PROBING HEME TRAFFICKING USING GENETICALLY ENCODED FLUORESCENT HEME SENSORS

A Dissertation
Presented to
The Academic Faculty

by

Osiris Martínez Guzmán

In Partial Fulfillment
of the Requirements for the Degree
Doctor of Philosophy in the
School of Chemistry & Biochemistry

Georgia Institute of Technology
December 2019

PROBING HEME TRAFFICKING USING GENETICALLY ENCODED FLUORESCENT HEME SENSORS

Approved by:

Dr. Amit Reddi, Advisor
School of Chemistry & Biochemistry
Georgia Institute of Technology

Dr. Loren Williams
School of Chemistry & Biochemistry
Georgia Institute of Technology

Dr. Adegboyega Oyelere
School of Chemistry & Biochemistry
Georgia Institute of Technology

Dr. Yury Chernoff
School of Biological Sciences
Georgia Institute of Technology

Dr. Raquel Lieberman
School of Chemistry & Biochemistry
Georgia Institute of Technology

Date Approved: [October 22, 2019]

ACKNOWLEDGEMENTS

I still remember the day I arrived in Atlanta to pursue my Ph.D. in Biochemistry, it was a bittersweet moment for me because while I has just made a huge leap towards my career, I was also leaving behind the most important part of my life, my family. Once I had my family arrive to help me settle in, I realized everything was going to be fine. I want to deeply thank my parents for teaching me the value of honest hard work and molding me into a caring and productive human being. For supporting me in every crazy idea I had. For loving me and providing me not only with the best household a kid could have but also with infinite care, this dissertation is for the both of you, los amo! To my siblings, I want to thank them for inspiring me, for always setting the best example and for not only being the best siblings but also best friends. To my sister and my brother-in-law David, I would like to thank them for giving me the best gift, my niece Osiris Marie. To my grandparents, thank you for all the love and support throughout my life, especially to my abuela Iris for always randomly calling to check on me, even though I know my abuelo Kike, abuelo Oscar and abuela Tati are still taking care of me from heaven, I love you all.

I am incredibly grateful to Eric, one of the best gifts' grad school could have ever given me. I am thankful for all your love and support through the years, for always being there in the hardest times. You definitely became my rock and none of this would have happened if I didn't have you in my life, I love you. I would also like to thank Eric's family, for adopting me as part of their own and giving me the warmth of a family when I most need it.

None of this could have been possible without having the best advisor, Dr. Amit Reddi. Thank you for always encouraging me to be a better scientist, to think on my own, to be more confident, and to fully develop my ideas. For teaching me to never be afraid of asking questions and for guiding me in my dream career of becoming a professor. I would also like to express my

gratitude to my committee members, Dr. Raquel Lieberman, Dr. Loren Williams, Dr. Adegboyega Oyelere and Dr. Yury Chernoff for their encouragement and advice throughout my graduate career.

To my lab mates and my friends, I thank you for making this process a lot of fun and for becoming a second family to me. I would like to specially thank Dr. Bindu Chandrasekharan, Dr. Rebecca Donegan, Claudia Montlor Albalate and Courtney Moore for not only making lab fun and welcoming but also for being incredible friends. I also would like to recognize the incredible work of Arushi Saini, that during her three years working as an undergrad under my mentorship accomplished magnificent things and made lab a lot more fun and gratifying.

Last but not least, I would like to recognize all the teacher and professors that spark the curiosity in science and guide me in the right path in order for me to accomplish this. Especially to my 7th grade teacher Elizabeth Torres who introduced me to the world of science. Also, thanks to my undergraduate advisor, Dr. Ezio Fasoli for giving me the opportunity to do research for the first time and introducing me to the Chemistry Department at Georgia Tech. To my Organic professor Dr. Margarita Ortiz Marciales, I am very grateful for being able to learn from her, for her enthusiasm, advise and care.

TABLE OF CONTENTS

ACKNOWLEDGEMENTS **iii**

LIST OF TABLES **x**

LIST OF FIGURES **xi**

LIST OF SYMBOLS AND ABBREVIATIONS **xiv**

SUMMARY **xxii**

CHAPTER 1: INTRODUCTION **1**

1.1 Heme in Cell Biology **2**

1.2 Heme Pathology **5**

1.3 Heme Mobilization and Trafficking **8**

1.3.1 Heme Transporters 10

1.3.2 Heme Buffering Factors 11

1.3.3 Exogenous Heme Uptake 12

1.4 Fist Generation Heme Sensor (HS1) **14**

1.5 Conclusion and Scope of the Thesis **16**

CHAPTER2: GENOME-WIDE DETERMINANTS OF HEME HOMESTASIS **17**

2.1 Introduction **17**

2.2 Results **19**

2.2.1 Development of High Through-put Screen for Cytosolic Heme Availability 19

2.2.2 Deletion Mutants with High Cytosolic Heme 21

2.2.3 Deletion Mutants with Low Cytosolic Heme 23

2.2.3.1 Validation of Genes with Low Heme Availability 25

2.2.3.2 Genes that Regulate Heme Availability through Total Heme Changes 30

2.3 Discussion **37**

2.4 Materials and Methods **41**

2.4.1 Cell Strains, Transformations, Growth Conditions and Plasmids 41

2.4.1.1 Yeast Strain and Growth 41

2.4.1.2 Yeast Transformations 41

2.4.1.3 Plasmids 41

2.4.2 Experimental Methods 42

2.4.2.1 High Through-put Transformations 42

2.4.2.2 High Through-put Screen 42

2.4.2.3 Total heme quantification 43

CHAPTER 3: GLYCERALDEHYDE 3-PHOSPHATE DEHYDROGENASE (GAPDH) AS A HEME BUFFERING FACTOR **44**

3.1 Thesis Attribution Statement for Chapter 3 **44**

3.2 Introduction **44**

3.3 Results **46**

3.3.1 GAPDH Regulates Cytosolic Heme Availability 46

3.3.2 Expression of GAPDH isoforms 47

3.3.3 Heme Dependent Processes in a GAPDH Deficient Mutants 48

3.3.3.1 Catalase Activity in a *tdh3*Δ 48

3.3.3.2 Heme Activator Protein, Hap1, activity in a *tdh3*Δ 49

3.3.4 GAPDH Complementation 49

3.3.5 Identification of Heme Binding Residues on GAPDH 50

3.4 Discussion **52**

3.5 Material and Methods **54**

3.5.1 Cell Strains, Culturing and Plasmids 54

3.5.1.1 Yeast Strains, Media and Growth Conditions 54

3.5.1.2 *E. coli* Strains, Media and Growth Conditions 54

3.5.1.3 Plasmids 55

3.5.2 Experimental Methods 55

3.5.2.1 Catalase Activity Measurements in Yeast 55

3.5.2.2 Total Heme Quantification in Yeast 56

3.5.2.3 Hap1 Transcriptional Reporter Assay 56

3.5.2.3 Immunoblotting 57

CHAPTER 4: THE HEME BIOSYNTHESIS ENZYME 5-AMINOLEVULINIC ACID SYNTHASE (ALAS), AND GTPASES IN CONTROL OF MITOCHONDRIAL DYNAMICS AND ER CONTACT SITES, REGULATE HEME MOBILIZATION TO THE NUCLEUS 58

4.1 Introduction 58

4.2 Results 62

4.2.1 Inter-compartmental heme transport kinetics 62

4.2.2 ALA synthase (ALAS) regulates mitochondrial-nuclear heme trafficking 71

4.2.3 Gem1, a GTPase that regulates ERMES, negatively modulates mitochondrial-nuclear heme trafficking 72

4.2.3.1 Mgm1 and Dnm1 are positive and negative regulators of mitochondrial-nuclear trafficking, respectively 75

4.2.3.2 Mitochondrial Fusion 76

4.2.3.3 Mitochondrial Fission 78

4.2.4 Mgm1 and Dnm1 regulate the activation of the nuclear heme-regulated transcription factor Hap1 81

4.3 Discussion 84

4.4 Materials and Methods 89

4.4.1 Cell strains, Transformations, Growth Conditions and Plasmids 89

4.4.1.1 Yeast Strains and Growth Conditions 89

4.4.1.2 Yeast Transformations 90

4.4.1.3 Plasmids 90
4.4.2 Experimental Methods 91
4.4.2.1 Heme Trafficking Dynamics Assay 91
4.4.2.2 Total heme quantification 93
4.4.2.3 Hap1 Activity 94
4.4.2.4 Isolation of the mitochondria and nuclei to confirm heme sensor localization 95
4.4.2.5 Confirmation of heme sensor localization by microscopy 97
4.4.2.6 Confirmation of mitochondrial morphology in fission and fusion 98
CHAPTER 5: UPTAKE AND UTILIZATION OF HEME AND HEME INTERMEDIATES 99
5.1 Introduction 99
5.2 Results 100
5.2.1 A *hem1*Δ Mutant can use intact Exogenous Heme 100
5.2.2 Heme Availability for Different Compartments of a *hem1*Δ Mutant Provided with Exogenous Heme and Heme Intermediates 103
5.2.3 Heme Dependent Processes of a *hem1*Δ with Supplementation of Exogenous Heme and Heme Intermediates 106
5.2.4 Heme Uptake Improvement by Iron Starving *S. cerevisiae* 108
5.2.5 Heme Uptake Improvement under Iron Starvation is controlled by Heme Oxygenase 110
5.2.6 High through-put screen for the identification of genes that regulate heme uptake 110
5.2.6.1 Genes that regulate heme acquisition 112
5.2.7 Role of *mfm1*Δ in heme uptake 115
5.3 Discussion 116

5.4 Materials and Methods **121**

5.4.1 Cell Strains, Transformation, Growth Conditions and Plasmids 121

5.4.1.1 Yeast Strain and Growth 121

5.4.1.2 Yeast Transformation 121

5.4.1.3 Plasmids 121

5.4.2 Experimental Methods 122

5.4.2.1 Catalase Activity Measurements in Yeast 122

5.4.2.2 Total Heme Quantification in Yeast 122

5.4.2.3 Hap1 Transcriptional Reporter Assay 123

5.4.2.4 Immunoblotting 123

5.4.2.5 High Through-put transformation 124

5.4.2.6 High Through-put screen 124

CHAPTER 6: CONCLUSION AND FUTURE WORK **125**

6.1 Genome-Wide Determinants of Heme Homeostasis **125**

6.2 GAPDH **126**

6.3 The Heme Biosynthesis Enzyme, 5-aminolevulinic Acid Synthase (ALAS), and GTPases in Control of Mitochondrial Dynamics and ER Contact Sites, Regulate Heme Mobilization to the Nucleus **127**

6.4 Uptake and Utilization of Heme and Heme Intermediates **129**

6.5 Conclusion **130**

APPENDIX A. SUPPLEMENTAL TABLES AND FIGURES **131**

A.1 Introduction **131**

A.2 Supplemental Table **131**

A.3 Supplemental Figure **134**

References **135**

LIST OF TABLES

Table 2.1	Validation screen for heme availability prioritized by Ratio of Ratios values.	26
Table 2.2	Total Heme measurements of low heme availability genes from the genome-wide screen.	32
Table 5.1	Genes identified to improve heme acquisition from the high through-put screen.	113
Table A.1	Kinetic parameters derived from fits to the heme trafficking data using Equation 2.	131

LIST OF FIGURES

Figure 1.1	Heme *b* chemical structure, which is the most common form of heme.	1
Figure 1.2	Heme biosynthesis in eukaryotes[1].	5
Figure 1.3	Eukaryotic model of heme transport and trafficking[2].	9
Figure 1.4	Model of HS1 derived from the X-ray structures of mKATE (PDB: 3BXB) and CG6 (PDB: 3U8P).	14
Figure 1.5	Validation of the sensor.	15
Figure 2.1	Genome-wide high through-put screen data for endogenous heme availability.	20
Figure 2.2	Cellular component enrichment for high cytosolic labile heme deletion mutants.	21
Figure 2.3	Biological process enrichment for high cytosolic labile heme deletion mutants.	22
Figure 2.4	Cellular component enrichment for low cytosolic labile heme deletion mutants.	23
Figure 2.5	Biological process enrichment for low cytosolic labile heme deletion mutants.	24
Figure 2.6	Percent of heme bound to the sensor on low cytosolic labile heme deletion mutants related to ESCRT proteins and vacuolar function.	25
Figure 2.7	Labile heme sensitivity to heme depletion using the heme biosynthetic inhibitor, succinylacetone (SA) and affinity variants of the heme sensor.	31
Figure 2.8	Total heme levels of specific functional groups of deletion mutants with low cytosolic heme.	32
Figure 2.9	The proposed mechanism for heme mobilization via intracellular vesicle-mediated trafficking.	40
Figure 3.1	Tdh3p regulates intracellular heme availability.	47
Figure 3.2	Immunoblot analysis of GAPDH and SOD1 (loading control) for the three isoforms of GAPDH in yeast.	47

Figure 3.3	Tdh3 deficient mutant displayed normal amounts of catalase activity.	48
Figure 3.4	Hap1p activity in the indicated strains as measured by a transcriptional reporter that used EGFP driven by the CYC1 promoter, a Hap1p target gene.	49
Figure 3.5	Heme availability and expression measurements for the complemented GAPDH deficient strain.	50
Figure 3.6	GAPDH heme binding is essential for regulating cytosolic labile heme and delivery to nuclear Hap1p.	51
Figure 4.1	The sub-cellular localization of HS1 was assessed by laser scanning confocal microscopy and cell fractionation and immunoblotting.	63
Figure 4.2	Validation that mitochondrial and nuclear-targeted HS1 does not respond to cytosolic heme.	64
Figure 4.3	Inter-compartmental heme trafficking dynamics as measured by heme sensor HS1.	66
Figure 4.4	A 500 μM dose of succinylacetone (SA) depletes total heme and heme-loading of the heme sensor, HS1, to values similar to heme deficient *hem1*Δ cells.	68
Figure 4.5	Heme sensor expression does not perturb the rates of heme synthesis or heme trafficking dynamics to the cytosol.	69
Figure 4.6	ALA synthase (Hem1) negatively regulates mitochondrial-nuclear heme trafficking.	71
Figure 4.7	Gem1 is a negative regulator of mitochondrial-nuclear heme trafficking.	75
Figure 4.8	Mgm1 is a positive regulator of mitochondrial-nuclear heme trafficking.	78
Figure 4.9	The effects of mgm1Δ and dnm1Δ on steady-state HS1 heme loading and heme synthesis.	79
Figure 4.10	Dnm1 is a negative regulator of mitochondrial-nuclear heme trafficking.	80
Figure 4.11	Mitochondrial-nuclear heme trafficking regulates Hap1 activity and sensitivity to new heme synthesis.	83
Figure 5.1	Growth rescue of hem1Δ with ALA treatment.	101

Figure 5.2	Growth rescue of hem1Δ with higher concentrations of ALA, PPIX and heme treatment.	102
Figure 5.3	Total heme concentrations of heme deficient cells supplemented with heme and heme intermediates.	103
Figure 5.4	ALA supplementation populates our sensor in the cytosol better than any other treatment.	104
Figure 5.5	PPIX supplementation binds to our nuclear sensor more than any other treatment or compartment.	105
Figure 5.6	No treatment made heme bioavailable in the mitochondria.	105
Figure 5.7	PPIX displayed the highest Hap1 activity correlating with heme availability in the nucleus.	107
Figure 5.8	Only endogenous heme by supplementing with ALA presented catalase activity and expression.	108
Figure 5.9	Heme acquisition improves during iron starvation conditions.	109
Figure 5.10	Iron starvation facilitates heme uptake in every quantified organelle.	109
Figure 5.11	Heme acquisition improvement by iron starvation is dependent upon heme oxygenase expression	110
Figure 5.12	Genome-wide high through-put screen data for heme acquisition.	111
Figure 5.13	Mfm1 is a negative regulator for heme acquisition.	115
Figure 5.14	Mfm1 deletion facilitates heme uptake through changes in mitochondrial membrane potential.	116
Figure A.1	Validation of the mitochondrial network morphology defects in yeast fission and fusion mutants.	134

LIST OF SYMBOLS AND ABBREVIATIONS

μL	microliter
μM	micromolar
°C	Degrees Celsius
Aβ	Amyloid-β
ALA	Aminolevulinic acid
ALAD	Aminolevulinic acid dehydratase
ALAS	Aminolevulinic acid synthase
Atx1	Copper chaperone
BPS	bathiphenanthrolinedisulfonic acid disodium salt hydrate (iron chelator)
BY4741	Wild type cell
C. albicans	*Candida albicans*

C. elegans	*Caenorhabditis elegans*
Ccs1	Copper chaperone
CO	Carbon monoxide
COX4	Cytochrome c oxidase gene
CPOX	Coproporphyrinogen oxidase
Cyt b_{562}	Cytochrome b562
DAPI	4,6-diamidino-2-phenylindole
E. coli	*Escherichia coli*
eGFP	Enhances green fluorescent protein
EMC	ER membrane protein complex
ER	Endoplasmic Reticulum
ERMES	ER-mitochondria encounter structure

ESCRT	Endosomal sorting complex required for transport
FABS	Fatty acid binding protein
FAD	Flavin adenine dinucleotide
FECH	Ferrochelatase
fL	femtoliters
FLVCR	Feline Leukemia Subgroup C Cellular Receptors
FRET	Fluorescence resonance energy transfer
GAPDH	Glyceraldehyde 3-phosphate dehydrogenase
GSH	Reduced glutathione
Hb	Hemoglobin
HBP	Heme binding protein
HGR	Heme responsive genes

Hmx1	Heme oxygenase 1
HO	Heme oxygenase
HOPS	homotypic fusion and protein sorting
HPLC	High-Performance Liquid Chromatography
IM	Inner membrane
IMS	Mitochondrial intermembrane space
iNOS	inducible Nitric oxide synthases
KanMX4	Antibiotic for deletion mutants in the collection
K_d	Dissociation constant
kDa	kilodalton
LH	Labile heme
MAMs	Mitochondrial associate's membranes

MEF	Mouse embryo fibroblast
MFS	Major facilitators superfamily
mg	milligrams
MICOS	mitochondrial contact site and cristae organizing system
mKATE2	Katushka 2
mL	milliliters
MVB	Multivesicular bodies
NADPH	Nicotinamide adenine dinucleotide phosphate
nM	nanomolar
nm	nanometer
OM	Outer membrane
PANTHER	Protein analysis through evolutionary relationships

PBG	Porphobilinogen
PBGD	Porphobilinogen deaminase
PC	Phosphatidylcholine
PE	Phosphatidylethanolamine
PGRMC1	Progesterone membrane receptor component 1
PMF	post-mitochondrial fraction
PNF	post-nuclear fraction
PPOX	Protoporphyrinogen oxidase
PRX1	Peroxiredoxin-1
PS	Phosphatidylserine
ROS	Reactive Oxygen Species
S. cerevisiae	*Saccharomyces cerevisiae*

S. pombe	*Schizosaccharomyces pombe*
SA	Succinyl acetone
SC	Synthetic complete medium
SCE	Synthetic complete medium with ergosterol and tween
Shu1	Suppressor of HU sensitivity-1
SNARE	Soluble N-ethylmaleimide-sensitive factor attachment protein receptor
Str3	Sulfur transfer-3
Tdh3p	Triose-phosphate Dehydrogenase
TNG	Trans-Golgi Network
UROD	Uroporphyrinogen decarboxylase
UROS	Uroporphyrinogen synthase
vCLAMPS	mitochondrial- vacuolar contact sites

WT	Wild Type
YPD	Yeast extract peptone dextrose

SUMMARY

Heme (iron protoporphyrin IX) is an essential but inherently cytotoxic metallocofactor and signaling molecule. Although essential for life, heme and its biosynthetic precursors may also act as toxins, necessitating that cells carefully handle the synthesis and trafficking of this compound. The hydrophobicity and redox activity of heme causes it to disrupt membrane structure, become mis-associated with certain proteins, and deleteriously oxidize various biomolecules. Despite the tremendous importance of heme in physiology, the cellular and molecular mechanisms that govern the safe assimilation of heme from its sites of synthesis or uptake into metabolism remain poorly understood. Herein, we utilized genetically encoded fluorescent heme sensors to identify factors that regulate heme uptake, trafficking, and bioavailability.

In this thesis, we describe genetic screens in Baker's yeast to identify factors that regulate **a.** steady-state heme availability, **b.** the dynamics of heme mobilization to different subcellular compartments as it is being synthesized, and **c.** heme uptake. Regarding steady-state heme availability, the *Saccharomyces cerevisiae* haploid gene deletion library was transformed with cytosolic heme sensors and mutants with altered heme availability were discovered in order to identify possible heme transporters, trafficking factors, and buffering proteins. The screen identified 114 strains with high cytosolic heme and 323 strains with low cytosolic heme.

Amongst the deletion mutants with high heme, we found that the glycolytic enzyme glyceraldehyde phosphate dehydrogenase (GAPDH) is responsible for buffering intracellular heme and regulating the activity of the nuclear heme-dependent transcription factor heme activator protein (Hap1p). Additionally, we found that a conserved His residue, His53 in human and His51 in yeast, is responsible for heme binding to GAPDH and its cellular role in heme buffering and activation of Hap1. Amongst the deletion mutants with low heme, we found that Golgi-to-vacuolar

vesicular trafficking is a key requirement to for ensuring heme is accessible to the cytosol. We propose a model in which heme is transported from endosomes into the cytosol. Altogether, for the first time, we identified genome-wide determinants of heme bioavailability.

In order to probe heme distribution dynamics as heme is being synthesized, we developed a live-cell assay in yeast to monitor inter-compartmental heme trafficking kinetics to different subcellular compartments, including the mitochondrial matrix, cytosol, or nucleus. Surprisingly, we found that heme trafficking rates from the matrix side of the IM, where heme is made, to the mitochondrial matrix and cytosol are similar, while trafficking to the nucleus is ~25% faster. These data indicate that heme is distributed from the mitochondrial IM to other locales simultaneously via multiple parallel pathways rather than sequentially. Moreover, we discovered that the heme biosynthetic enzyme, aminolevulinic acid synthase (ALAS) negatively regulates mitochondrial-nuclear heme trafficking, highlighting the close coordination of heme synthesis and trafficking. In addition, we identified GTPases that directly (Gem1) and indirectly (Dnm1 and Mgm1) regulate ERMES as being modulators of nuclear heme transport. Based on our results, we propose a model in which heme is trafficked via ER- mitochondrial membrane contact sites to other organelles such as the nucleus.

Most eukaryotes have the capacity to both make and import heme. We used fluorescent heme sensors in *Saccharomyces cerevisiae* to determine if heme availability and utilization differs whether heme is derived from exogenous or endogenous sources. Our results demonstrate that *S. cerevisiae* is capable of acquiring and utilizing exogenous heme under high concentrations but not in an efficient way. Biosynthesized heme is more available than exogenous heme and is more efficient at activating heme dependent processes such as catalase activity and Hap1 activity, a heme dependent transcription factor. We observed conditions such as iron starvation promoted

heme availability from exogenous sources in a heme oxygenase (HO) dependent manner. In addition, we screened the yeast deletion collection for factors that altered heme uptake and utilization and identified 33 deletion mutants that displayed an improvement in heme uptake, including *mfm1*Δ cells, which lacks a magnesium transporter and has a defect in mitochondrial membrane potential.

Overall, our work probing heme homeostasis with genetically encoded heme sensors have identified a host of new factors that regulate heme trafficking dynamics and availability from both endogenous and exogenous heme sources. The tools and approaches described herein to identify new heme trafficking factors in Baker's yeast are now being applied to probe heme homeostasis in human cell lines, where defects in heme metabolism cause a number of diseases, and in bacterial and fungal pathogens, which require heme for virulence.

CHAPTER 1. INTRODUCTION

Heme (iron protoporphyrin IX, heme b) is an essential metallonutrient required for virtually all aerobic life. (**Figure 1.1**) Biology exploits the Lewis acidity, redox activity and hydrophobicity of heme to act as a protein cofactor and signaling molecule. As a cofactor, heme facilitates several processes that span electron transfer, chemical catalysis, gas synthesis, storage and transport[3]. As a signaling molecule, heme handles a set of proteins that collectively control pathways spanning iron homeostasis, oxygen sensing, the oxidative stress response, mitochondrial respiration and biogenesis, mitophagy, apoptosis, circadian rhythms, cell cycle progression, proliferation, and protein translation and degradation[2, 4]. There are three major types of heme in eukaryotes: heme *a*, heme *b*, and heme *c*, which differ in the nature of the substituents on the porphryin ring[5]. Heme *b* it is the most ubiquitous form and constitutes the cofactor of most hemoprotein such as myoglobin and hemoglobin[5]. Heme *a* is only found in cytochrome *c* oxidase of the electron transport chain[5]. Heme *c* is different from heme *b* in that it is covalently bound to proteins via a thioether linkage and is found in respiratory proteins such as cytochrome c and the *bc1* complex[5]. Since heme *b* is the most abundant form of heme, and the pre-cursor for hemes *c* and *a*, we will be discussing heme *b* trafficking and availability throughout this work.

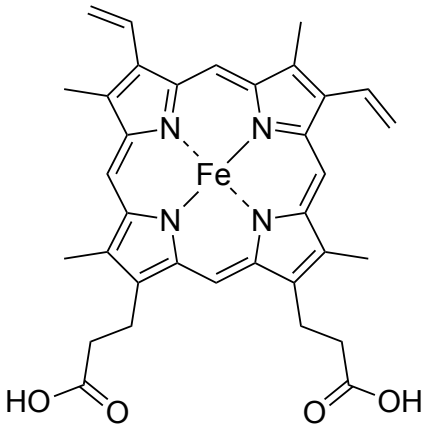

Figure 1.1- Heme *b* chemical structure, which is the most common form of heme.

The very same properties of heme that make it essential for life also render it potentially toxic if mishandled by cells. For instance, the misincorporation of heme into various biomolecules, including certain proteins and lipid membranes, alters macromolecular structure and function[6, 7]. Moreover, heme is capable of catalyzing the formation of reactive oxygen species (ROS), thereby damaging DNA, lipid membranes and the cytoskeleton[8, 9]. Therefore, heme concentration and bioavailability must be tightly regulated. Heme concentration is regulated by its biosynthesis and degradation, two well-understood processes. However, the molecules and mechanisms governing heme bioavailability, including its transport and trafficking, to hemoproteins residing in every subcellular compartment are not well understood. In this chapter, we will discuss the role of heme in cell biology, heme biosynthesis and degradation, heme toxicity and detoxification, heme related pathologies such as, porphyria and Alzheimer's disease, and what is currently known about heme transport and trafficking.

1.1 Heme in Cell Biology

The canonical role of heme in cell biology is as a protein cofactor[10]. For example, in hemoglobin and myoglobin heme is used for oxygen transport and storage respectively[1, 2, 4]. Other biological functions for heme include its ability to facilitate electron transfer and catalysis. In addition, heme can act as a dynamic signaling molecule in the regulation of transcription factors, ion channels, kinases, and cell surface receptors[1, 2, 4]. Heme in biology is composed of two major pools, an exchange inert heme pool and an exchange labile heme pool[2, 4]. Exchange inert heme is tightly bound to high affinity hemoproteins like goblins and cytochromes and cannot exchange between various proteins. Labile heme is readily exchangeable between proteins and represents the mobile pool of heme accessible for trafficking and signaling. Studies with activity and fluorescence-based heme reporters in *Saccharomyces cerevisiae* and various non-erythroid human

cell lines estimated the labile heme pool in the cytosol to be ~25-300 nM[3, 11, 12], which corresponds to 10% of the total cellular heme concentration.

In order to reduce heme toxicity, heme concentration and heme availability need to be tightly regulated in the cells. Heme concentration is regulated by its synthesis and degradation. Eukaryotic heme biosynthesis is a very well understood highly conserved pathway, called the Shemin pathway, and involves eight enzymatic steps that take place in between the cytosol and mitochondria[13]. (**Figure 1.2**) This pathway starts with the condensation of glycine and succinyl-CoA to form 5-aminolevulinic acid (5-ALA), which is catalyzed by ALA synthase (ALAS) in the mitochondrial matrix. ALAS is the rate limiting step of heme biosynthesis. 5-aminolevulinic acid is then transported from the mitochondrial matrix into the cytosol, where it is condensed by ALA dehydratase (ALAD) to form porphobilinogen (PBG). Four PBG molecules are condensed into hydroxymethylbilane via the cytosolic enzyme PBG deaminase (PBGD). Next, hydroxymethylbilane is then cyclized by uroporphyrinogen synthase (UROS) to make uroporphyrinogen III. For the final cytosolic biosynthesis step, uroporphyrinogen III is decarboxylated to form coproporphyrinogen III via uroporphyrinogen decarboxylase (UROD). Coproporphyrinogen III is then trafficked to the mitochondrial intermembrane space (IMS) for oxidation to protoporphyrinogen IX helped by coproporphyrinogen oxidase (CPOX). Protoporphyrinogen IX is mobilized to the matrix and consequently oxidized to protoporphyrin IX by protoporphyrinogen oxidase (PPOX). In the the last step of heme synthesis, iron is inserted into protoporphyrin IX in a reaction catalyzed by ferrochelatase (FECH).

Heme degradation is facilitated by heme oxygenase (HO), which catalyzes the O_2-dependent catabolism of heme into biliverdin, carbon monoxide (CO) and free iron[1, 4, 14]. HO dependent heme degradation starts with the formation of a ferric heme-HO complex in which the iron center gets

reduced to its ferrous state by the first electron donated from NADPH-cytochrome P450 reductase[14]. Molecular oxygen then binds to the complex to from a stable oxy-form, in which the iron bound oxygen is converted into a hydroperoxide intermediate by getting another electron from the reductase and a proton from water[14]. To finish, the terminal oxygen of the hydroperoxide intermediate attacks the α-carbon of the porphyrin ring to form biliverdin or ferric α-meso-hydroxyheme[14]. Biliverdin is further catabolized to bilirubin by biliverdin reductase, an NADPH dependent oxidoreductase, [9].

As an iron tetrapyrrole complex, heme presents characteristics of both a metal and a lipid[4]. Therefore, heme might be mobilized as a metal or a lipid or alternatively it could be mobilized in a specific way that combines both. As a metal, heme transport and mobilization could be governed by its coordination chemistry and oxidation state, which may suggest the existence of heme chaperones, buffers and transporters[4]. As a lipid, heme could be mobilized as a phospholipid-like molecule in which trafficking might be dictated by the hydrophobic, ionic and hydrogen bonding interactions of heme and putative carrier proteins[4]. This suggests heme is mobilized like other mitochondrial derived lipids through membrane tethering complexes, lipid transfer proteins, vesicular trafficking or organelle contact points[4]. Currently, there is very little known about the mechanisms and factors that regulate heme homeostasis. Knowledge of these pathway would aid in the understanding of the numerous disorders associated with defects in heme management.

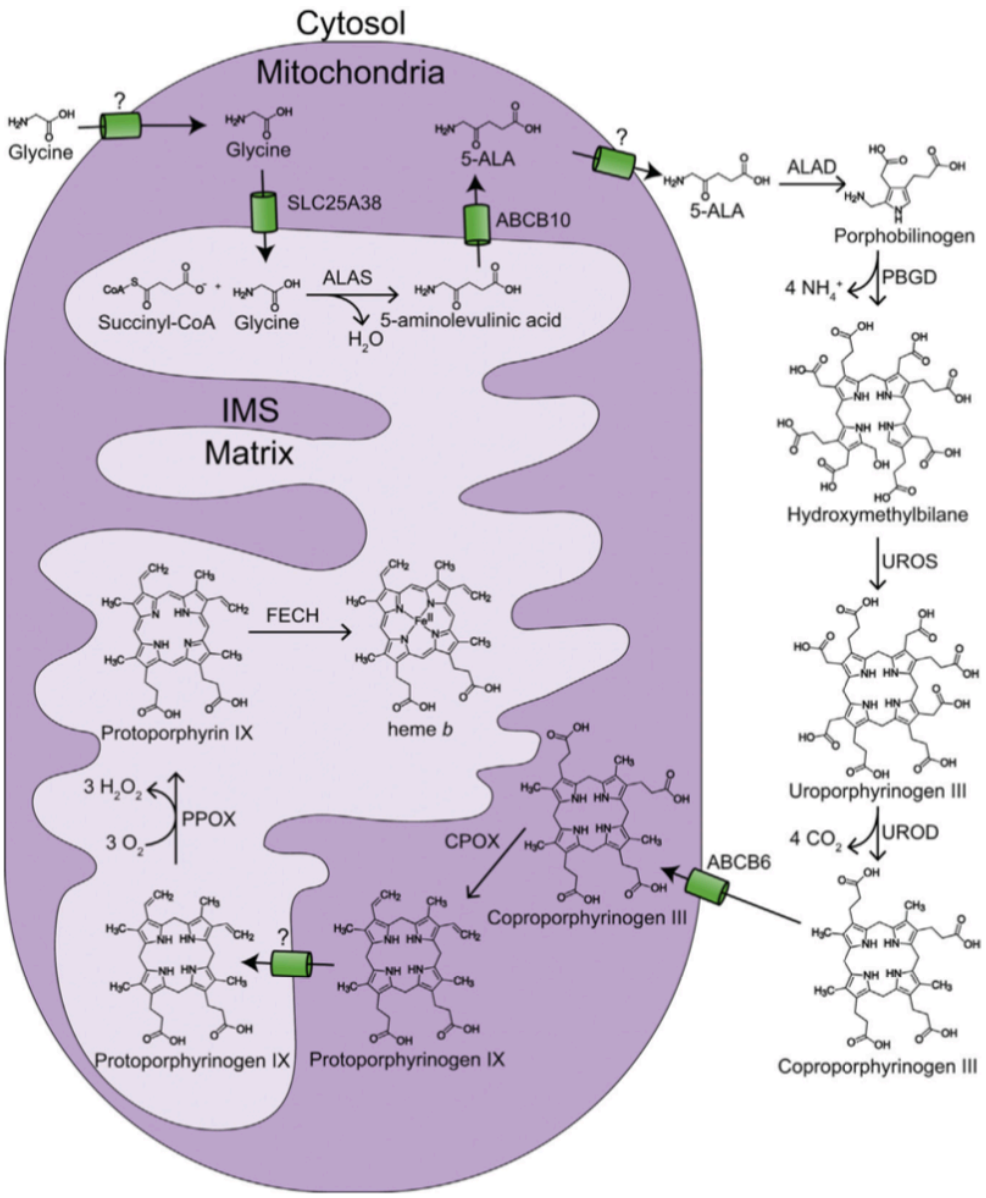

Figure 1.2 - Heme synthesis in eukaryotes. Heme is synthesized in eukaryotes via the Shemin pathway consisting of eight highly conserved enzymes, four in the mitochondria and four in the cytoplasm. Figure adapted with permission from: Donegan, R. K., et al. (2019). "Handling heme: The mechanisms underlying the movement of heme within and between cells." Free Radic Biol Med **133**: 88-100. Copyright © 2019 Elsevier Inc.

1.2 Heme pathology

In cases of severe hemolysis and myolysis, which are common in diseases such as sickle cell, malaria and ischemia reperfusion, high amounts of toxic free heme is released, causing organ

and tissue damage. During these cases, the large amount of heme that accumulates overwhelms the HO-mediated system for heme detoxification. This leads to a variety of heme toxicity mechanisms, a major mode being from its ability to catalyze peroxidation reactions and hydroxyl radical production via Fenton chemistry. Deleterious heme-dependent redox reactions in part contribute to vascular disorders like hemolytic anemia, vasculitis, reperfusion injury and arteriosclerosis. The generation of ROS by heme has also being implicated in lipid oxidation, DNA damage, apoptosis and protein degradation that causes aggregates[9]. Another pathway for heme toxicity is through its ability to aggregate in lipid membranes, disrupting membrane structure and permeability, which can lead to cell lysis and death. This is common in hemolysis in which the red cell membranes gets oxidized and disrupted to the point that stimulates potassium loss and swelling[9]. Heme also has the ability to alter the conformation of the cytoskeleton, which can damage red blood cells[9]. Heme, acting as a pro-inflammatory signaling molecule, can also reorganize the neutrophil cytoskeleton by increasing the polymerization of actin [9].

Another mode of heme toxicity is its missincorporation into certain proteins, such as in Alzheimer's disease. Amyloid-β (Aβ), the pathogenic protein that causes AD, can bind heme contributing toward the cytotoxicity of the disease through the peroxidase activity of the heme complex[6]. Moreover, heme sequestration by Aβ leads to cells feeling heme starved, causing them to turn on heme synthesis. Another aspect of AD is that there is increased heme and hemoglobin in the brain due to a weakened blood brain barrier, which further makes Aβ more toxic due to deleterious heme interactions. [7, 15-17]. Indeed, tissue analysis of patients demonstrated an increase of heme in the temporal lobe[7] and high amount of hemoglobin mRNA in other specific parts of the brain[18]. Moreover, heme accumulates and colocalizes with Aβ deposits in the brain tissues of Alzheimer's disease patients[18]. Additionally, heme and hemoglobin have been observed to bind

Aβ and alter its aggregation state[7, 15, 16]. Recent data demonstrated heme and hemoglobin significantly decrease the Aβ-mediated expression of pro-inflammatory cytokines in astrocytes[19]. Altogether, these results indicate a new heme-related perspective in the cytotoxicity of Alzheimer's disease that has not been fully appreciated.

To protect the cells from heme toxicity, a number of detoxification mechanisms have evolved, including the heme oxygenase system for degrading heme and heme scavenging systems such as hemopexin, albumin and reduced glutathione (GSH)[9]. HO protects cells by not only degrading excess heme, but also the products of heme degradation, such as biliverdin and bilirubin, are themselves cytoprotective by acting as antioxidants and anti-inflammatory agents. Carbon monoxide, another heme degradation product, can stimulate the expression of the iron storage protein, ferritin, to prevent the toxicity associated with iron release from heme degradation. Bilirubin is capable of scavenging peroxyl radicals, CO inhibits pro-inflammatory cytokines and ferritin scavenge free iron.

In terms of heme scavenging, hemopexin is a high affinity heme binding protein that reduces the toxicity of heme by forming a complex with it[9]. The role of this protein is binding free heme in the blood and transporting it to the liver for degradation[20]. Albumin, like hemopexin, also scavenges heme, but acts more like a heme buffer in the serum. Rather than being directed for degradation in the liver, albumin buffers heme until more hemopexin is available for heme detoxification. Reduced glutathione (GSH) is capable of protecting against heme-induced oxidative stress by not only scavenging ROS generated by heme but also by being able to non-enzymatically degrade heme in the presence of oxygen and at neutral pH[21].

Proper regulation of heme synthesis is also important to maintain heme homeostasis. Abnormal function of any of the eight enzymes responsible for heme biosynthesis results in the

accumulation of toxic heme biosynthetic intermediates, leading to a family of disorders called porphyrias. Porphyrias are a group of eight metabolic disorders in the heme biosynthesis pathway that cause symptoms such as skin lesions due to the build up of photo-sensitive porphyrin and porphyrin precursors, as well as zinc-protoporphyrin in one case. Moreover, the lack of heme leads to decreases in liver and gastrointestinal function. All of the porphyrias are associated with partial enzyme deficiencies, accounting for why patients survive to adulthood.

Other situations in which heme is important in physiology is in infectious diseases. Pathogenic bacteria and fungi require iron for survival and evolved a number of pathways for iron uptake. Since heme represents the major form of iron in humans, they contain sophisticated machineries for heme uptake that contribute to virulence [22]. The majority of these pathogens uptake heme and degrades it in order to use the iron[22]. Better understanding of heme acquisition and utilization in infectious disease will allow us to design heme-based therapeutics.

1.3 Heme Mobilization and Trafficking

Once heme is made on the matrix side of the inner-membrane of the mitochondria, it must be delivered to hemoproteins throughout the cell, including cytochromes in the mitochondrial respiratory complexes, globins in the cytosol, catalases in peroxisomes, P450 enzymes in the ER, NADPH oxidases at the plasma membrane, and heme-regulated transcription factors in the nucleus, e.g. p53, Bach1, and Reverb. The hierarchy for heme distribution, *i.e.* which organelles acquire heme the fastest and/or prioritize holding on to heme the longest in the face of heme depletion, is not known. Also, very little is known about the transport and trafficking of heme and the dynamics of heme mobilization out of the mitochondria.

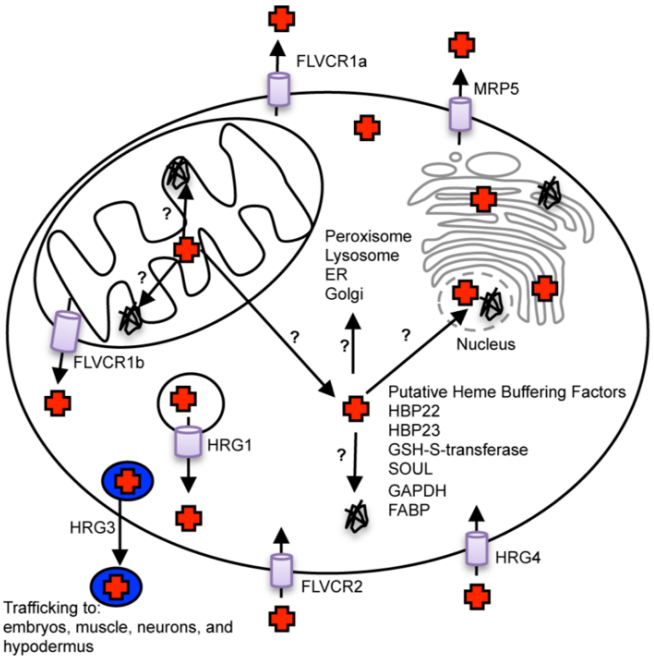

Figure 1.3 – Model of eukaryotic heme transport and trafficking. After heme synthesis is done in the mitochondrial matrix, heme must be transported out of it and incorporated into a multitude of hemoproteins found in different compartments. Proteins previously implicated in heme transport, trafficking, or buffering are identified, and trafficking pathways that are currently unknown are marked with question marks. Figure adapted with permission from: Hanna, D. A., et al. (2017). Biochemistry **56**(13): 1815-1823. Copyright © 2017 American Chemical Society.

In the context of our model that conceptualizes total cellular heme as being the sum of exchange inert and labile heme, one can envision two primary pathways for heme trafficking and mobilization. One pathway is that there may be post-translational modifications that cause a hemoprotein that does not otherwise dissociate heme to release heme. For instance, S-nitrosation of heme ligating thiolates were previously found to cause heme dissociation of certain thiolate-coordinating heme enzymes[1, 4]. The second pathway for heme transfer consists of the exchange of labile heme between buffering factors, heme chaperones, transporters and apo-hemoproteins through differences in their expression level and/or affinity for heme. (**Figure 1.3**)

As an iron-protoporphyrin IX complex, heme displays characteristics of a transition metal and a lipid[4]. Therefore, it could be mobilized as a metal, as a lipid or in a hybrid way. As a metal

heme transport and mobilization would be dependent on the presence of heme chaperones, buffers and transporters[4]. Since the dissociation of heme is the rate-limiting step of ferrochelatse (FECH), we can suggest the idea of heme binding proteins or chaperones that catalase the transfer of heme from FECH (45). Protein such as the progesterone membrane receptor component 1 (PGRMC1), a heme chaperone, was found to interact with FECH as part of a heme biosynthetic complex or heme metabolon, possibly accepting heme prior its mobilization[23, 24]. As a lipid, heme would be mobilized like phospholipids, with trafficking being dictated by the hydrophobic, ionic and hydrogen bonding interactions between the porphyrin and client proteins[4]. In that case and given the hydrophobic nature heme, it would be mobilized like other mitochondrial derived lipids, through membrane tethering complexes like the ER-mitochondria encounter structure (ERMES) or mitochondrial associates membranes (MAMs), lipid transfer proteins, vesicular trafficking or organelle contact points[4]. Heme could be mobilized to other organelles via the ER and trans Golgi network and secretory pathways[1]. Alternatively, heme could be mobilized in ER or Golgi-derived vesicles that fuse into different organelles to deliver heme to the hemoproteins throughout the cell[1].

1.3.1 Heme Transporters

Over the years, a few heme transporters have been identified, including Feline Leukemia Subgroup C Cellular Receptors (FLVCR)[25], heme responsive genes HRG1 and HRG4 [26], and multidrug resistance protein 5 (MRP-5)[27]. The FLVCRs are proteins that are members of the major facilitator superfamily (MFS) involved in heme import and heme export, in which two splice variants have been identified: FLVCR1a and FLVCR1b[28]. FLVCR1a, the plasma membrane exporter, is a ~60 kDa protein predicted to have the common MFS protein twelve hydrophobic transmembrane domains[29]. In the case of the mitochondrial heme exporter, FLVCR1b, is a ~28 kDa with a six predicted transmembrane domain[30]. The expression of these heme exporters in

mammals is present in high levels in the brain, liver, kidney, intestine and bone marrow[25]. Although the expression of the transporter FLVCRb have been demonstrated to be crucial for erythroid cell differentiation, presumably because it enables the export of mitochondrial heme and its delivery to globins, direct evidence that it transports heme and its precise localization is still not known[25].

The heme transporter, MRP5, was first identified on *Caenorhabditis elegans* as a necessary heme exporter in the intestines[27]. MRP5 seems to be crucial for the transport of heme from the cytosol into the secretory pathway in which can subsequently be mobilized to hemoproteins within the pathway, to the cellular membrane or to the extracellular space[27]. Two other heme transporters identified in *C. elegans* are the HRG-1 and HRG-4, important for transport and utilization of exogenous heme[26]. These two heme transporters are ~19 kDa with four predicted transmembrane domains. HRG-1 is localized in the membranes of endosomal/ lysosomal compartments transporting exogenous heme into the cytosol and necessary for the recycling of heme by macrophages[31]. HRG-4 mobilized heme across the plasma membrane into the cytosol primarily involved in the heme uptake of the intestines[26].

1.3.2 Heme Buffering Factors

The cytosol is the organelle with the highest concentration of labile heme in the cell consisting of 20-340 nM, which is more than the < 1 nM found in the nucleus or the mitochondria (21-23). Due to the relatively high concentration of cytosolic LH, heme likely must be buffered and trafficked with chaperones and heme binding proteins in order to mitigate the cytotoxicity of this biomolecule. Based on interactions with hemin-agarose or blue sepharose, a number of heme-binding proteins have been identified and proposed to have a role in heme homeostasis, including heme binding proteins HBP22[32] and HBP23[33], glutathione S-transferase (GSH-S transferase)[34],

HBP-1 (also known as SOUL)[35] and fatty acid binding protein (FABS)[36]. [32]. Even though these heme-binding proteins may prevent toxicity by binding and buffering excess of heme in the cytosol, the lack of *in vivo* and biochemical characterization raises even more questions on not only how these proteins play a role in heme homeostasis but also how heme is mobilized and transported by them throughout the cell.

The heme binding protein HBP23, which is also the peroxiredoxin PRX1, is a recently characterized heme buffering factor. PRX1 is a thiol peroxidase that binds heme with an affinity of 170 nM and binds heme in a 1:1 stoichiometry[37]. This protein binds heme through the coordination of a cysteine, specifically Cys52, that upon heme binding loses the thiol peroxidase activity[37]. Since PRX1 is so abundant in the cytosol and is able to bind heme, this protein could be serving two roles, as a peroxide scavenging thiol peroxidase and as a heme buffering factor or storage protein[1]. However, *in vivo* experiment with PRX1 are necessary in order to demonstrate its role in heme homeostasis[37]. Overall, not much is known about the proteins that buffer heme and regulate heme homeostasis. The proteins that have been suggested based on their ability to bind heme in vitro, have not been found to regulate heme homeostasis *in vivo*.

1.3.3 Exogenous Heme uptake

Even though some organisms are capable of heme assimilation and heme acquisition, the cellular components required for these processes are not well understood. In order to understand the mechanism of heme uptake in eukaryotes, several organisms like *Schizosaccharomyces pombe* and *Candida albicans* have been utilized. For *S. Pombe* two iron acquisition pathways have been previously described[38]: one being a high affinity iron uptake complex composed of a ferrireductase and a ferroxidase-permease[39] and the second consisting of the generation and uptake of siderophores[40]. Through the use of genome-wide studies and transcript levels under conditions of

iron depletion or repletion, specific genes responsible for heme uptake on *S. pombe* have been identified. Two iron regulated plasma membrane proteins known as Shu1 and Str3 were identified to transport heme into the yeast cell under iron starvation conditions[41, 42]. Shu1 is a 25 kDa GPI anchored transporter in which utilization of exogenous heme is dependent on the vacuolar transporter Abc3 and has a heme affinity of 2.2 μM[41, 43]. Str3 is a 12 transmembrane domain containing protein from the major facilitator superfamily (MFS) of transporters that was discovered to uptake heme in a Shu1 deficient cell[42]. These two proteins work by tuning their expression in an iron depending manner in which Str3 has a lower affinity to heme than Shu1 but is only expressed under high iron concentrations while the high affinity transporter Shu1 is expressed under low iron concentration. This data is very interesting since it demonstrate how tightly regulated heme uptake and heme concentration are since the cell tunes the expression of different affinity transporters depending on exogenous heme concentrations.

In the case of the fungal pathogen *C. albicans* it can utilize heme and hemoglobin as the sole iron source through their recognition and binding to cell surface receptors and consequently transferred across the cell wall for endocytosis at the inner membrane. Rbt5, Rbt51 and Pga7 are *C. albicans* heme and hemoglobin (Hb) binding proteins that are GPI anchored within the cell wall and required in heme uptake by either binding heme or Hb[44-46]. The pathway of heme-iron utilization is through the recognition of heme or Hb by Rbt5 localized in the extracellular part of the cell membrane and then it gets transferred to the Pga7, due to the higher heme affinity, that will eventually get endocytosed, degraded by the heme oxygenase and made iron available by the vacuole iron permease[44]. Since proteins involved in the endosomal sorting complex required for transport (ESCRT) are necessary for the heme uptake in *C. albicans*, it is believed the transfer across the plasma membrane is through endocytosis[46].

1.4 Genetically Encoded Fluorescent Heme Sensors (HS1)

One of the reasons for the poor understanding of heme trafficking and the factors that regulate subcellular heme pools is that, until recently, there were no tools available to probe labile heme. In order to probe heme homeostasis, the Reddi lab developed a genetically encoded ratiometric fluorescent heme sensor and expressed it in the model unicellular eukaryote, *Saccharomyces cerevisiae.* The heme sensor, referred to as HS1, is a tri-domain chimeric protein consisting of a heme binding domain, cytochrome b_{562} (Cyt b_{562}), fused to a pair of fluorescent proteins, eGFP and mKATE2 (**Figure 1.4**). The fluorescence of eGFP is quenched by heme through a fluorescence resonance energy transfer (FRET) mechanism **(Figure 1.5a)**. On the other hand, mKATE2 is not a good FRET acceptor of heme, making mKATE2 fluorescence relatively unaffected by heme binding **(Figure 1.5b).** Thus, HS1 is designed to act as an excitation-emission ratiomentric probe in which the ratio of heme sensitive eGFP fluorescence to heme insensitive mKATE2 fluorescence provides a readout of cellular heme independently of sensor concentration[3] (**Figure 1.5c and d**).

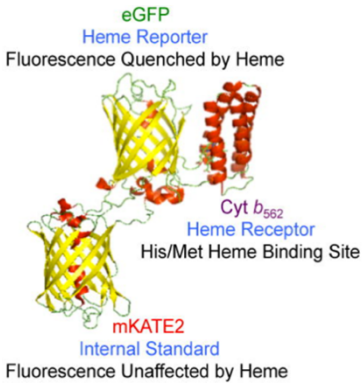

Figure 1.4 - Model of HS1 is derived from the X-ray structures of mKATE (PDB: 3BXB) and CG6 (PDB: 3U8P). Figure adapted with permission from: Hanna et al. (2016) *Proc Natl Acad Sci USA* ***113****(27):7539-7544.*

HS1 binds heme using His_{102} and Met_7 of the Cyt b_{562} binding domain to coordinate the heme iron atom. Previous experiments in the lab found that HS1 has very high affinities for ferrous and ferric heme, sub-nanomolar heme dissociation constants, and is 100% saturated with heme in

cells[3]. The most optimal poise for a sensor is to be ~50% bound so as to best monitor both increases and decreases in analyte. In order to address this, the Reddi lab has also engineered a large library of primary binding site mutants of HS1 that have varying heme affinities. One such variant, HS1-M7A, which has Met_7 mutated to Ala, is ~20-50% bound[3]. As seen in **Figure 1.5,** HS1-M7A is selective for ferrous heme over ferric heme, exhibiting ferric and ferrous heme dissociation constants of 2 uM and 25 nM, respectively[3]. Thus, HS1-M7A is poised to monitor labile ferrous heme in cells[3]. In order to measure heme distribution in other compartments, the HS1 and HS1-M7A sensors were targeted to the mitochondria and the nucleus by attaching localization sequences such as N-terminal COX4 mitochondrial matrix for the mitochondria and a C-terminal SV40 for the nucleus.

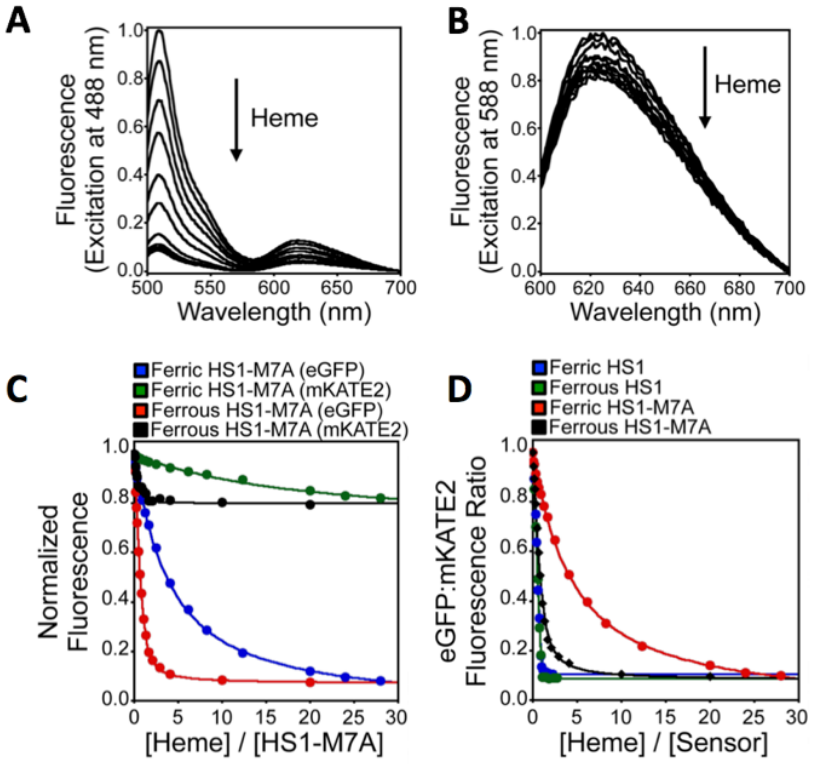

Figure 1.5 - Validation of the sensor. **A**. eGFP signal for an in vitro heme titration of the sensor showing that is getting quenched with the addition of heme. **B**. The mKATE2 signal for the in vitro heme titration of the sensor showing that is independent of heme binding. **C**. Sensor titration with ferrous and ferric heme showing the sensor binds better to ferrous heme. **D**. Change in eGFP: mKATE2 fluorescence ratios for HS1 and HS1-M7A. Figure adapted with permission from: Hanna et al. (2016) *Proc Natl Acad Sci USA* ***113****(27):7539-7544.*

1.5 Conclusions and Scope of Thesis

In the past, heme was viewed as a static cofactor that was tightly bound and buried in heme enzymes. But thanks to the development of new tools to measure and image heme and their ability to be integrated with biochemical, cell biological and genetic approaches revealed heme to be a very dynamic signaling molecule that can be mobilized to elicit adaptations to various stimuli. Our discovery of the existence of a labile heme pool invalidated the idea that heme is made on demand and any excess is degraded. However, the existence of this labile heme pool raised even more questions regarding how cells manage heme. What are the factors that transport, traffic, and mobilize labile heme for heme dependent functions throughout the cell? Overall, this thesis is focused on integrating genetically encoded heme sensors with yeast molecular genetics in order to elucidate novel heme trafficking pathways. In particular, our focus was to identify factors that regulate: **a.** steady-state cytosolic heme availability, **b.** the inter-compartmental distribution dynamics as heme is being synthesized in the mitochondria, **c.** and heme uptake and utilization from exogenous heme sources. Altogether, our work has revealed a host of proteins and pathways previously not known to regulate heme trafficking.

CHAPTER 2. GENOME-WIDE DETERMINANTS OF HEME HOMESTASIS

2.1 Introduction

Heme is an essential protein cofactor and the most abundant form of iron in mammals due to the fundamental need in hemoglobin for oxygen binding and transport. From the 3 to 4 grams of total iron typically found in the human body, 95% is in the heme iron form[47]. Although essential for life, heme may also act as a toxin, necessitating that cells carefully handle this compound[2, 4]. The hydrophobicity and redox activity of heme causes it to disrupt membrane structure, become misincorporated into certain proteins, and deleteriously oxidize various biomolecules[2, 4]. Due to these qualities, heme concentration and mobilization from its site of synthesis in the mitochondria to hemoproteins present in virtually every subcellular compartment need to be carefully regulated. However, the mechanisms governing the mobilization of heme out of the mitochondria, and the spatio-temporal dynamics of these processes, are poorly understood. Additionally, only a handful of factors have been found to regulate inter- and intra-cellular heme concentrations.

The two main processes that are thought to prevent heme toxicity and regulate heme concentration in the cell are heme biosynthesis and degradation[48]. These two mechanisms are very well studied and understood; it is known heme biosynthesis occurs between the cytosol and the mitochondria in which eight heme biosynthetic proteins facilitate this process and have been very well characterized[13]. Heme is enzymatically degraded by heme oxygenase (HO), which converts heme into biliverdin, carbon monoxide (CO) and free iron[1, 4, 14]. The free iron released by heme catabolism is detoxified by the iron storage protein ferritin.[9] Reduced glutathione (GSH) is capable

of non-enzymatically degrading heme. Heme can also be detoxified through scavenging systems such as hemopexin and albumin[9].

Based on their interactions with hemin-agarose or blue sepharose, a number of heme-binding proteins have been identified and proposed to have a role for heme homeostasis, such as heme binding proteins HBP22[32] and HBP23[33], glutathione S-transferase (GSH-S transferase)[34], HBP-1 (also known as SOUL)[35] and fatty acid binding protein (FABS)[36]. Even though these proteins have been suggested to play a role in heme homeostasis based on their ability to bind heme *in vitro*, there is currently no *in vivo* evidence for their roles in regulating heme trafficking and availability. Herein, we utilized genetically encoded heme sensors to identify new heme homeostatic factors from genome wide screens in *Saccharomyces cerevisiae* (Baker's yeast).

There are several qualities that make *Saccharomyces cerevisiae* (Baker's yeast) the perfect model organism for investigating heme trafficking. Being a single-cell eukaryote, it is inexpensive and fast to culture and shares many of the same metabolic pathways as higher eukaryotes. Importantly, given that transition metal trafficking and heme synthesis and degradation are highly conserved, it is very likely that factors governing heme trafficking and availability in yeast will also be conserved in higher organisms. Since Baker's yeast is a very well-studied and genetically tractable model organism, it is amenable for genome-wide screening. *S. cerevisiae* has ~6,000 genes and approximately 5,000 deletion mutants are viable and commercially available in a haploid yeast gene deletion collection.

Herein, we described a genome-wide screen for heme availability using genetically encoded fluorescent heme sensor in combination with the commercially available yeast knockout library in order to identify new regulators of heme synthesis and degradation, as well as factors that regulate heme trafficking and distribution. Of the 5154 deletion mutants in the yeast haploid knockout

collection we were able to transform and stably express the heme sensor in 4470 deletion mutants. The screen identified 114 strains with a Z-score of +1.5 or higher, indicating that these strains had high cytosolic heme availability and 323 strains with a Z-score of -1.5 or lower, indicating low cytosolic heme availability. Functional groups like ESCRT proteins and vesicular trafficking proteins were identified to have an important role in heme homeostasis and distribution.

2.2 Results

2.2.1 Development of High Through-put Screen for Cytosolic Heme Availability

The commercially available yeast deletion collection was transformed in masse with genetically encoded fluorescent heme sensors using a liquid handling robotics system. Deletion mutants with altered heme availability as measured by the sensors will reveal factors regulating heme trafficking and distribution, as well as novel regulators of heme synthesis and degradation. When using sensors to measure analytes like heme, it is very important to take into consideration the binding affinities of the probe and the concentration of the analyte. For accurate measurements of increases and decreases of a specific analyte, the dissociation constant K_d of the probe must be similar to the concentration of the analyte to ensure the probe is 50% bound[2]. To address this concern, we utilized a moderate affinity heme sensor, HS1-M7A, that is 30-50% bound with heme in the cytosol, ensuring that we can optimally monitor both increases and decreases heme.

5,154 of the ~6,000 genes in the *S. cerevisiae* genome can be individually deleted are available in the yeast knockout collection. Through the use of a high through-put transformation protocol employing lithium acetate[49, 50], we were able to stably express the cytosolic heme sensor in 4,470 deletion mutants. In order to identify genes presenting a disruption in cytosolic labile heme availability, we screened these 4,470 deletion mutants for alterations in the fluorescence of HS1-M7A in the cytosol. The heme sensor is designed as an excitation-emission ratiometric probe

in which the ratio of heme-sensitive eGFP fluorescence to heme-insensitive mKATE2 fluorescence provides a readout of cytosolic heme independent of sensor concentration[3]. The sensor ratios from the deletion mutants were z-scored, (**Figure 2.1a**), with a positive z-score indicating an increase in heme availability and a negative z-score indicating a decrease in heme availability.

Figure 2.1a highlights the distribution in z-scores from the deletion screen. For reference, WT yeast exhibit a z-score close to 0, indicating that it has an amount of heme that is on par with the average amount of heme in a typical mutant. Heme deficient *hem1*Δ cells, which lack the first enzyme in the heme biosynthetic pathway, exhibit a z-score < - 1.5. From this screen, we were able to identify 114 strains with a z-score of +1.5 or higher and 323 strains with a z-score of -1.5 or lower. The mutants identified to have altered heme availability could be regulators of heme trafficking, synthesis, or degradation, directly traffic heme, e.g. heme chaperones or buffering factors, or transport heme into or out of the cytosol. We are now just beginning to uncover the roles of these newly identified mutants in heme homeostasis.

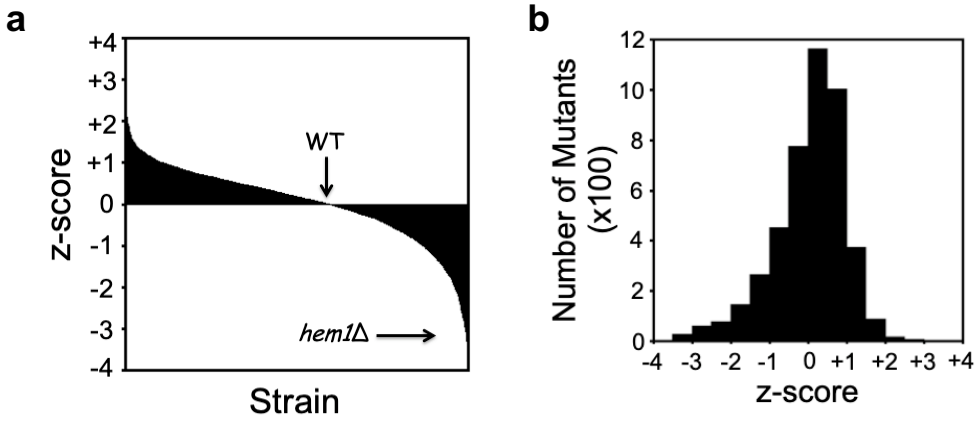

Figure 2.1 – Genome-wide high through-put screen data for endogenous heme availability. **a**. Z-scores were calculated from the fluorescence ratios eGFP/mKATE2 expressed on the mutants on which positive Z-score indicate high cytosolic labile heme and negative Z-scores indicate low cytosolic labile heme. **b.** To calculate the Z-score sensor ratios on the pates were average and the sensor ratio of the mutant was subtracted and divided by the standard deviation of the plate. Data was calculated from duplicated samples.

2.2.2 Deletion Mutants with High Cytosolic Heme

114 deletion strains displayed a z-score of +1.5 or higher. One deletion mutant that we identified was *tdh3*Δ, which lacks the major isoform of glyceraldehyde phosphate dehydrogenase (GAPDH). We will discuss this mutant in greater detail in Chapter 3, where we describe a new role for GAPDH in heme trafficking and buffering. Beyond *tdh3*Δ, we sought to determine if there were any common patterns in the localization or function of the genes identified that negatively regulate heme homeostasis. (**Figure 2.2**) In order to identify if there was any organelle prioritization by these genes, the list of 114 genes were analyzed using PANTHER (http://www.pantherdb.org/), which is a publicly available web-based resources that conducts gene ontology analysis. Locales that are enriched in the dataset of mutants with increased heme include non-membrane bounded organelles, the cytosol, and the ribosome.

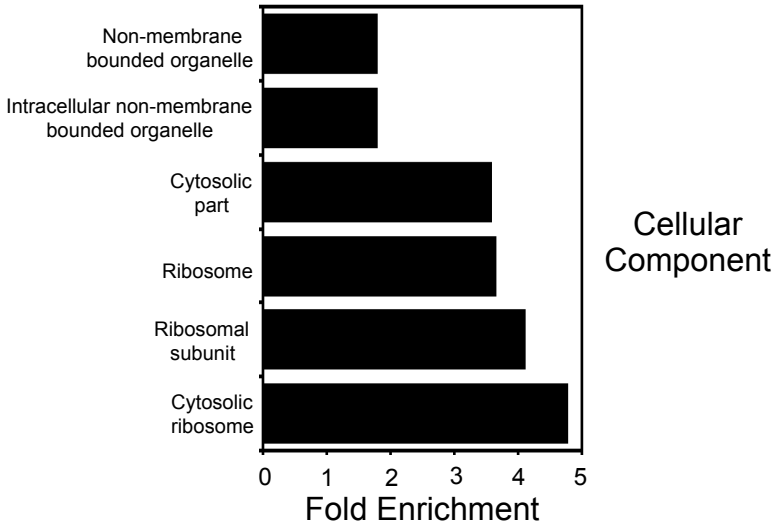

Figure 2.2 – Cellular component enrichment for high cytosolic labile heme deletion mutants. Genes were submitted to the data base PANTHER (protein analysis through evolutionary relationship) in order to predict compartmental protein association networks. The enrichment is base of the number of genes coming out from a certain compartment in comparison to the number of possible ones.

We next assessed the biological function of these genes in order to determine if there were common pathways that might regulate heme availability. Using PANTHER, we identified that the most enriched functions were translation factors (23 genes), peptide metabolic processes (20

genes), protein complex disassembly (12 genes) and amide metabolic process (23 genes). (**Figure 2.3**) ~18 uncharacterized genes were also identified to be important for maintaining heme homeostasis, raising the opportunity to discover novel roles for these proteins.

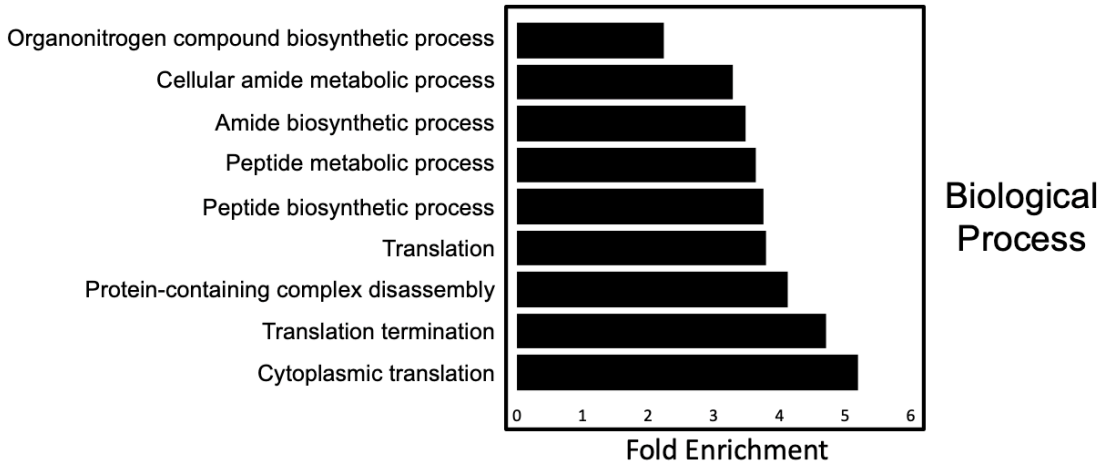

Figure 2.3 – Biological process enrichment for high cytosolic labile heme deletion mutants. Genes were submitted to the data base PANTHER (protein analysis through evolutionary relationship) in order to predict functional protein association networks. The enrichment is base of the number of genes coming out from a certain process or function in comparison to the number of possible ones.

The main pathway represented in mutants with increased heme is protein translation. We also identified cell division (11 genes) and proteins involved in cytoskeleton structure (4 genes). The screen identified 5 transporters (VBA5, TPO1, SMF2, VNX1 and ACB1) that have not previously been reported to mobilize heme. Further work on these transporters may reveal new functions in heme transport. In terms of heme chaperones or buffering factors, we were able to identify glyceraldehyde 3-phosphate dehydrogenase as a heme buffering factors in which further characterization is described in Chapter 3. Identification of more heme chaperones or buffering factors could be facilitated by classifying this group of genes by their abundance, solubility, molecular weight and localization and further characterize targeted genes.

In summary, we were able to utilize the heme sensors to identify 114 deletion mutants with higher cytosolic heme availability. In Chapter 3, we discuss a novel role for GAPDH, a glycolytic

protein, in heme trafficking and buffering. However, this is just the tip of the ice berg. Our lab is now working to determine how the transporters, translation factors, and cell division works to alter labile heme.

2.2.3 Deletion Mutants with Low Cytosolic Heme

We identified 323 deletion mutants with low cytosolic heme (z-score < -1.5). In order to determine if these genes were predominantly present in a specific organelle, analysis of these genes using PANTHER revealed that most of the mutants identified are associated with the endosomal sorting complex required for transport (ESCRT), endosomal membranes, and intracellular vesicles (**Figure 2.4**).

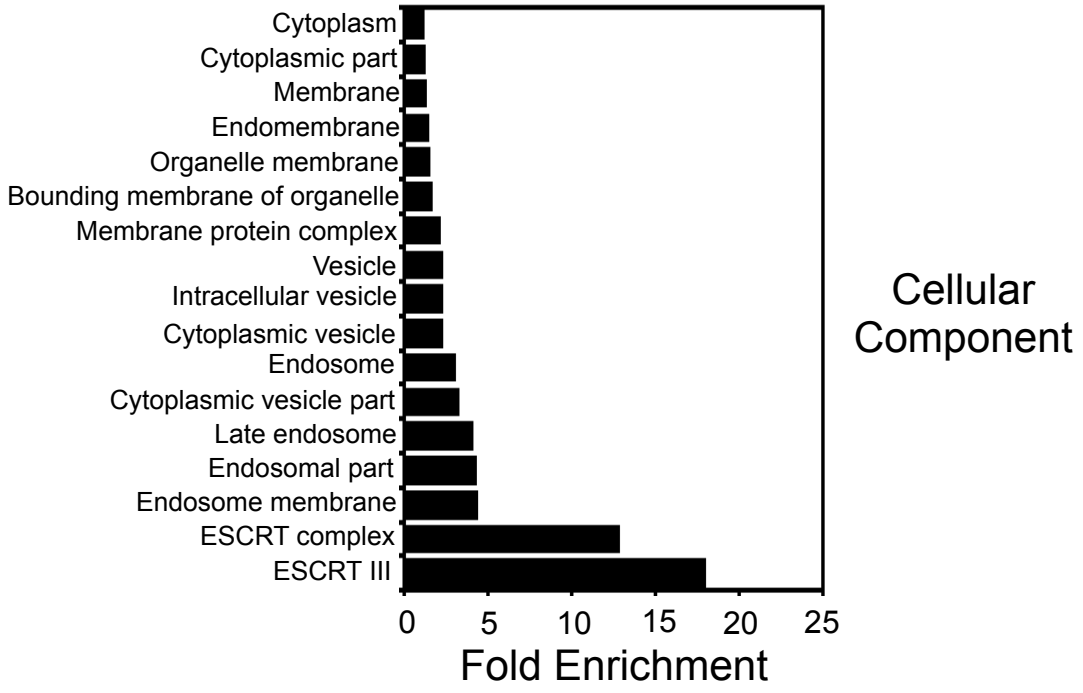

Figure 2.4 - Cellular component enrichment for low cytosolic labile heme deletion mutants. Genes were submitted to the data base PANTHER (protein analysis through evolutionary relationship) in order to predict compartmental protein association networks. The enrichment is base of the number of genes coming out from a certain compartment in comparison to the number of possible ones.

In terms of biological function, we find that there is considerable enrichment of factors that regulate vesicle formation and proteins involved with the ESCRT complex and endosomal transport. In addition, 20 genes were identified as having roles in ion transport, nucleotide mobilization, carbohydrate derivative transport, ATP transport and vacuole transport. (**Figure 2.5**) Further, a large number of metabolic enzymes, including hydrolases, isomerases, ligases, oxidoreductases, proteases, and transferases also deplete cytosolic heme when deleted, most excitingly, 50 uncharacterized genes were identified as having low heme availability, raising the possibility that we have discovered novel heme homeostatic factors.

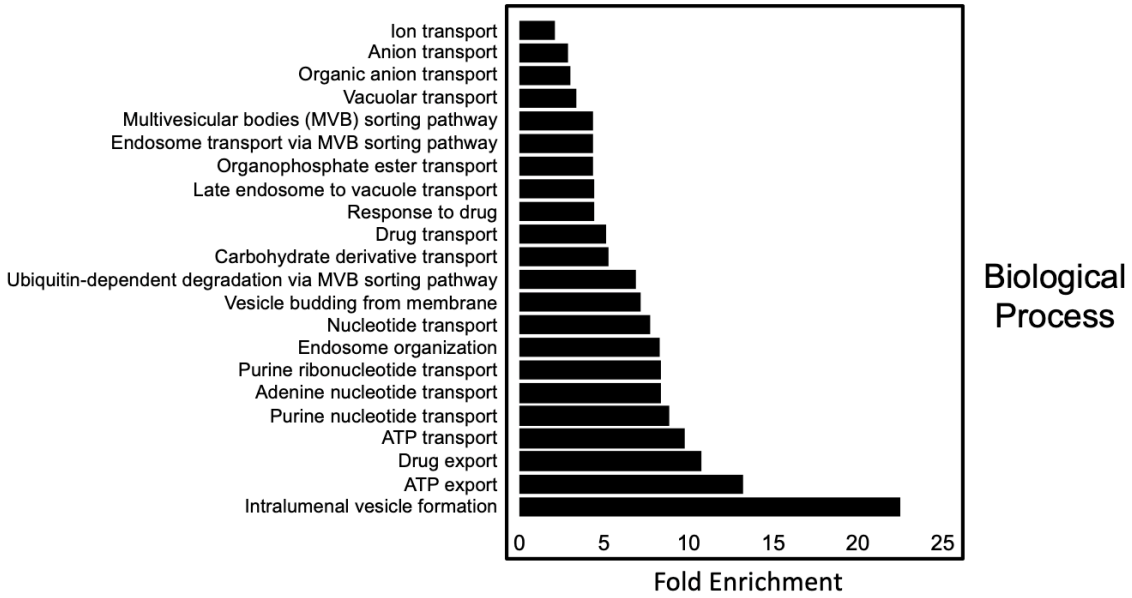

Figure 2.5 – Biological process enrichment for low cytosolic labile heme deletion mutants. Genes were submitted to the data base PANTHER (protein analysis through evolutionary relationship) in order to predict functional protein association networks. The enrichment is base of the number of genes coming out from a certain process or function in comparison to the number of possible ones.

A large numer of mutants expected to have defects in heme synthesis were also identified in our screen, thereby validating our approach to use genetically encoded heme sensors to fish out new heme homeostatic factors. It is known heme synthesis requires iron, succinyl-CoA, and glycine. Deletion mutants that affect availability of succinyl CoA, including mitochondrial

pyruvate transporters and pyruvate dehydrogenase, glycine, including a mitochondrial glycine transporter, and iron, including mitochondrial iron transporters and homeostatic factors all come out in our screen. In addition, factors required for the maturation of certain heme biosynthetic enzymes, such as mitochondrial FAD transporters, which is required for the heme biosynthetic enzyme porphyrinogen oxidase, and the chaperone that inserts pyridoxyl-5-phosphate into ALAS, the first enzyme in heme synthesis, also have low heme availability as expected.

We also identified copper trafficking factors, ATX1, which delivers copper to the Golgi, and CCS1, which delivers copper to the antioxidant enzyme SOD1, as having low heme. Genes encoding proteins that regulate the proteasome, a protein complex that degrades proteins, were also identified in the screen. However, the major pathway responsible for maintaining heme availability in the cytosol involves the endosomal sorting complex that facilitates the formation of multivesicular bodies, endosomes, and Golgi-vacuolar trafficking. (**Figure 2.6)**

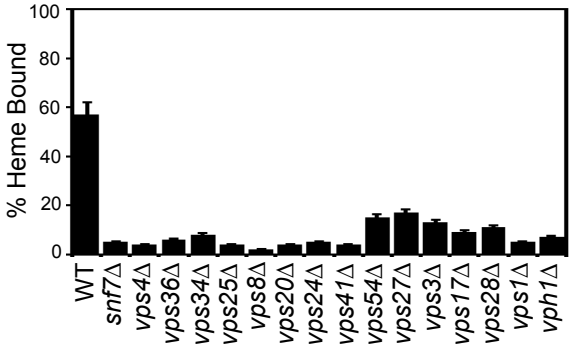

Figure 2.6 – Percent of heme bound to the sensor on low cytosolic labile heme deletion mutants related to ESCRT proteins and vacuolar function. The percent bound calculation was derived from the fluorescence ratiometric readouts of the mutant minus the Rmin (*hem1*Δ ratios) divided by Rmax (WT ratios) minus Rmin. All data represent the mean ± SD of triplicate cultures and the statistical significance was assessed using a two-sample t-test.

2.2.3.1 Validation of Genes with Low Heme Availability

We were able to identify 323 deletion mutants displaying low levels of labile heme in the cytosol from our initial screen. In order to validate these mutants as having low heme, we re-

streaked these cells to single colonies and analyzed sensor ratios from three independent clones. We selected 75 deletion mutants representing genes from unique non-redundant pathways in the initial list of 323 and verified that independent clones in these pathways did indeed have decreased heme. 87% of the deletion mutants were validated by assessing the ratio of sensor ratios between mutant and WT cells (**Table 2.1**). These genes will be further characterized in the future for their roles in heme homeostasis.

Table 2.1 - Validation screen for heme availability prioritized by Ratio of Ratios values.

Strain	Sensor Ratio	STDEV	Ratio of Ratios (Mutant/WT)
*met12*Δ	7.5	0.2	N/A
*snf7*Δ	11.2	1.1	N/A
*tmn3*Δ	16.6	6.7	3.7
*vph1*Δ	11.0	1.5	2.9
*pep12*Δ	10.8	1.2	2.8
YKL096C	13.3	3.0	2.5
*erg4*Δ	13.0	0.6	2.4
*dfg16*Δ	12.7	1.0	2.4
*aim11*Δ	12.4	2.9	2.3
*suc2*Δ	11.9	0.8	2.3
*hom6*Δ	11.7	0.6	2.2
YOR342C	7.4	1.5	2.1
YIL015C-A	6.5	0.2	2.1
*sps4*Δ	7.1	0.9	2.0

Table 2.1 (continued)

YER137C	7.0	0.3	2.0
YLR358C	10.3	0.5	2.0
*etr1*Δ	9.6	0.4	1.9
*lge1*Δ	10.2	2.1	1.9
*vps36*Δ	10.2	0.6	1.9
YIL055C	10.1	0.5	1.9
*sul1*Δ	9.9	0.6	1.9
*irc21*Δ	9.9	1.3	1.9
*tbs1*Δ	5.7	0.5	1.9
*pex8*Δ	6.7	1.2	1.9
*opt2*Δ	9.6	2.4	1.8
*aim18*Δ	6.3	0.6	1.8
*atr2*Δ	9.4	0.8	1.8
*tml25*Δ	9.3	0.7	1.8
*mak31*Δ	9.3	0.9	1.7
*ald3*Δ	9.0	0.9	1.7
*dit2*Δ	9.2	1.5	1.7
YMR181C	6.0	1.1	1.7
*hua1*Δ	9.0	0.9	1.7
*gnp1*Δ	10.4	0.1	1.7
*srl4*Δ	8.7	2.3	1.6

Table 2.1 (continued)

*pex2*Δ	5.9	0.6	1.6
*his7*Δ	8.7	1.3	1.6
*fur4*Δ	7.3	0.4	1.6
*cox15*Δ	7.1	1.1	1.6
*pdr18*Δ	8.4	2.5	1.6
YJL213W	5.5	0.8	1.6
YJL132W (Plate 44)	8.2	2.0	1.5
YOR289W	8.2	0.6	1.5
*dcv1*Δ	8.0	0.4	1.5
*pex3*Δ	8.1	1.1	1.5
*tpo3*Δ	8.5	0.9	1.5
YGR050C	7.9	0.6	1.5
YDL157C	5.3	0.5	1.5
*nst1*Δ	7.7	1.7	1.4
*oca5*Δ	9.4	0.7	1.4
YOL075C	7.4	1.5	1.4
*mcs2*Δ	7.2	1.3	1.4
*cys3*Δ	7.2	0.1	1.4
YNL097C-A	7.2	0.5	1.4
*ccs1*Δ	6.4	0.1	1.4
YBR090C	7.1	1.2	1.3

Table 2.1 (continued)

*fen2*Δ	6.0	0.2	1.3
*dif1*Δ	7.0	0.6	1.3
*dal4*Δ	7.4	0.7	1.3
*oca6*Δ	7.7	0.9	1.3
*put2*Δ	6.9	1.4	1.3
YKL075C	6.8	2.0	1.3
*mtc3*Δ	6.7	0.1	1.3
*oye3*Δ	6.7	1.4	1.3
*cox10*Δ	6.7	0.3	1.2
*ept1*Δ	6.5	0.5	1.2
YCR016W	6.3	1.0	1.2
*enb1*Δ	6.4	0.6	1.2
*sdd1*Δ	6.1	0.5	1.2
*atx1*Δ	6.0	0.5	1.1
YBR184W	3.9	1.3	1.1
*tpi1*Δ	3.9	1.7	1.1
YPR195C	3.9	0.5	1.1
YGL108C	5.2	0.3	1.0
*dia1*Δ	5.0	0.5	0.9
*cmg1*Δ	3.1	0.5	0.9

2.2.3.2 Genes that Regulate Heme Availability through Total Heme Changes

In order to differentiate between factors that affect heme biosynthesis versus bioavailability, we sought to determine if the mutants with low bioavailable heme exhibited a decrease in total heme. Towards this end, we first determined how sensitive labile heme was to total heme by measuring the effects of succinylacetone (SA), a heme synthesis inhibitor, on total heme, heme loading of the high affinity sensor HS1, and heme loading of the weaker binding HS1-M7A sensor used in the screen. In Figure 2.7a we can observe 5 μM SA is enough for the sensor fluorescence ratio of HS1-M7A to be similar to the *hem1*Δ deletion mutant that cannot make heme. The data indicate that a 15% reduction of the total heme concentration is sufficient to completely deplete heme binding to HS1-M7A. (**Figure 2.7a and 2.7b**) In the case of the tight binding sensor HS1, a 60% reduction in total heme completely depleted heme loading of HS1 (**Figure 2.7c and 2.7d**). Thus, we found that labile heme levels are exquisitely sensitive to total heme and a modest ~15% decrease in total heme can completely deplete the HS1-M7A heme sensor.

Total heme concentration was measured in 73 deletion mutants with low cytosolic labile heme. These values were then normalized to the WT heme concentration. We found that 41 of the 73 deletion mutants exhibited WT-levels of total heme, with < 15% change in total heme. (**Table 2.2**) 32 of the 73 deletion mutants with low bioavailable heme exhibited a > 15% decrease in total heme. (**Table 2.2**) Examples of mutants with unaltered total heme are the copper chaperone mutants, *ccs1*Δ and *atx1*Δ, which exhibit WT-levels of total heme, suggesting that defects in copper homoeostasis can alter labile heme levels through an unknown mechanism. (**Figure 2.8a**) Examples of mutants with lowered total heme include the heme *a* biosynthetic mutant, *cox10*Δ and *cox15*Δ, suggesting that the inability to synthesize heme *a* may negatively feedback to attenuate heme biosynthesis. (**Figure 2.8b**)

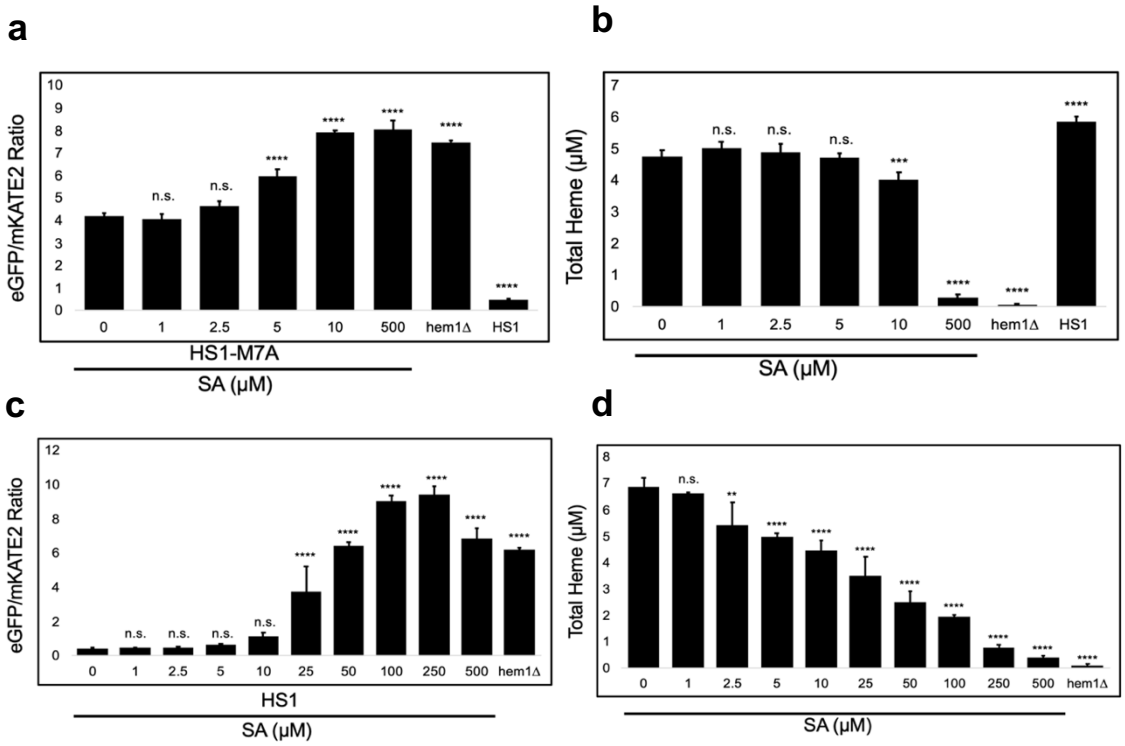

Figure 2.7 – Labile heme sensitivity to heme depletion using the heme biosynthetic inhibitor, succinylacetone (SA) and affinity variants of the heme sensor. **a**. Labile heme was measured in HS1-M7A **c**. or HS1 expressing cells cultured in SCE media for 16 hours with the indicated concentration of SA prior to measurement of the eGFP/mKATE2 fluorescence ratios. (**b**) Total heme measured in the cultures depicted in **a** or in heme deficient *hem1*Δ cells. **d**. HS1 total heme data from cultures depicted on **c**. All data represent the mean ± SD of triplicate cultures and the statistical significance was assessed using a two-sample t-test. Black asterisks represent the statistical significance by a Dunnett's multiple comparison relative to 0 μM [SA]. * $P < 0.05$, ** $P < 0.005$, *** $P < 0.001$, n.s. not significant.

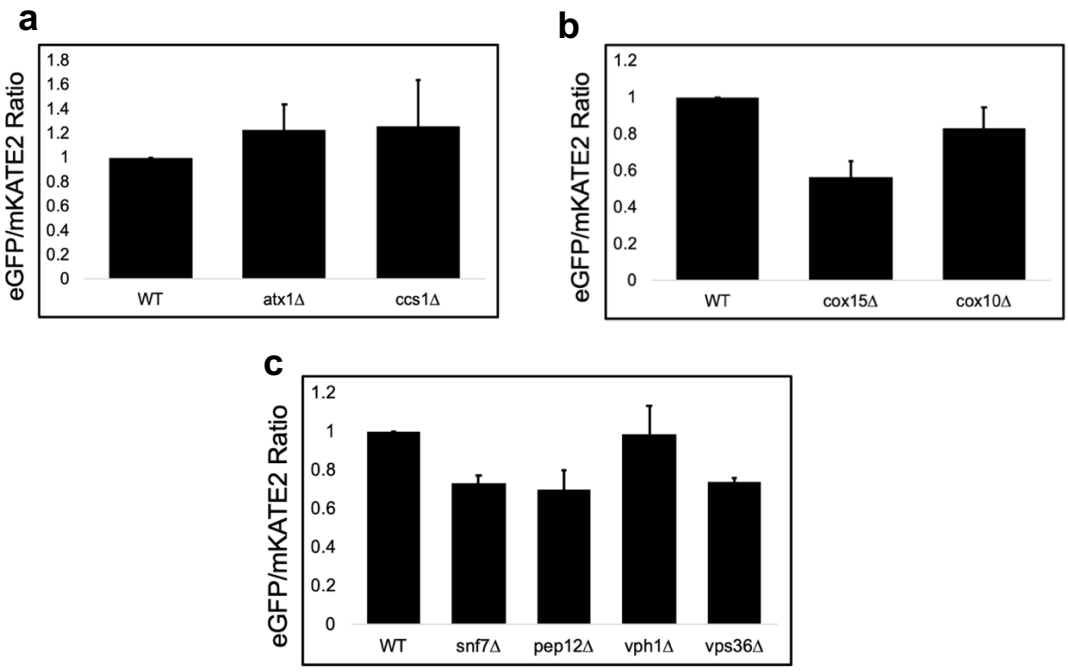

Figure 2.8 – Total heme levels of specific functional groups of deletion mutants with low cytosolic heme. Total heme concentrations were measures for a. Copper chaperones, b. heme a maturation proteins and c. vacuolar or ESCRT proteins in order to identify if they have a role in heme biosynthesis or degradation. All data represent the mean ± SD of triplicate cultures and the statistical significance was assessed using a two-sample t-test.

Table 2.2 - Total Heme measurements of low heme availability genes from the genome-wide screen.

Strain	Total Heme per cell	STDEV	Normalize to WT
*oye3*Δ	9.6E-06	7.3E-07	1.3
*ccs1*Δ	1.3E-05	4.01E-06	1.3
*pex3*Δ	1.3E-05	1.5E-06	1.2
*atx1*Δ	1.3E-05	2.2E-06	1.2
*fen2*Δ	1.3E-05	1.9E-06	1.2
*enb1*Δ	1.2E-05	2.3E-06	1.2

Table 2.2 (continued)

*nst1*Δ	1.2E-05	2.3E-06	1.2
YPR195C	9.7E-06	6.1E-07	1.2
*dfg16*Δ	8.2E-06	1.3E-06	1.2
*cmg1*Δ	9.6E-06	2.9E-07	1.1
YKL075C	1.5E-05	4.7E-06	1.1
*sdd1*Δ	1.1E-05	4.8E-07	1.1
*dia1*Δ	1.1E-05	5.6E-07	1.1
*srl4*Δ	1.1E-05	1.3E-06	1.1
*hua1*Δ	7.8E-06	1.8E-07	1.1
*erg4*Δ	1.1E-05	-1.3E-06	1.1
YKL096C	1.4E-05	4.3E-07	1.0
*tpi1*Δ	8.6E-06	3.5E-07	1.0
*oca5*Δ	7.4E-06	1.1E-06	1.0
*oca6*Δ	7.4E-06	2.4E-07	1.0
*cys3*Δ	7.6E-06	7.4E-08	1.0
YCR016W	1.4E-05	2.8E-06	1.0
*gnp1*Δ	4.7E-06	3.4E-07	1.0

Table 2.2 (continued)

*dcv1*Δ	1.0E-05	1.2E-06	1.0
*vph1*Δ	1.0E-05	1.1E-06	1.0
YBR184W	8.2E-06	3.8E-06	1.0
*put2*Δ	7.0E-06	3.8E-07	1.0
*pex2*Δ	9.8E-06	1.8E-06	1.0
YBR090C	1.3E-05	4.3E-07	1.0
*sps4*Δ	8.0E-06	1.1E-06	1.0
*aim11*Δ	9.7E-06	2.3E-07	1.0
YJL132W (Plate 44)	1.3E-05	1.9E-06	1.0
YGR050C	1.3E-05	7.9E-07	1.0
*opt2*Δ	7.0E-06	2.3E-06	0.9
*ept1*Δ	6.5E-06	4.0E-07	0.9
*lge1*Δ	9.9E-06	2.8E-07	0.9
*tml25*Δ	1.2E-05	4.1E-07	0.9
*irc21*Δ	1.2E-05	2.0E-07	0.9
YDL157C	7.4E-06	5.6E-07	0.9
*met12*Δ	8.7E-06	1.7E-07	0.9

Table 2.2 (continued)

*dit2*Δ	6.3E-06	6.0E-07	0.9
*atr2*Δ	6.3E-06	6.2E-07	0.9
YNL097C-A	9.1E-0.6	5.6E-07	0.8
*pdr18*Δ	6.0E-06	7.1E-07	0.8
*cox10*Δ	8.8E-06	1.2E-06	0.8
*ald3*Δ	6.1E-06	4.0E-07	0.8
YER137C	6.8E-06	5.7E-07	0.8
YIL055C	1.1E-05	4.5E-07	0.8
YOL075C	5.8E-06	3.0E-07	0.8
*pex8*Δ	8.0E-06	2.6E-06	0.8
*dif1*Δ	5.9E-06	6.5E-07	0.8
*sul1*Δ	5.9E-06	6.5E-07	0.8
*mcs2*Δ	5.8E-06	4.0E-07	0.8
*dal4*Δ	7.6E-06	2.2E-07	0.8
*mak31*Δ	5.4E-06	2.0E-07	0.8
YOR342C	6.3E-06	4.2E-07	0.8
*hom6*Δ	5.5E-06	2.0E-07	0.7

Table 2.2 (continued)

*vps36*Δ	7.4E-06	2.0E-07	0.7
*snf7*Δ	7.3E-06	4.6E-07	0.7
*pep12*Δ	7.4E-06	1.1E-06	0.7
YJL213W	6.8E-06	4.7E-07	0.7
*tbs1*Δ	5.6E-06	1.2E-06	0.7
*suc2*Δ	4.9E-06	6.2E-08	0.7
*aim18*Δ	6.1E-06	7.1E-08	0.6
*tpo3*Δ	2.8E-06	2.1E-07	0.6
YIL015C-A	6.0E-06	7.9E-07	0.6
YLR358C	6.0E-06	1.4E-07	0.6
*cox15*Δ	6.0E-06	9.8E-07	0.6
YOR289W	5.1E-06	1.5E-07	0.5
*tmn3*Δ	5.1E-06	1.3E-07	0.5
*his7*Δ	3.3E-06	5.5E-07	0.5
*fur4*Δ	4.5E-06	2.7E-07	0.4
YMR181C	2.8E-06	1.7E-06	0.3
*etr1*Δ	2.5E-06	8.7E-07	0.2

2.3 Discussion

Heme, which is an essential but cytotoxic cofactor, must be tightly regulated. The factors and processes involved in heme trafficking, distribution and homeostasis are not well known. Herein, we conducted a genome-wide screen in yeast to identify new heme homeostatic factors using genetically encoded heme sensors. Of the 5,000 genes available in the yeast haploid deletion library, we were able to transform and stably express the heme sensor in 4,470 genes. Of these, we identified 114 deletion mutants with a +1.5 z-score or higher, indicating high cytosolic labile heme, and 323 deletion mutants with a z-score of -1.5 or lower, indicating low cytosolic labile heme.

We observed that labile heme in WT cells was higher than in the average mutant. We believe this result indicates that deletion of a large number of pathways can indirectly affect heme synthesis or availability. Heme biosynthesis is not only regulated by the eight heme biosynthetic enzymes, in reality a multitude of factors may regulate the expression and maturation of the heme biosynthetic enzymes, as well as the concentrations of heme biosynthetic precursors. The network of proteins that directly or indirectly regulate heme synthesis is likely very substantial.

In the case of the 114 deletion mutants exhibiting high cytosolic labile heme, we observed that the majority of these genes were enriched in the cytosol. This is not surprising given that we are probing cytosolic heme. A large number of the strains with high labile heme are ribosomal protein mutants. It is possible that certain ribosomal proteins bind and buffer heme. Upon their deletion, more heme would be accessible to the heme sensor. It is intriguing to speculate that the ribosome acts as a heme sink to provide heme for hemoproteins as they are being translated. It has been reported that hemin is responsible for enhancing polyribosome stabilization and lead treatments can cause a heme inhibition resulting into disaggregation of polyribosomes following

a decreased in protein synthesis[51]. Our future work will involve determining if heme associates with ribosomes and the specific ribosomal proteins identified in our deletion screen.

Deletion mutants of certain cytoskeleton proteins were identified to exhibit an increase in heme availability. It has been previously demonstrated that heme can bind and alter the conformation of the cytoskeleton[9], as well as increase the polymerization of actin [9]. Previously a role for hemopexin in the reorganization of actin cytoskeleton specifically in podocytes was reported[52]. It was observed that WT podocytes cells reorganized the actin from a stress fiber to cytoplasmic aggregates and membrane ruffles after 30 minutes of hemopexin treatment[52]. However, it was thought to be by a nephrin dependent signaling, not necessarily by a direct interaction of heme and the cytoskeleton. It would be tempting to speculate that heme is transported along the cytoskeleton network. However, there is currently no direct evidence for this.

Deletion mutants of cell division proteins also exhibited high heme. Cell cycle regulation by heme is a topic that has been studied in HeLA cells by Weizhen Ye and Li Zhang, who demonstrated heme control of the expression of some cell cycle regulators[53]. They observed that heme synthesis inhibition with succinylacetone caused a cell cycle arrest in the S phase and that it also induced the expression of molecular markers associated with senescence and apoptosis[53]. This could suggest heme having a signaling role for triggering cell cycle progression either by direct activation of cell cycle modulators or through changes in heme concentration acting as a signaling molecule and regulating the expression of the molecular factors favoring division.

A large fraction of the 323 deletion mutants with low heme availability play a role in the ESCRT complex, vacuolar function, or Golgi-vacuolar protein trafficking via multivesicular bodies. We propose that heme could be mobilized from multivesicular bodies with the help of ESCRT proteins or possibly be sent to the vacuole where it can be transported out of. Heme could

be mobilized after its synthesis from the mitochondria to the ER or to the Golgi in order to be packaged into transport vesicles. This transport vesicle could be targeted to go to the membrane, cytosol or maybe even fuse with the early endosomes. The early endosomes could be sent to be recycled to the membrane that could transport heme into the cell membrane if necessary, but it could also merge with other early endosomes in order to form the late endosomes or multivesicular bodies. Transporters in these multivesicular bodies could mobilize heme into the cytosol, making it available for other heme buffering factors to regulate it and deliver it when necessary. These multivesicular bodies may also fuse with the vacuole /lysosome, where heme can be stored and transported out of. We are testing this hypothesis by deleting genes in the ESCRT pathway and measuring heme distribution in different organelles. (**Figure 2.9**) For example, VPH1 is a gene that displayed low labile heme but normal amount of total heme and is in responsible for the vacuolar ATPase. This gene would be a good target to test if heme is stored and trafficked from the vacuole and if vacuole function is crucial for heme distribution. We could also test proteins like Snf7, a subunit of ESCRT complex III, or Vps36, a subunit of the ESCRT complex II, or, Pep12, a target receptor for vesicular intermediates traveling between the Golgi and the vacuole. All of these experiments will reveal if vesicular sorting and ESCRT proteins are crucial for heme distribution and which step is the most important for making heme bioavailable.

The notion that heme is trafficked via endosomes is supported by a number of lines of evidence. First, work performed by Di Fiore and Di Camilli has demonstrated membrane trafficking as a potential process for regulating and distributing various signaling metabolites. [54]. In *C. elegans*, intracellular heme can be found in lysosomal related organelles that are very dynamic[55]. Zinc has also been found to be stored in and mobilized from these *C. elegans* lysosomal-related organelles. [56].

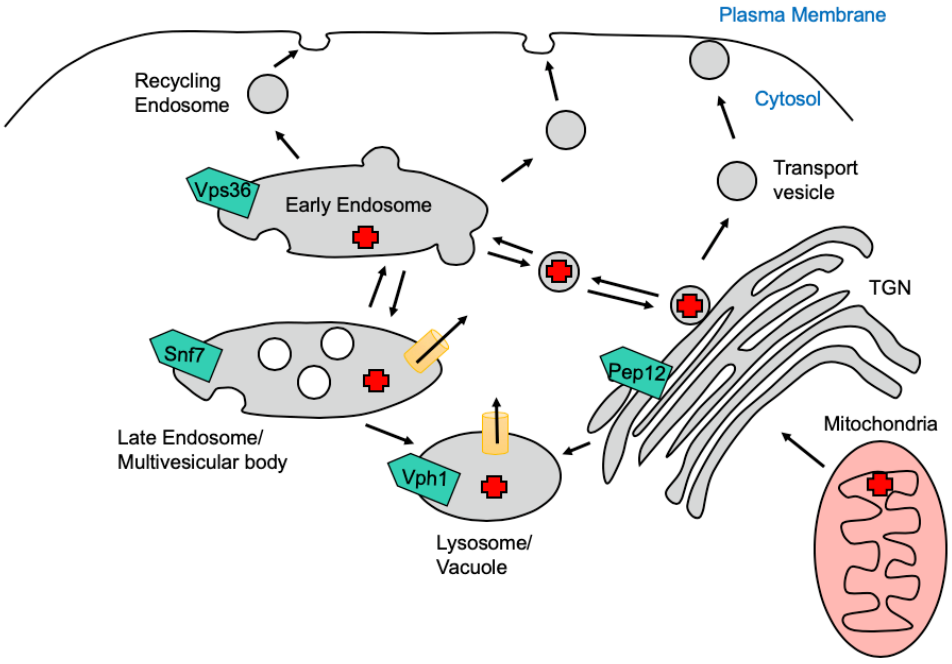

Figure 2.9 – The proposed mechanism for heme mobilization via intracellular vesicle-mediated trafficking. Endocytic pathway it displayed, in which heme could be mobilized out of the Trans-Golgi Network (TGN) facilitated by Pep12, heme could be mobilized into early endosomes in which Vps36 could be playing a role for heme mobilization. Endosomes will mature into multivesicular bodies (MVB) with Snf7 possible transporting out heme and making it bioavailable. Heme could also be mobilized to the cytosol and made bioavailable by Vph1, which is a vacuolar ATPase.

In summary, we successfully utilized genetically encoded fluorescent heme sensors to screen the yeast haploid gene deletion collection to identify genes important for heme homeostasis. We not only identified genes known to affect heme biosynthesis, as expected, but we found a large number of new genes that impact both heme synthesis and availability. Two major findings include GAPDH, which was found to buffer and traffic heme to the nucleus and is discussed in Chapter 3, and endosomal trafficking of heme. Overall, this work will help in the understanding of heme trafficking, the regulation of heme homeostasis, and identifying heme buffering elements and new heme biosynthesis and degradation factors.

2.4 Materials and Methods

2.4.1 Cell Strains, Transformation, Growth Conditions and Plasmids

2.4.1.1 Yeast Strains and Growth

S. cerevisiae strains used in this study were derived from BY4741 (MATa, *his3*Δ1, *leu2*Δ0, *met15*Δ0, *ura3*Δ0). Deletion mutant strains were obtained from the yeast gene deletion collection (Thermo Fisher Scientific). We also utilized the previously reported strain DH001b-3 (*hem1*Δ::*HIS3*)[3]. All strains derived from the yeast deletion collection were confirmed by sequencing the unique barcodes flanking the *KanMX4* deletion cassette.

2.4.1.2 Yeast Transformation

Yeast transformations were performed by the lithium acetate procedure [49]. Strains were maintained at 30° C on either enriched yeast extract (1%) - peptone (2%) based medium supplemented with 2% glucose (YPD) and G418 (200 μg/mL) or synthetic complete medium (SC) supplemented with 2% glucose and the appropriate amino acids to maintain selection[3]. Cells cultured on solid media plates were done so with YPD or SC media supplemented with 2% agar [3]. Selection for yeast strains containing the KanMX4 marker was done with YPD agar plates supplemented with G418 (200 μg/mL) [3]. Cells for the screen were resuspended in SC media supplemented with 15 mg/mL of ergosterol and 0.5% Tween-80 (SCE). All liquid cultures were maintained at 30 °C and most were done in standing cultures.

2.4.1.3 Plasmids

Cytosolic, mitochondrial, and nuclear-targeted heme sensors, HS1, were sub-cloned into pRS415 and driven by *ADH*, *TEF*, or *GPD* promoters as previously described[3]. PCR based

mutagenesis was used to generate the affinity variants of HS1 (M7A)[3]. The Hap1 reporter plasmid in which eGFP is driven by the *CYC1* promoter was also previously described [3].

2.4.2 Experimental Methods

2.4.2.1 High Through-put transformation

Yeast high through-put transformations were performed in the standard clear sterile 96 well plates and by: a. preculturing the cells in 200 µL YPD G418 (200 µg/mL) media until saturation (48 hours); b. diluted the cells in 200 µL of YPD G418 and grown for 14-16 hour at 30°C standing; c. transforming cells using the lithium acetate procedure adapted for 96 well plates[57]; d. incubating the cells with the transformation reagents for 6 hours at 42°C on the standing incubator on a Mary bath set up; e. resuspending cells in SCE media with the appropriate amino acids to maintain selection[3]. Plates were incubated for 96 hours and then diluted in fresh SCE media supplemented with the appropriate amino acids to confirm and maintain selection until saturation (48 hours.).

2.4.2.2 High Through-put Screen

Cytosolic HS1-M7A expressing cells were cultured in standard clear sterile 96 well plates. Duplicate cultures were seeded in 200 µLof SCE media with the appropriate amino acids to maintain selection[3] standing until saturation (48 hours.). The cells were diluted into 200 µL SCE-LEU and grown standing for 14-16 hours at 30°C. After culturing cells were harvested, washed twice in 200 µL of sterile ultrapure water and finally resuspended in 200 µL of 1x PBS. HS1-M7A fluorescence was monitored on 200 uL of a 4 OD/mL (2 x 10^7 cells/mL) cell suspension using black Greiner Bio-one flat bottom fluorescence plates and a Synergy Mx multi-modal plate reader. eGFP (ex. 488 nm, em. 510 nm) and mKATE2 (ex. 588 nm, em. 620 nm) fluorescence was recorded every 30 seconds for 5 min. Z-scores values were calculated by subtracting the sensor

fluorescence ratio for a given strain screened to the average sensor fluorescence ratio of the all samples screened in the plate and dividing it by the STDEV of the sensor fluorescence ratio of all the strains screened in the plate.

2.4.2.3 Total heme quantification

Measurements of total heme were accomplished using a fluorimetric assay designed to measure the fluorescence of protoporphyrin IX upon the release of iron from heme as previously described [58]. For all total heme measurements, ~1 x 10^8 cells were harvested, washed in sterile ultrapure water, and resuspended in 500 µL of 20 mM oxalic acid and stored in a closed box at 4 °C overnight (16-18 hours). Next, an equal volume (500 µL) of 2 M oxalic acid was added to the cell suspensions in 20 mM oxalic acid. The samples were split, with half the cell suspension transferred to a heat block set at 95 °C and heated for 30 minutes and the other half of the cell suspension kept at room temperature (~25 °C) for 30 minutes. All suspensions were centrifuged for 2 minutes on a table-top microfuge at 21000 x g and the porphyrin fluorescence (ex: 400 nm, em: 620 nm) of 200 µL of each sample was recorded on a Synergy Mx multi-modal plate reader using black Greiner Bio-one flat bottom fluorescence plates. Heme concentrations were calculated from a standard curve prepared by diluting 500-1500 µM hemin chloride stock solutions in 0.1 M NaOH into ultrapure water, which was then added back to extra cell samples as prepared above. In order to calculate heme concentrations, the fluorescence of the unboiled sample (taken to be the background level of protoporphyrin IX) is subtracted from the fluorescence of the boiled sample (taken to be the free base porphyrin generated upon the release of heme iron). The cellular concentration of heme is determined by dividing the moles of heme determined in this fluorescence assay and dividing by the number of cells analyzed, giving moles of heme per cell, and then converting to a cellular concentration by dividing by the volume of a yeast cell, taken to be 50 fL [3].

CHAPTER 3. GLYCERALDEHYDE 3-PHOSPHATE DEHYDROGENASE (GAPDH) AS A HEME BUFFERING FACTOR

3.1 Thesis Attributions Statement for Chapter 3.

Portions of this chapter are adapted from previously published work: "David A. Hanna; Raven M. Harvey; Osiris Martinez-Guzman; Xiaojing Yuan; Bindu Chandrasekharan; Gheevarghese Raju; F. Wayne Outten; Iqbal Hamza; and Amit R. Reddi. 'Heme Dynamics and Trafficking Factors Revealed by Genetically Encoded Fluorescent Heme Sensors. Proc Natl Acad Sci, 2016;113:7539-7544.'" And also work from: "Elizabeth A. Sweeny; Anuradha Bharara Singh; Ritu Chakravarti; Osiris Martinez-Guzman; Arushi Saini; Mohammad Mahfuzul Haque; Greer Garee; Pablo D. Dans; Luciana Hannibal; Amit R. Reddi; and Dennis J. Stuehr. "Glyceraldehyde-3-phosphate dehydrogenase is a chaperone that allocates labile heme in cells." Journal of Biological Chemistry 293(37): 14557-14568."

3.2 Introduction

Heme is an incredibly important metallonutrient for many essential biological functions, but very little is known about the proteins involved in its trafficking and homeostasis. As mentioned in Chapter 2, glyceraldehyde 3-phosphate dehydrogenase (GAPDH) was identified as a possible heme trafficking factor in a genome wide screen for cytosolic heme availability using genetically encoded fluorescent heme sensors. GAPDH is a member of the dehydrogenase enzyme family and an essential protein for glucose metabolism. GAPDH catalyzes the conversion of glyceraldehyde-3-phosphate to 1,3 bis-phosphoglycerate, the sixth step on glycolysis. This glycolytic enzyme is ubiquitously expressed comprising around 10-20% of the total cellular protein content[59], and is localized in different organelles such as the cytoplasm, mitochondria, nucleus lipid particles and

cell wall. GAPDH, which has a molecular mass of 37 kDa, is most typically a homotetramer, but can also be found as a monomer or dimer. [60, 61] Interestingly, the monomeric form is localized to the nucleus during cell proliferation[62, 63]. *Saccharomyces cerevisiae* encodes three isoforms of GAPDH: *TDH1*, *TDH2*, and *TDH3*. These isoforms are very similar in sequence and structure[64, 65]. Tdh2p and Tdh3p are expressed mainly during exponential growth, whereas Tdh1p is primarily expressed during stationary growth phase[66].

In addition to its role in glycolysis, GAPDH is known to have non-canonical roles in transcriptional activation by binding to DNA and RNA[59, 67-69], regulating apoptosis[70], catalyzing microtubule formation and polymerization[71-73], NO sensing[74, 75] and facilitating vesicular transport between the ER and Golgi[76]. Post-translational modification of GAPDH may play a critical role in regulating its diverse functions. For example, in the cytosol of human monocytes, it has been observed that a S-thiolation of the reactive sulfhydryl groups on GAPDH can facilitate a metabolic shift from anaerobic respiration to the pentose phosphate pathway[77]. Another reversible modification in GAPDH is the S-nitrosylation, in which the addition of the nitric oxide (NO) group to the thiol side chain of cysteine regulates the activity of this protein. [78, 79]. Irreversible posttranslational modifications, e.g. sulfonation, mobilizes GAPDH from the cytosol to other cellular compartments for signaling purposes[80].

Previously, GAPDH from macrophages was proposed to be a heme binding protein on the basis of its interactions with hemin-agarose [81]. They proposed GAPDH was able to control the activation of inducible NO synthase (iNOS) by regulating heme insertion in a NO-sensitive manner[81]. They observed that a GAPDH deficient cell was incapable of heme insertion into the iNOS and exposure to NO, which causes S-nitrosylation of GAPDH, inhibits glycolytic activity and heme binding[81]. Is GAPDH truly a heme binding protein? What role does GAPDH play in

heme homeostasis? Does GAPDH have a role for heme allocation in the cell? What is the affinity for heme? What are the heme binding residues of GAPDH?

In order to provide some answers to these questions, we decided to screen the three isoforms of GAPDH in *S. cerevisiae* and measure heme availability using genetically encoded fluorescent heme sensors. We also wanted to measure how heme distribution was affected upon the deletion of this glycolytic protein through activity measurement of heme dependent processes in different organellar compartments. By integrating our heme sensors with genetic screens, we found that the glycolytic enzyme glyceraldehyde phosphate dehydrogenase (GAPDH) is responsible for buffering intracellular heme and regulating the activity of the nuclear heme-dependent transcription factor heme activator protein (Hap1p). Additionally, the His53 for hGAPDH and His51in yeast GAPDH were identified as the residues crucial for heme binding and delivery to transcription factors such as Hap1.

3.3 Results

3.3.1 GAPDH Regulates Cytosolic Heme Availability

In order to identify genes that regulate LH, we transformed the cytosolic HS1-M7A into the yeast knockout collection and screened for mutants that exhibited altered sensor fluorescence ratios. After partial screening, we identified TDH3, which encodes an isoform of the glycolytic enzyme GAPDH, to be a determinant of LH. We observed that only the *tdh3*Δ mutant, but not *tdh1*Δ or *tdh2*Δ mutants, increases cytosolic labile heme as measured by HS1-M7A (**Figure 3.1A**). In-situ calibration of the sensors as described previously indicates that labile heme levels increase from ~20 nM to ~60 nM upon deletion of *TDH3.* These results suggest that the GAPDH isoform Tdh3p, buffers intracellular heme. Quantification of total heme was done on all of the GAPDH isoforms to determine if the changes in labile heme were due to a disruption in heme biosynthesis.

Acid-acetone extraction of heme from cells and heme quantification using High-Performance Liquid Chromatography (HPLC) revealed that total heme levels are not affected by deletion of GAPDH isoforms (**Figure 3.1B**). These data suggest that Tdh3p regulates bioavailable heme pools, not total heme.

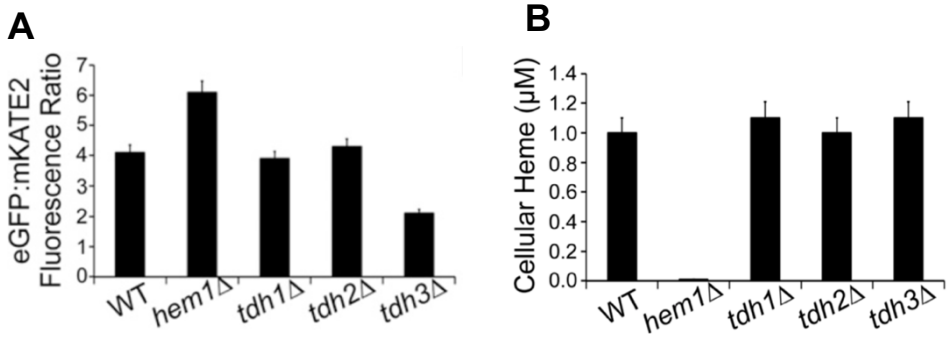

Figure 3.1- Tdh3p regulates intracellular heme availability. (**A**) Fluorimetric determination of EGFP/mKATE2 fluorescence ratios of the indicated yeast strains expressing HS1-M7A. (**B**) Total heme levels of the indicated strains as determined by HPLC. Figure adapted with permission from: Hanna et al. (2016) Proc Natl Acad Sci USA **113**(27):7539-7544.

3.3.2 Expression of GAPDH isoforms

Why is the effect of GAPDH on labile heme specific for Tdh3p? In fact, Tdh1p and Tdh2p share > 95% sequence identity with Tdh3p. In order to test the contribution of each isoform to the total GAPDH pool, we immunoblotted for GAPDH in WT, *tdh1*Δ, *tdh2*Δ, and *tdh3*Δ cells. The results from the western blot suggest that the Tdh3p isoform is the primary contributor toward total GAPDH (**Figure 3.2**). These results explain the Tdh3p-specific effect on labile heme, namely that Tdh3p is the primary isoform present under the conditions of the experiment.

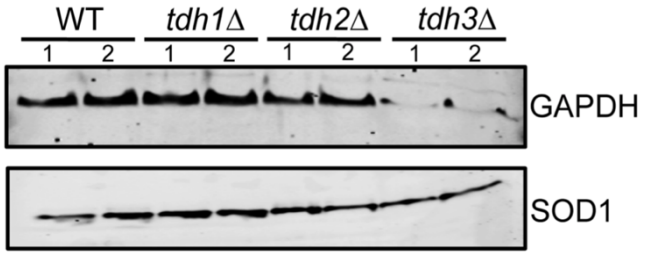

Figure 3.2 - Immunoblot analysis of GAPDH and SOD1 (loading control) for the three isoforms of GAPDH in yeast. Figure adapted with permission from: Hanna et al. (2016) Proc Natl Acad Sci USA **113**(27):7539-7544.

3.3.3 Heme Dependent Processes in a GAPDH Deficient Mutant

Previously it was described how the glycolytic enzyme glyceraldehyde phosphate dehydrogenase (GAPDH) constitutes a major cellular heme buffer without affecting total heme levels. It is also very well-known that heme is involved in many biological functions like oxygen transfer, catalysis, electron transfer, energy metabolism, apoptosis, cell proliferation and gene expression[5, 82]. In order to characterize the role of GAPDH in heme homeostasis and the effect Tdh3p deletion has on the heme pool in other organelles, we decided to test the activity of several heme dependent processes. For example, cytosolic catalase (Ctt1p) activity provides an indicator of cytosolic heme homeostasis. The activity of the nuclear transcription factor heme activator protein, Hap1p, provides an indicator of nuclear heme homeostasis.

3.3.3.1 Catalase Activity in a *tdh3*Δ

Catalase is a tetrameric enzyme that catalyzes the decomposition of hydrogen peroxide to water and oxygen. It requires four heme molecules, or one heme per monomer, in order to be active. A colorimetric assay for catalase was employed that exploits the ability of heme bound catalase to catalyze the peroxide-dependent oxidation of dopamine, which turns purple[83]. The amount of purple coloration reports on how active the protein is. Since *tdh3*Δ cells exhibit a defect in cytosolic labile heme levels, we probed the activity of the cytosolic catalase activity, Ctt1p. The *tdh3*Δ mutant did not display any disruption in catalase activity in comparison to the WT strain (**Figure 3.3**).

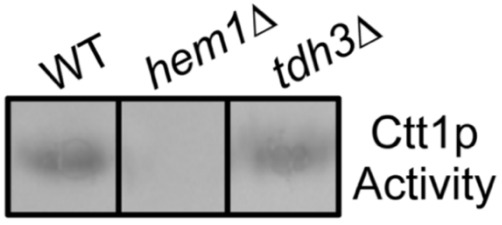

Figure 3.3 – Tdh3 deficient mutant displayed normal amounts of catalase activity. In-gel activity assay for cytosolic catalase, Ctt1p, in the indicated strains. Cells were grown to mid-log phase in YPDE. Immunoblots and catalase activity are representative of two independent trials. Figure adapted with permission from: Hanna et al. (2016) Proc Natl Acad Sci USA **113**(27):7539-7544.

3.3.3.2 Heme Activator protein, Hap1, activity in a *tdh3*Δ

Heme Activator Protein, Hap1p, is a zinc finger transcription factor involved in adapting metabolism to O_2 via its ability to sense and bind heme, a O_2-dependent metabolite.[84, 85]. In order to probe Hap1p activity, we designed a transcriptional reporter plasmid that drives the expression of green fluorescent protein (GFP) under the control of the CYC1 promoter, which is activated by Hap1p in the presence of heme. GFP fluorescence is therefore a measure of the availability of heme for Hap1p since heme-activation of Hap1p is required to turn-on CYC1 expression. Using this reporter construct, our data indicate that GAPDH seems to have a role in Hap1p activation since *tdh3*Δ cells have ~3-fold lower GFP expression comparted to WT (**Figure 3.4**). These data suggest that GAPDH regulates Hap1p, presumably by acting as a heme source for Hap1p.

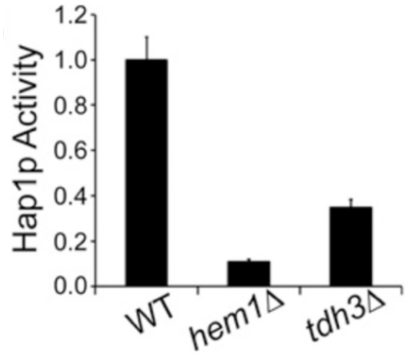

Figure 3.4 - Hap1p activity in the indicated strains as measured by a transcriptional reporter that used EGFP driven by the CYC1 promoter, a Hap1p target gene. All data represent the mean ± SD of triplicate mid-log-phase yeast extract-peptone-dextrose media supplemented with ergosterol and tween-80 (YPDE) cultures. Figure adapted with permission from: Hanna et al. (2016) Proc Natl Acad Sci USA **113**(27):7539-7544

3.3.4 GAPDH Complementation

To confirm the increase in cytosolic labile heme was due to the deletion of the major isoform of GAPDH, Tdh3p, complementation experiments were performed. In these experiments, the expression of GAPDH was reintroduced in a deficient mutant through the use of a p416-GPD plasmid. WT and *tdh3*Δ cells expressing empty vector (p416-GPD) or *TDH3* (p416- GPD-TDH3) and p415-ADH1-HS1-M7A were cultured in order to measure the cytosolic heme availability. We

observed that episomal expression of TDH3 in *tdh3*Δ cells restored cytosolic labile heme to WT levels (**Figure 3.5A**). Immunoblot analysis of GAPDH and SOD1 (loading control) were also done in these strains to confirm the recovery in expression of GAPDH in the TDH3 deficient mutants. A full restoration of GAPDH expression was observed in the *tdh3*Δ strains that were expressing the p416-GPD-TDH3 and not in the ones expressing empty vector (**Figure 3.5B**). It can be concluded that the phenotypes observed were due to the lack of GAPDH expression, and that indeed this glycolytic enzyme is acting as a heme buffer in the cell.

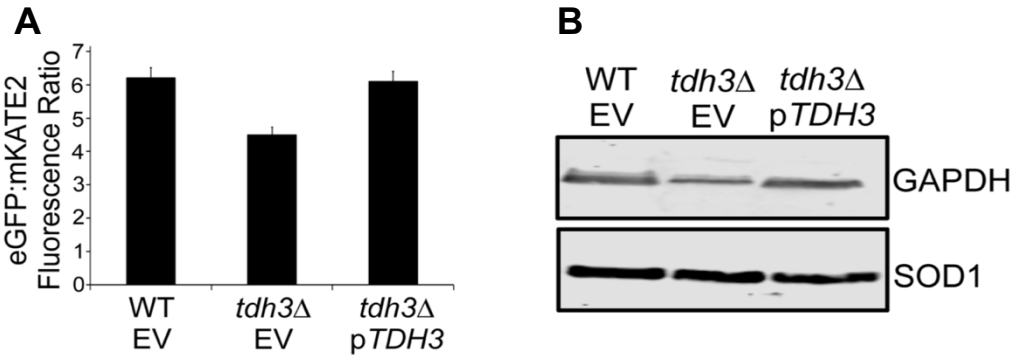

Figure 3.5 – Heme availability and expression measurements for the complemented GAPDH deficient strains. (**A**) WT and *tdh3*Δ cells expressing empty vector (p416-GPD) or *TDH3* (p416- GPD-TDH3) and p415-ADH1-HS1-M7A were cultured in SCE-LEU-URA media for 15 hours and EGFP:mKATE2 fluorescence ratios were recorded. The fluorescence data represent the mean ± SD of duplicate cultures. (**B**) Immunoblot analysis of GAPDH and SOD1 (loading control) in the strains from Panel A. Figure adapted with permission from: Hanna et al. (2016) Proc Natl Acad Sci USA **113**(27):7539-7544.

3.3.5 Identification of Heme Binding Residues on GAPDH

One of the most commons heme binding ligands in hemo-proteins is histidine (His)[86]. Previous studies with rabbit GAPDH (rGAPDH) identified a histidine residue as the ligand that would facilitate heme binding to GAPDH. In order to determine the important heme binding residues in human GAPDH (hGAPDH), our collaborators at the Cleveland Clinic performed sequencing alignments of GAPDH from a large number of species and selected three highly-conserved His residues in hGAPDH. According to our collaborator's computer modeling of these residues, His53

was the most probable heme binding residue due to it being localized on a flexible loop at the inter-protomer interface of the tetramer[87]. They also observed that only the H53A mutation cause a decrease in the hGAPDH heme binding affinity. In order to further study the role of GAPDH as a heme buffer and identify the crucial residues that facilitate this function, we decided to probe labile heme with various GAPDH mutants.

First, we screened heme availability of a *tdh3*Δ strain and confirmed the increase in cytosolic heme levels. When we transformed the *tdh3*Δ mutant with the plasmid that provides the expression of the native TDH3 or hGAPDH, both of them resulted in the restoration of WT cytosolic labile heme levels. In the case of transforming the *tdh3*Δ strain with the TDH3 H51A mutant (*S. cerevisiae* mutant equivalent of H53A) or the hGAPDH H53A mutants, the WT cytosolic labile heme levels were not rescued. This data indicates that the heme coordinating ability of GAPDH regulates the intracellular labile heme and that this characteristic is conserved in humans.

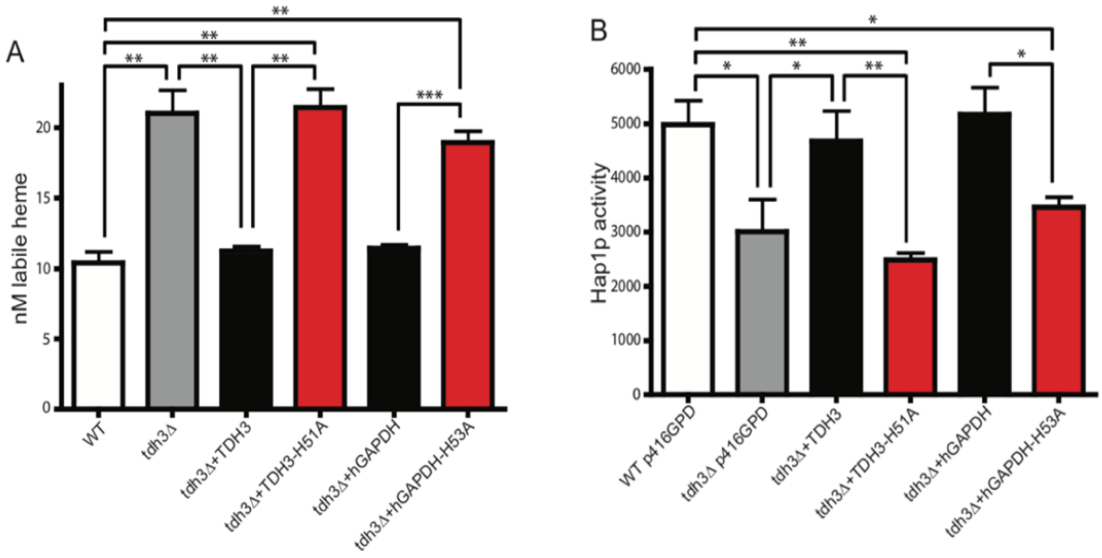

Figure 3.6 - GAPDH heme binding is essential for regulating cytosolic labile heme and delivery to nuclear Hap1p. **(A)** Sensor-detected labile heme levels in WT and tdh3Δ (GAPDH deletion) yeast strains with or without transfection with yeast and human GAPDH variants. (**B**) Corresponding Hap1p activation in yeast. Figure adapted from: Sweeny et al. (2018) Journal of Biological Chemistry. **293** (37):14557-14568.

We next wanted to study if the His heme binding residue also was required for the heme activation of Hap1p. We observed the *tdh3*Δ strain expressing the transcriptional reporter resulted in decreased levels of Hap1p activation in comparison to a WT. The *tdh3*Δ mutant transformed with yeast TDH3 or hGAPDH, resulted in restoration of Hap1p activity to WT levels. In the case of transforming the *tdh3*Δ strain with the TDH3 H51A mutant or the hGAPDH H53A mutants, we still observed the lower levels of Hap1p activation.

3.4 Discussion

Although essential for life, heme may also act as a toxin, necessitating that cells carefully handle this compound[2, 4]. However, the factors that govern heme bioavailability, including the molecules that transport, traffic, and buffer it, are largely unknown. There are a number of proteins characterized as being heme binding proteins due to their *in vitro* interactions with hemin-agarose, including glutathione-S-transferase[88], heme-binding proteins (HBPs)[89, 90] and fatty acid binding proteins (FABPs)[91]. Direct evidence of heme binding ability and their role in heme homeostasis is often lacking.

From the genome-wide screens for heme availability, we were able to identify GAPDH as a possible heme buffering factor that, upon deletion, increases the labile heme pool in the cytosol. Previous work proposed that GAPDH delivers heme to the inducible nitric oxide synthases (iNOS) in an NO-dependent manner, in which S-nitrosylation prevents heme binding in GAPDH[81]. Our results were able to confirm GAPDH is a heme buffering factor in the cytosol that also regulates heme mobilization and delivery to nuclear heme dependent transcription factors such as Hap1. Additionally, we also identified His53 in hGAPDH and His51 in yeast as crucial for heme binding, buffering, trafficking to Hap1. It has been demonstrated that oxidative stress such as NO supplementation can lead to S-nitrosylation, preventing heme binding to GAPDH[81]. Our lab has

also described how NO can dynamically mobilize heme, especially in the nucleus.[3]. Can GAPDH be responsible for the labile heme release observed upon NO supplementation? The addition of NO can cause posttranslational modifications on GAPDH such as S-nitrosylation in the catalytic cysteine. This can induce the release of heme from the glycolytic protein, generating an increase in heme availability.

These results provide new insights into heme gets distributed within the cell. Instead of acting as a heme chelator or heme sink to protect the cell from heme toxicity, GAPDH seems to be acting more as a facilitator that makes heme bioavailable and regulates its delivery to downstream target proteins like Hap1. Our data suggest that the GAPDH heme pool is in equilibrium with the overall labile heme pool in the cell that is detected by the heme sensor, and that GAPDH is responsible to manage a significant portion of it. Once GAPDH binds heme, it makes it bioavailable for being inserted into cytosolic proteins like iNOS and for delivery to heme dependent transcription factors like Hap1p.

The mechanism underlying GAPDH mediated heme delivery to Hap1p is still unknown. We speculate that one possibility is that GAPDH directly delivers heme to Hap1p via its nuclear translocation and interaction with Hap1. This idea is supported by evidence that demonstrates that GAPDH is mobilized from the cytosol to the nucleus under specific conditions[92]. In addition, it is known that the inhibition of GAPDH through S-nitrosylation leads to GAPDH binding to an E3 ubiquitin ligase, Siah-1, which translocate as a GAPDH-Siah complex to the nucleus triggering apoptosis[75, 93-95]. We propose that there is a protein interaction or a posttranslational modification that can also cause the nuclear translocation of GAPDH in a similar manner, to deliver heme to Hap1. A second possibility is through an intermediary that could accept heme from GAPDH and deliver heme to Hap1 in the nucleus. The identification of GAPDH as a heme buffering factor

helps to expand the knowledge of how intracellular heme is trafficked and how heme homeostasis is maintained. It also validates the idea of the existence of heme chaperones and motivates the need to identify more proteins like this so we would get a better understanding of heme trafficking and regulation.

3.5 Materials and Methods

3.5.1 Cell Strains, Culturing and Plasmids

3.5.1.1 Yeast Strains, Media and Growth Conditions

S. cerevisiae strains used in this study were derived from BY4741 (*MAT*a, *his3*Δ1, *leu2*Δ0, *met15*Δ0, *ura3*Δ0). *tdh1*Δ::*kan*MX4, *tdh2*Δ::*kan*MX4, and *tdh3*Δ::*kan*MX4 strains were obtained from the yeast gene deletion collection (Thermo Fisher Scientific). A *hem1*Δ::HIS3 strain was generated by deleting *HEM1* using the *hem1*::HIS3 deletion plasmid, pDH001. Yeast transformations were performed by the lithium acetate procedure[96]. Strains were maintained at 30° C on either enriched yeast extract-peptone based medium supplemented with 2% glucose (YPD), or synthetic complete medium (SC) supplemented with 2% glucose and the appropriate amino acids to maintain selection. Culturing of *hem1*Δ cells required supplementing YPD or SC media with 50 μg/mL of 5-aminolevulinic acid (5-ALA) or 15 mg/mL of ergosterol and 0.5% Tween-80 (YPDE or SCE, respectively)[97].

3.5.1.2 E. coli Strains, Media and Growth Conditions

For routine cloning, sub-cloning grade chemically competent *E. coli* cells, strain 10G E. cloni (Lucigen), were used according to the manufacturer's specifications. Unless otherwise stated, all *E. coli* strains were cultured in Lysogeny broth (LB)[98] with the appropriate antibiotic selection, either 100 μg/mL ampicillin or kanamycin.

3.5.1.3 Plasmids

HAP1 Transcriptional Reporter, prCYC1-EGFP. In order to monitor HAP1 activity, a transcriptional reporter was generated in which EGFP was driven by the CYC1 promoter, which is a gene that is positively regulated by HAP1. A 5'/3' BamHI/HindIII EGFP fragment was amplified and sub-cloned in p416-CYC1, containing the CYC1 promoter.

GAPDH and mutant's expression plasmids. The yeast Tdh3p expression plasmid was generated by amplifying *TDH3* from yeast genomic DNA and sub-cloning it into the SpeI/BamHI sites of p416-*GPD*[99] to generate plasmid pAR1031. The yeast Tdh3-H51A mutation was generated by Quick Change mutagenesis (Agilent Technologies) using pAR1031 as a template, generating pAR1033. The yeast hGAPDH and hGAPDH-H53A expression plasmids were generated by amplifying hGAPDH from pGex4T2-GST-hGAPDH or pGex4T2-GST- hGAPDH-H53A and sub-cloning it into the SpeI/BamHI sites of p416-*GPD*[99] to generate plasmids pAR1035 and pAR1036, respectively.

3.5.2 Experimental Methods

3.5.2.1 Catalase Activity Measurements in Yeast

WT yeast cells expressing empty vector (p415-GPD), or HS1-M7A driven by the GPD, TEF1, or ADH1 promoters (p415-GPD-HS1-M7A, p415-TEF1-HS1-M7A, p415-ADH1-HS1-M7A) were cultured in SC-LEU media for ~14-16 hours to mid-exponential phase (an optical density at 600 nm of $OD_{600\ nm}$ ~ 1-2). Cells were harvested and lysed in phosphate buffer and 10 μg of protein lysate were subjected to native PAGE on a 10% tris-glycine gel (Invitrogen). After electrophoresis, an in-gel activity stain was utilized to measure catalase activity[100]. Briefly, a catalase staining solution containing 1 part Dopamine (20mg/mL) in pH 8 0.2 M KP_i buffer, 1 part para-phenylenediamine (3.5mg/mL) in pH 8 0.2M KP_i, 1 part 15 % H_2O_2, and 2 parts DMSO

were mixed in the order listed. The staining solution was added directly to the gel and allowed to stain for 2 minutes, followed by rinsing in Milli-Q water and imaging.

3.5.2.2 Total Heme Quantification in Yeast

Heme was quantified using a protocol adapted from the method of Woods and Simmonds[101]. Briefly, yeast was cultured in 25 mL of YPDE media for 15 hours to a density of 1 $OD_{600\ nm}$ /mL. Cells were harvested, washed in ice-cold Milli-Q water, and lysed in three pellet volumes of acid-acetone (9.75 mL acetone, 0.250 mL concentrated HCl). Lysis was achieved at 4 C using one pellet volume of zirconium oxide beads and a bead beater (Bullet Blender, Next Advance) on a setting of 8 for 3 minutes. After homogenization, lysates were clarified by centrifugation at maximum speed on a table-top centrifuge. 50 µL of an acid-acetone extract of heme was diluted into 50 µL of 0.1% trifluoroacetic acid in a 1:1 mixture of water and acetonitrile. Heme was quantitated by HPLC using a flow rate of 1 mL/min and elution gradients going from 50% acetonitrile in water, 0.1% TFA to 100% acetonitrile, 0.1% TFA over 10 minutes on a C-18 column (Poroshell 120, SB-C18, 4.6 x 100 mm, 2.7 um). Heme was quantified relative to hemin chloride standards run in parallel and normalized for cell number. Cellular heme concentration was determined by assuming a yeast cell volume of 50 fL. Heme was unambiguously identified from its retention time and characteristic UV/visible spectrum using a photodiode array detector coupled to the HPLC.

3.5.2.3 HAP1 Transcriptional Reporter Assay

Yeast cells expressing p416-CYC1- EGFP, or EGFP driven by the Hap1p regulated CYC1 promoter, were cultured in 10 mL of SCE-URA media for 15 hours to a to a density of 1 $OD_{600\ nm}$ /mL. Cells were resuspended in PBS to a concentration of 1×10^8 cells/mL and 100 uL was used to measure EGFP fluorescence (ex. 488 nm, em. 510 nm). As a positive and negative control,

WT and *hem1*Δ cells were cultured for each experiment. Background auto- fluorescence of cells not expressing EGFP was recorded and subtracted from the EGFP expressing strains.

3.5.2.4 Immunoblotting

Yeast were cultured in 10 mL of SC media for 15 hours to a density of 1 OD600 nm /mL. Cells were harvested, washed in ice-cold Milli-Q water, and lysed in two pellet volumes of phosphate buffer supplemented with protease inhibitors as described previously[102, 103]. Lysis was achieved at 4 C using one pellet volume of zirconium oxide beads and a bead beater (Bullet Blender, Next Advance) on a setting of 8 for 3 minutes[102, 103]. Lysate protein concentrations were determined by the Bradford method (Bio-rad) and 12% tris-glycine gels (Invitrogen) were employed for SDS-PAGE[102, 103]. Anti-GFP rabbit or anti-GAPDH polyclonal antibodies (Genetex) and a goat anti-rabbit secondary antibody conjugated to a 680 nm emitting fluorophore (Biotium) were used to probe for GAPDH. All gels were imaged on a LiCOR Odyssey Infrared imager[102, 103].

CHAPTER 4. THE HEME BIOSYNTHESIS ENZYME, 5-AMINOLEVULINIC ACID SYNTHASE (ALAS), AND GTPASES IN CONTROL OF MITOCHONDRIAL DYNAMICS AND ER CONTACT SITES, REGULATE HEME MOBILIZATION TO THE NUCLEUS

4.1 Introduction

Heme (iron protoporphyrin IX) is an essential but inherently cytotoxic metallocofactor and signaling molecule[3]. As a cofactor, heme facilitates diverse processes that span electron transfer, chemical catalysis, and gas synthesis, storage and transport[3]. As a signaling molecule, heme regulation of an array of proteins, including transcription factors[85, 104-106], kinases[107, 108], ion channels[109], and micro RNA processing proteins[110], collectively control pathways spanning iron homeostasis, oxygen sensing, the oxidative stress response, mitochondrial respiration and biogenesis, mitophagy, apoptosis, circadian rhythms, cell cycle progression, proliferation, and protein translation and degradation[2, 4]. Although essential for life, heme and its biosynthetic precursors may also act as toxins, necessitating that cells carefully handle the synthesis and trafficking of this compound. The hydrophobicity and redox activity of heme causes it to disrupt membrane structure, become mis-associated with certain proteins, and deleteriously oxidize various biomolecules[8, 9]. Porphyrin and porphyrinogen, heme biosynthetic intermediates, are photosensitizers that can catalyze the formation of reactive oxygen species like singlet oxygen[111]. Indeed, a number of diseases are associated with defects in heme management, including certain cancers[112], cardiovascular disease[113], aging and age-related neurodegenerative diseases[7, 114, 115], porphyrias[116], and anemias[117]. Despite the tremendous importance of heme in physiology, the

cellular and molecular mechanisms that govern the safe assimilation of heme into metabolism remain poorly understood.

In eukaryotes, heme is synthesized via a highly conserved eight-step process. The first and the last three reactions in metazoans (first and last two in the yeast *Saccharomyces cerevisiae*) take place in the mitochondria and the remaining reactions occur in the cytosol[23]. The first committed step of heme synthesis is the condensation of glycine with succinyl coenzyme A to form 5-aminolevulinic acid (ALA), which is catalyzed by ALA synthase (ALAS). ALA is then exported from the mitochondria into the cytosol where it is converted to coproporphyrinogen III in four steps by the enzymes porphobilinogen synthase (PBGS), hydroxymethylbilane synthase (HMBS), uroporphyrinogen III synthase (UROS), and uroporphyrinogen III decarboxylase (UROD). Coproporphyrinogen III is transported back into the mitochondria where it is converted to protoporphyrin IX (PPIX) in two steps by the enzymes coproporphyrinogen oxidase (CPOX) and protoporphyrinogen oxidase (PPOX). In the final step of heme synthesis, ferrochelatase (FECH) catalyzes the insertion of ferrous iron into PPIX to make heme.

Interestingly, it was recently proposed that the mitochondrial heme biosynthetic enzymes, ALAS, PPOX, and FECH, form a super complex, or metabolon, that includes additional factors like iron and porphyrinogen transporters, and putative heme chaperones[24, 118]. The biochemical rationale for the assembly of a heme metabolon is that it would facilitate the channeling of potentially toxic reactive substrates, including porphyrinogen, porphyrin, and iron, for efficient production and trafficking of heme, thereby mitigating their ability to diffuse freely throughout the cell in an unproductive and deleterious manner. However, given this rationale, it is unclear why ALAS would interact with FECH in the heme metabolon if the product of the ALAS-catalyzed reaction, ALA, were not the immediate substrate for super-complex factors PPOX or FECH.

Rather, ALAS may play a regulatory role in heme synthesis or trafficking from FECH beyond simply catalyzing the production of ALA.

Once heme is synthesized by FECH on the matrix side of the mitochondrial inner membrane (IM), it must be mobilized to heme proteins present in virtually every subcellular compartment[2, 4]. However, the specific factors that govern the transport and trafficking of heme to target hemoproteins are not well-understood[2, 4]. The current paradigm for subcellular heme trafficking is a *sequential* one in which mitochondrial heme transporters export heme into the cytosol, where it can then be distributed to other locales. The transporter-mediated sequential paradigm for heme distribution was established with the discovery of feline leukemia virus subgroup C cellular receptor 1b (FLVCR1b), the only putative mitochondrial heme transporter identified to date[30]. FLVCR1b was proposed to transport heme from the mitochondria into the cytosol on the basis that it was required for the hemoglobinization of developing erythrocytes and its ablation results in increased mitochondrial heme content[30].

An alternative, but far less studied potential mechanism for heme distribution is through mitochondrial membrane contact sites[2, 4, 23]. Endoplasmic reticulum (ER)-mitochondrial encounter structures (ERMES), one type of mitochondrial-ER contact site[119], are highly dynamic tethers that physically link the mitochondrial and ER networks and have been proposed to play a role in the transfer of lipids and regulate iron homeostasis[120-122]. The frequency of ERMES is in part dependent on mitochondrial division[119]. ER tubules facilitate mitochondrial fission by wrapping around and constricting mitochondria in an ERMES-dependent fashion, thereby ensuring that the GTPase Dnm1 can oligomerize around a compressed mitochondrial outer-membrane to catalyze the scission of mitochondria[123]. Following fission, the GTPase Gem1 disengages ERMES to dissolve the ER-mitochondrial contact site[124]. As a consequence, ERMES assembly may be

dependent on mitochondrial fission and fusion dynamics[119] . Indeed, mutants with defects in fission have increased ERMES foci, presumably because Dnm1-dependent fission is required for Gem1 to disengage ERMES[119] . On the other hand, mutants with defects in fusion have decreased ERMES foci[119], presumably due to the relative increase in mitochondrial fission over fusion.

Herein, using genetically encoded ratiometric fluorescent heme sensors (HS1) targeted to the mitochondrial matrix, cytosol, or nucleus[3, 87, 125], we developed a live-cell assay in yeast to monitor heme distribution kinetics to probe the role of ALAS and ER-mitochondrial contact sites and dynamics on subcellular heme trafficking. Surprisingly, we find that heme trafficking rates from the matrix side of the IM to the mitochondrial matrix and cytosol are similar, while trafficking to the nucleus is ~25% faster. We propose that the increased rate of nuclear heme trafficking is required for heme-based mitochondrial-nuclear retrograde signaling. These data also indicate that heme is distributed from the mitochondrial IM to other locales *simultaneously* via multiple parallel pathways rather than *sequentially.* Moreover, we discovered that the heme biosynthetic enzyme, ALAS, negatively regulates mitochondrial-nuclear heme trafficking, highlighting the close coordination of heme synthesis and trafficking. In addition, we identified GTPases that directly (Gem1) and indirectly (Dnm1 and Mgm1) regulate ERMES as being modulators of nuclear heme transport. Based on our results, we propose a model in which heme is trafficked via ER-mitochondrial membrane contact sites to other organelles such as the nucleus. In total, the development of a live cell assay for probing heme trafficking dynamics coupled with molecular genetics approaches have revealed new insights into subcellular heme distribution.

4.2 Results

4.2.1 Inter-compartmental heme transport kinetics

In order to probe inter-compartmental heme trafficking in yeast, we developed an *in vivo* pulse-chase assay in which, upon the initiation of heme synthesis, heme mobilization into the mitochondrial matrix, cytosol and nucleus is monitored using genetically encoded ratiometric fluorescent heme sensors (HS1)[3]. HS1 is a tri-domain fusion protein consisting of a heme-binding moiety, the His/Met coordinating 4-alpha-helical bundle hemoprotein cytochrome *b*562 (Cyt *b*562), fused to a pair of fluorescent proteins, eGFP and mKATE2, that exhibit heme-sensitive and –insensitive fluorescence, respectively[3]. Heme binding to the Cyt *b*562 domain results in the quenching of eGFP fluorescence via resonance energy transfer but has little effect on mKATE2 fluorescence. Thus, the ratio of eGFP fluorescence (ex: 488 nm, em: 510 nm) to mKATE2 fluorescence (ex: 588 nm, em: 620 nm) reports cellular heme independently of sensor concentration, with the eGFP/mKATE2 ratio inversely correlating with heme binding to the sensor[3]. Throughout this study, unless otherwise noted, the sensor is expressed on a centromeric plasmid and the *GPD* promoter (p*GPD*) is used to drive HS1 expression.

HS1 is targeted to the mitochondria and nucleus by appending N-terminal Cox4 mitochondrial matrix or C-terminal SV40 nuclear localization sequences, respectively, as previously demonstrated[3] and indicated herein by microscopy (**Figure 4.1a**) and organelle isolation and immunoblotting (**Figures 4.1b and 4.1c**). Indeed, the eGFP and mKATE2 fluorescence emission of nuclear and mitochondrial-targeted HS1 overlay with 4,6-diamidino-2-phenylindole (DAPI) stained nuclei and mitochondria, respectively (**Figure 4.1a**), using a labeling procedure that enables the selective visualization of mitochondrial or nuclear DNA by varying DAPI concentration or exposure time[126, 127]. On the other hand, HS1 lacking nuclear or

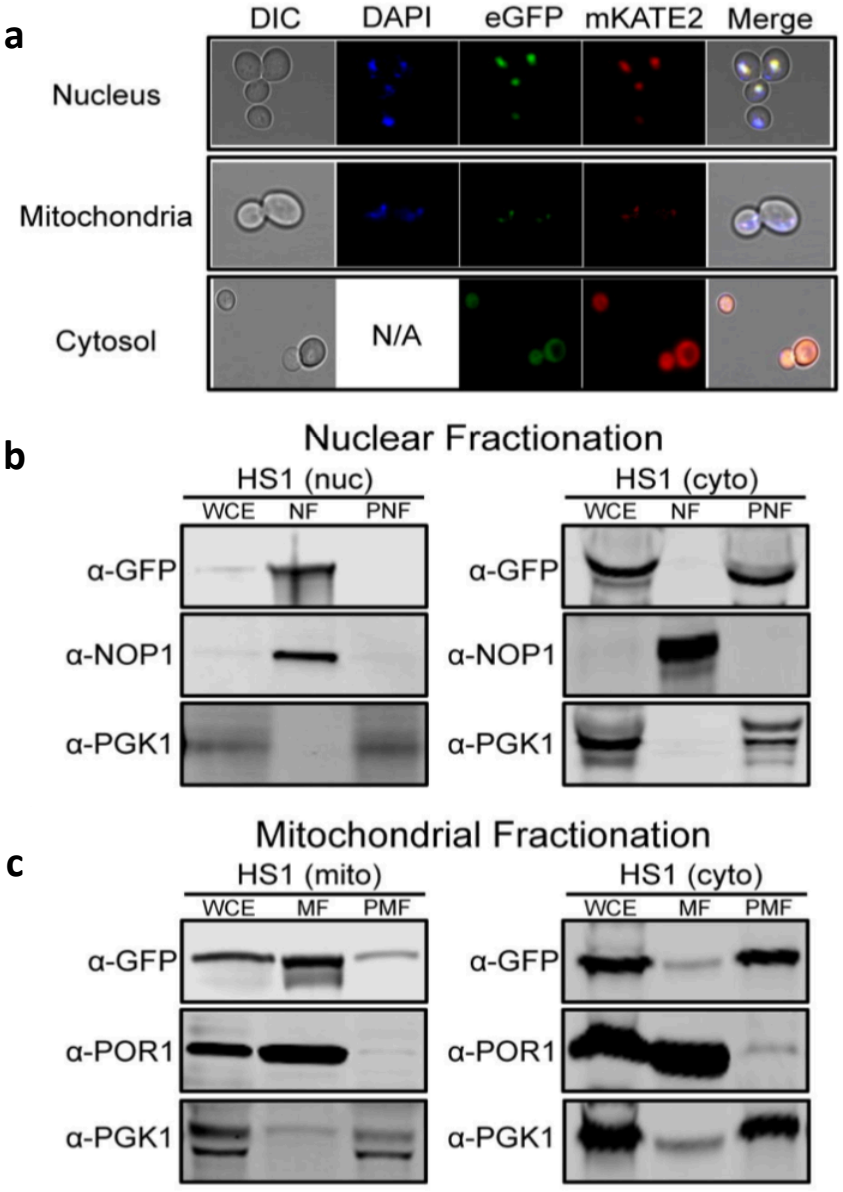

Figure 4.1 - (**a)** The sub-cellular localization of HS1 was assessed by laser scanning confocal microscopy. Cells expressing nuclear or mitochondrial targeted HS1 were stained with DAPI to label nuclei or mitochondria and live cells were imaged. "Merge" is the merged images of fluorescence from the DAPI, EGFP, and mKATE2 fluorescence channels. (**b** and **c**) Confirmation of mitochondrial (mito), nuclear (nuc), and cytosolic (cyto) HS1 localization as assessed by cell fractionation and immunoblotting.

mitochondrial targeting sequences results in a diffuse pattern of expression throughout the cytosol of the cell. Moreover, isolation of nuclei and mitochondria and immunoblotting for HS1 further confirms the subcellular targeting of mitochondrial and nuclear HS1 (**Figures 4.1b and 4.1c**). HS1 lacking the nuclear or mitochondrial targeting sequence is found primarily in cytosolic fractions, *i.e.* post-nuclear (PNF) and post-mitochondrial (PMF) fractions and is not present in significant amounts in mitochondrial or nuclear fractions (**Figure 4.1b and 4.1c**).

It is possible that a small fraction of mitochondrial or nuclear-targeted sensor may be present in the cytosol and confound analysis of sub-compartmental heme. In order to assess if this were the case, we permeabilized heme-deficient cells lacking *HEM1*, which encodes the first enzyme in the heme biosynthetic pathway, ALAS, with digitonin, a mild non-ionic detergent that selectively permeabilizes the plasma membrane but not mitochondrial or nuclear membranes, and treated cells with heme. As indicated in **Figure 4.2**, only cells expressing cytosolic HS1 exhibited a significant heme-dependent reduction in eGFP/mKATE2 fluorescence ratio, with no significant perturbations to the fluorescence of mitochondrial and nuclear-targeted HS1. These data indicate that mitochondrial and nuclear-targeted HS1 is unresponsive to cytosolic heme. Thus, altogether, our data indicate that cytosolic, nuclear, and mitochondrial heme can be robustly monitored *in vivo* using HS1.

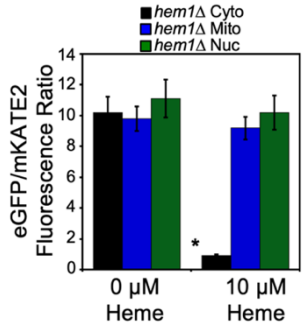

Figure 4.2 - Validation that mitochondrial and nuclear-targeted HS1 does not respond to cytosolic heme. *hem1*Δ cells expressing cytosolic, nuclear, or mitochondrial HS1 were permeabilized with digitonin, a plasma membrane specific permeabilizing agent, and incubated with the indicated concentration of heme. Fluorimetry data represent the mean ± SD of three biological replicates and the statistical significance relative to no heme treatment is indicated by asterisks using an ordinary one-way ANOVA with Dunnett's post-hoc test. * $p < 0.00001$.

Inter-compartmental heme trafficking rates are monitored by: **a.** inhibiting heme synthesis with 500 μM succinylacetone (SA), an inhibitor of PBGS, for ~16 hours in sensor expressing cells; **b.** removing the block in heme synthesis by re-suspending cells into media lacking SA; and **c.** monitoring the time-dependent change in the eGFP/mKATE2 ratio (R) of HS1 localized to different locations upon the re-initiation of heme synthesis (**Figures 4.3a-d**). As described in the Materials and Methods section and **Equation 1**, the fractional saturation of HS1 (% Bound) is calculated by considering R relative to the HS1 fluorescence ratio when the sensor is 0% bound (Rmin) and 100% bound (Rmax) (**Figure 4.3e**), which are parameters derived from parallel cultures of cells continually maintained in media with and without SA[3, 125] (**Figures 4.3a-c**).

$$[\%\ \text{Bound}] = ([R - R\text{min}] / [R\text{max} - R\text{min}])*100 \quad \textbf{Equation 1}$$

In order to confirm the SA-mediated block in heme synthesis, we determined that SA-conditioned wild type (WT) cells exhibit intracellular heme concentrations[128] (**Figure 4.4a**) and HS1 eGFP/mKATE2 ratios[3] (**Figure 4.4b**) similar to *hem1*Δ cells, which cannot make heme due to the deletion of the first enzyme in the heme biosynthetic pathway, ALAS[3]. SA pre-conditioned cells shifted to media lacking SA exhibit a time-dependent decrease in HS1 eGFP/mKATE2 ratio (**Figures 4.3a-c**) in the cytosol, nucleus, and mitochondria, which is characteristic of increased heme loading of the sensor due to newly synthesized heme (**Figure 4.3e**). By contrast, the HS1 eGFP/mKATE2 ratios in cells continuously maintained with or without SA remain characteristically high or low, respectively (**Figures 4.3a-c**), albeit there are some modest time dependent changes for currently unknown reasons.

The change in sensor heme saturation (% Bound) following the re-initiation of heme synthesis reveals three distinct phases: a lag phase, an exponential phase, and a stationary phase (**Figure 4.3e**). The lag phase can be interpreted as the time required to alleviate the SA-mediated

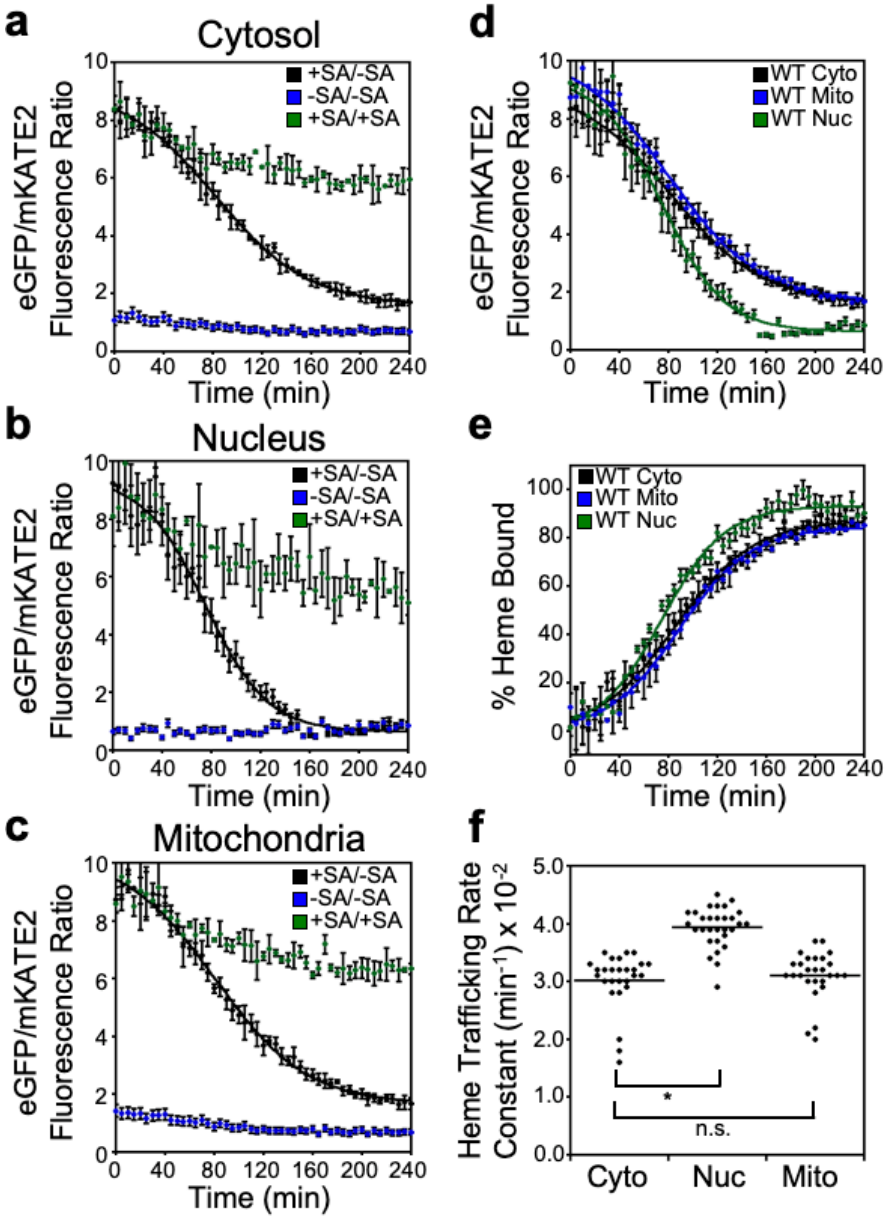

Figure 4.3 - Inter-compartmental heme trafficking dynamics as measured by heme sensor HS1. WT cells expressing HS1 in the cytosol (**a**), nucleus (**b**), or mitochondria (**c**) were depleted of heme using 500 μM succinylacetone (SA), the heme biosynthetic inhibitor and, upon the re-initiation of heme synthesis, the rates of heme trafficking to the indicated subcellular locations were monitored by measuring the time-dependent change in sensor eGFP/mKATE2 fluorescence ratio (**d**) or the fractional saturation of HS1 (**e**), which is determined using **equation 1** and the "raw" fluorescence ratio values in **a**-**c**. The data in **d** and **e** are fit to **equation 2**. (**f**) The rate constants for cytosolic, nuclear, and mitochondrial heme trafficking, which were extracted from fits to the data represented in panel "**e**", from triplicate cultures in nine independent experimental trials are shown. The statistical significance relative to the rate constants for cytosolic heme trafficking is indicated by an asterisk using an ordinary one-way ANOVA with Dunnett's post-hoc test. * $p < 0.0001$. The heme trafficking kinetics data shown in all figure panels represent the mean ± SD of independent triplicate cultures.

block in heme synthesis and re-initiate heme production. The exponential phase represents the rate of heme binding to HS1, which is governed by the relative rates of heme synthesis and trafficking to the different subcellular locations. However, when comparing HS1 heme saturation kinetics between different compartments within a given strain, the data strictly represent the inter-compartmental heme trafficking rates since the contribution from heme synthesis is a constant. Indeed, expression of cytosolic, nuclear, or mitochondrial HS1 does not perturb heme synthesis (**Figure 4.5a**). Since the final step of heme synthesis occurs with the insertion of ferrous iron into protoporphyrin IX, a reaction catalyzed by FECH at the matrix side of the mitochondrial IM, the heme trafficking rates reflect heme mobilization from the mitochondrial IM to the matrix, cytosol, or nucleus. Given the high affinity of HS1 for both ferric and ferrous heme, K_D^{III} = 10 nM and K_D^{II} < 1 nM at pH 7.0[3], and the negligible differences in FRET between eGFP and ferric and ferrous heme[3], we cannot resolve the two oxidation states of heme. The stationary phase represents the maximum limiting heme saturation of the sensor 4 hours after alleviating the SA-mediated block in heme synthesis and typically spans ~70-100%.

The kinetics of heme binding to HS1 (**Figure 4.3e**) can be fit to the logistic function described in **Equation 2**, where [A] is the maximal value of HS1 fractional saturation (amplitude), k is the first order rate constant (min^{-1}), t is the time (min), and $t_{1/2}$ is the midpoint of the transition. The lag time can be defined as $t_{1/2} - 2/k$ [129].

$$\{\%\ \text{Bound}(t) = [A] / (1+e^{-k(t-t1/2)}) \quad \textbf{Equation 2}$$

Quite surprisingly, the kinetics of HS1 heme saturation indicate that heme trafficking to locations as disparate as the mitochondrial matrix, cytosol, and nucleus are similar, but with heme transport to the nucleus exhibiting a ~25% increase in rate constant relative to heme transport to

the cytosol and mitochondrial matrix (Figures 4.4e and 4.4f). This observation is highly reproducible and the rate constants for heme trafficking to the cytosol (k^{CYTO}), nucleus (k^{NUC}), and mitochondrial matrix (k^{MITO}) were found to be 0.030±.005 min^{-1}, 0.039±.003 min^{-1}, and 0.031±.004 min^{-1}, which are the average ± standard deviation from triplicate biological samples over nine independent experimental trials (**Figure 4.3f**). Importantly, in every trial conducted, even if the absolute rates were different, the relative differences always followed the same trend, *i.e.* $k^{NUC} > k^{CYTO} \sim k^{MITO}$. In addition, fitting of the "raw" unprocessed sensor ratios, *R*, reveal a similar trend in the relative rates of heme binding to HS1, with k^{NUC} (0.039±.003 min^{-1}) > k^{CYTO} (0.026±.001 min^{-1}) = k^{MITO} (0.027±.002 min^{-1}) (Figure 4.4d), albeit the absolute rate constants are different when fitting processed "% Bound" traces. This is due to the fact that, for reasons not completely understood, there are fluctuations in R_{min} and R_{max} over the course of a heme trafficking dynamics experiment (**Figures 4.3a-c**). Although the qualitative trends are similar between analyzing changes in "% Bound" and "*R*", "% Bound" is the preferred metric since it accounts for non-heme dependent changes in sensor fluorescence ratio, *i.e.* fluctuations in R_{min} or R_{max} over the course of an experiment.

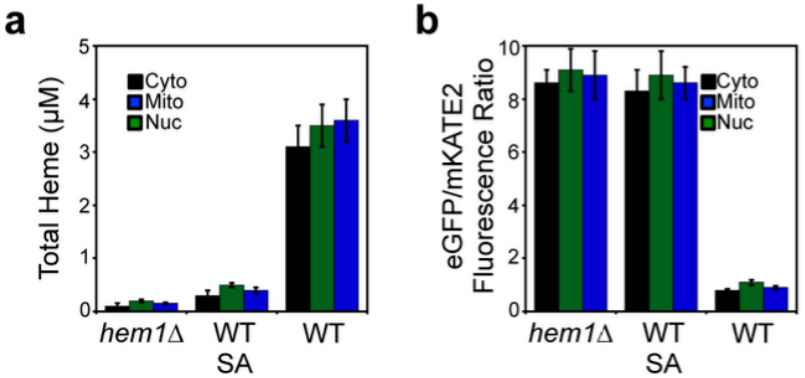

Figure 4.4 - A 500 μM dose of succinylacetone (SA) depletes (**a**) total heme and (**b**) heme-loading of the heme sensor, HS1, to values similar to heme deficient *hem1*Δ cells, which lack the 1st enzyme in the heme biosynthetic pathway. All data represent the mean ± SD of triplicate cultures.

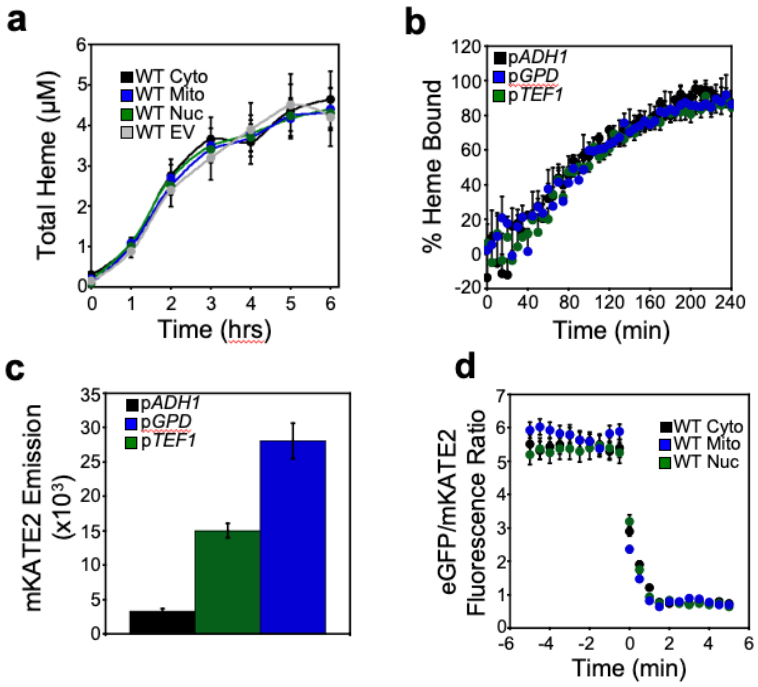

Figure 4.5 - Heme sensor expression does not perturb (**a**) the rates of heme synthesis or (**b**) heme trafficking dynamics to the cytosol. (**a**) WT cells expressing GPD driven cytosolic (Cyto, black), mitochondrial (Mito, blue), or nuclear (Nuc, green) HS1, or empty vector (EV, grey) were heme depleted with 500 μM succinylacetone (SA) for 15 hours and then the cells were resuspended in fresh SC-LEU media lacking SA, where the re-synthesis of heme was monitored by harvesting 2 x 10^8 cells every hour and analyzed for heme content as described in the Methods section. (**b**) The heme trafficking dynamics assay was conducted on cells expressing ADH (black), TEF (green) and GPD (blue) driven cytosolic HS1. Despite the ~10-fold increase in HS1 expression between ADH and GPD promoters, as measured by mKATE2 fluorescence in the right panel (**c**), cytosolic heme trafficking rates are virtually identical. All data represent the mean ± SD of triplicate cultures. (**d**) Heme binding kinetics of cytosolic, nuclear, and mitochondrial-targeted HS1.

The remarkable similarity in the observed rates of heme trafficking to different locales might suggest that heme binding to the sensor is rate limiting. However, measurements of the rate of heme binding to HS1 in cell lysates of WT cells depleted of heme indicate that heme binding to the cytosolic, mitochondrial, and nuclear sensors occurs in less than 2 minutes (**Figure 4.5c**), which is much faster than the ~90-120 minutes it takes 50% of: (i) total cellular heme to be synthesized (**Figure 4.5a**) or (ii) HS1 to become heme saturated in the SA pulse-chase assays (**Figure 4.3**).

In order to rule out any potential artifacts associated with heme sensor expression itself perturbing the observed heme trafficking rates, we expressed cytosolic HS1 under the control of weak (p*ADH1*), medium (p*TEF1*), or strong (p*GPD*) promoters and found that the observed heme trafficking rates were not affected despite a nearly 10-fold span in sensor expression (**Figure 4.5b**). These results are consistent with our previous findings that sensor expression does not perturb heme homeostasis or otherwise affect cell viability[3]. Analogous experiments titrating expression with mitochondrial and nuclear sensors could not be completed due to low sensor expression and correspondingly low sensor signal to noise ratios associated with p*TEF1*- or p*ADH1*-driven expression. Altogether, our data indicate that the SA-pulse chase assays can be used to measure the rates of heme trafficking to multiple compartments and that the rates of mitochondrial-nuclear heme trafficking are 25% faster relative to heme trafficking to the cytosol and mitochondria.

In order to rule out that the observed rates of inter-compartmental heme trafficking are due to artifacts associated with SA treatment, we re-capitulated the *in vivo* heme transport assay in *hem1*Δ cells pulsed with a bolus of ALA to initiate heme synthesis. As shown in **Figure 4.6a**, heme trafficking kinetics to the matrix, cytosol, and nucleus in *hem1*Δ cells are qualitatively similar to the results obtained from the SA pulse-chase assay using WT cells (**Figures 4.3e and 4.3f**), with transport to the nucleus (k^{NUC} = 0.059±.005 min^{-1}) being faster than to the cytosol (k^{CYTO} = 0.030±.003 min^{-1}) and mitochondrial matrix (k^{MITO} = 0.028±.004 min^{-1}) (**Appendix Table 1**). Notably, the rate enhancement for heme trafficking to the nucleus is greater in magnitude in *hem1*Δ cells pulsed with ALA (k^{NUC} / k^{CYTO} = 2.0 ± 0.1; **Figure 4.6a**) than in WT cells that have the SA- mediated block in heme synthesis alleviated (k^{NUC} / k^{CYTO} = 1.3 ± 0.2); **Figures 4.3e and 4.3f**), one-way ANOVA, $p < .01$, $n = 3$. This observation suggests that either the use of SA

suppresses nuclear heme trafficking or that the first enzyme in the heme biosynthetic pathway, ALAS, is a negative regulator of mitochondrial-nuclear heme trafficking.

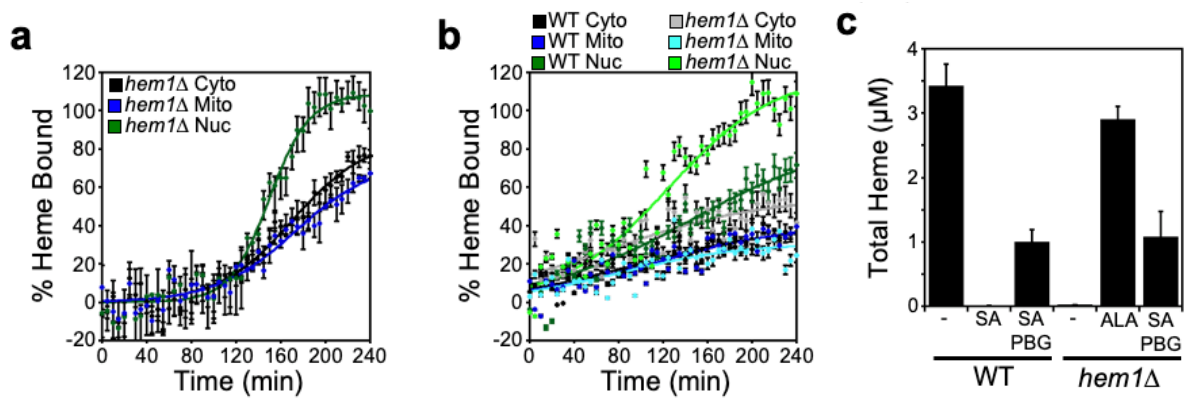

Figure 4.6 - ALA synthase (Hem1) negatively regulates mitochondrial-nuclear heme trafficking. (**a**) *hem1Δ* cells expressing HS1 in the cytosol (black), nucleus (green), or mitochondria (blue) were pulsed with a bolus of ALA to initiate heme synthesis and the rates of heme trafficking to the indicated subcellular locations were monitored by measuring the fractional saturation of HS1 over time. The reported averages and standard deviations are from three independent cultures. (**b**) WT and *hem1*Δ cells expressing sensor were pre-cultured with succinylacetone (SA) to deplete heme and pulsed with a bolus of porphobilinogen (PBG) to re-initiate heme synthesis. The rates of heme trafficking to the indicated subcellular locations were monitored by measuring the fractional saturation of HS1 over time. The indicated rate constants and data are the mean and standard deviations from independent triplicate cultures. (**c**) Analysis of total heme in WT and *hem1* strains treated with succinylacetone (SA), aminolevulinic acid (ALA), or porphobilinogen (PBG). The data represent the mean ± SD of duplicate cultures.

4.2.2 ALA synthase (ALAS) regulates mitochondrial-nuclear heme trafficking

In order to determine if ALAS plays a role in regulating heme distribution kinetics, we monitored inter-compartmental heme trafficking kinetics directly between WT and *hem1*Δ cells. Towards this end, we monitored heme distribution dynamics in WT and *hem1*Δ cells that had SA-inactivated PBGS pulsed with 500 μM porphobilinogen (PBG), the product of the reaction catalyzed by PBGS, to re-initiate heme biosynthesis. As with the SA-pulse chase experiment in WT cells (**Figures 4.3e and 4.3f),** the rates of heme trafficking to the nucleus are greater than trafficking to the cytosol and mitochondrial matrix in SA-treated WT cells pulsed with PBG

(**Figures 4.6b**); $k^{NUC} / k^{CYTO} = 1.5 \pm 0.2$ vs. $k^{MITO} / k^{CYTO} = 1.1 \pm 0.2$; one-way ANOVA, p = 0.05, n = 3. Strikingly, in SA-treated *hem1*Δ cells pulsed with PBG, heme trafficking to the nucleus is significantly augmented relative to WT cells (Figure 4.6b); $k^{NUC} / k^{CYTO} = 2.0 \pm 0.1$ in *hem1*Δ cells vs. $k^{NUC} / k^{CYTO} = 1.5 \pm 0.2$ in WT cells, one-way ANOVA, p = 0.05, n = 3. The relatively low final fractional saturation of the sensor using PBG can be attributed to the fact that heme-deprived cells are less efficient at using PBG to make heme (**Figures 4.6c**). WT and *hem1*Δ cells treated with SA and PBG make roughly ~33% of the heme that WT or *hem1*Δ cells treated with ALA make. Thus, it is all the more impressive that in *hem1*Δ cells pulsed with PBG, the nuclear sensor is completely saturated with heme, unlike in WT cells. Importantly, *hem1*Δ cells do not have a defect in synthesizing heme when supplied with PBG (**Figures 4.6c**). Thus, in total, our results demonstrate that ALAS negatively regulates mitochondrial-nuclear heme trafficking without impacting downstream steps of heme synthesis.

4.2.3 Gem1, a GTPase that regulates ERMES, negatively modulates mitochondrial-nuclear heme trafficking

Since the final step of heme synthesis occurs on the matrix side of the mitochondrial IM, our expectation was that heme would sequentially populate sensors in the mitochondrial matrix, cytosol, and nucleus. However, the data indicate that once heme is synthesized in the mitochondrial IM, it disperses to multiple compartments almost simultaneously, suggesting the existence of parallel routes for heme mobilization to distinct locales. Moreover, surprisingly, mitochondrial-nuclear heme trafficking occurs ~25% faster than to other compartments. Since mitochondria form dynamic physical contacts with other organelles like the ER[119, 121], we surmised that one potential route for the distribution of mitochondrial heme to other compartments like the nucleus could be

through such membrane contact sites. In this scenario, heme may be trafficked to the nucleus via the ER network, bypassing the cytosol, thereby accounting for the increased rate of nuclear heme trafficking. To test this idea, we probed heme distribution rates in deletion mutants with increased or decreased ER-mitochondrial contact sites.

The ER-mitochondrial encounter structure (ERMES), which constitutes one type of physical interface between these organelles, is a complex that consists of four proteins, Mmm1, Mdm10, Mdm12, and Mdm34[130-133]. Mmm1 and Mdm10 are anchored in the ER and outer mitochondrial membranes, respectively, while the cytosolic protein Mdm12 and the mitochondrial protein Mdm34 help to bridge the interaction between Mmm1 and Mdm10 in the ERMES complex[130-133]. The absence of any single ERMES protein results in dissociation of the entire complex, compromising the formation of ER-mitochondrial contact sites, mitochondrial division and morphology [38-41,134]. ERMES is negatively regulated by Gem1, which is a mitochondrial outer-membrane localized GTPase that disengages ERMES after mitochondrial division[124, 135].

As shown in **Figure 4.7a**, *gem1*Δ cells, which have increased ERMES, exhibit a significantly increased rate of mitochondrial-nuclear heme trafficking, with minimal impact on heme trafficking to the cytosol and mitochondrial matrix; $k^{NUC} / k^{CYTO} = 1.45 \pm 0.05$ in *gem1* cells vs. $k^{NUC} / k^{CYTO} = 1.1 \pm 0.1$ in WT cells, one-way ANOVA, $p < 0.01$, $n = 3$. These data suggest that more stable ER-mitochondrial contacts increase the flow of heme to the nucleus. However, in ERMES compromised *mdm12*Δ and *mdm10*Δ strains, heme trafficking rates are unaffected (Figures 4.8b and 4.8c).

ERMES has been implicated in the transfer of lipids, *e.g.* phosphatidylserine (PS), between the ER and mitochondria[131, 136, 137]. PS, an ER-synthesized lipid, is a precursor for the synthesis of

phosphatidylethanolamine (PE) in the mitochondria, which itself is a precursor for phosphatidylcholine (PC) synthesis back in the ER. Both phospholipids are constituents of mitochondrial membranes[138]. In order to rule out confounding contributions that may arise due to general defects in PE or PC in ERMES mutants, we tested heme trafficking dynamics in *psd1*Δ cells, which lack PS decarboxylase, the enzyme that catalyzes the formation of PE. As shown in **Figure 4.7d**, there are no defects in heme trafficking dynamics in *psd1*Δ cells.

ERMES are highly dynamic and sensitive to the presence of mitochondrial- vacuolar contact sites, termed vCLAMPs for vacuolar and mitochondrial patches. Like ERMES, vCLAMPs are important for lipid and metabolite trafficking between mitochondria and the endomembrane system[119]. The absence of one causes expansion of the other and ablation of both ERMES and vCLAMPs is lethal[119]. We therefore sought to determine if a defect in vCLAMPs also increases mitochondrial-nuclear heme trafficking rates as in *gem1*Δ cells, which have an increased number of ERMES foci like vCLAMP mutants. However, neither *vps39*Δ nor *ypt7*Δ cells (**Figures 4.7e and 4.7f**), which lack a component of the HOPS ('homotypic fusion and protein sorting') tethering complex (Vps39) and the Rab GTPase (Ypt7), core components of vCLAMPs[119, 121, 139], exhibit defects in heme distribution kinetics. We conclude that Gem1, but not the core components of ERMES and vCLAMP machineries, regulates mitochondrial-nuclear heme trafficking.

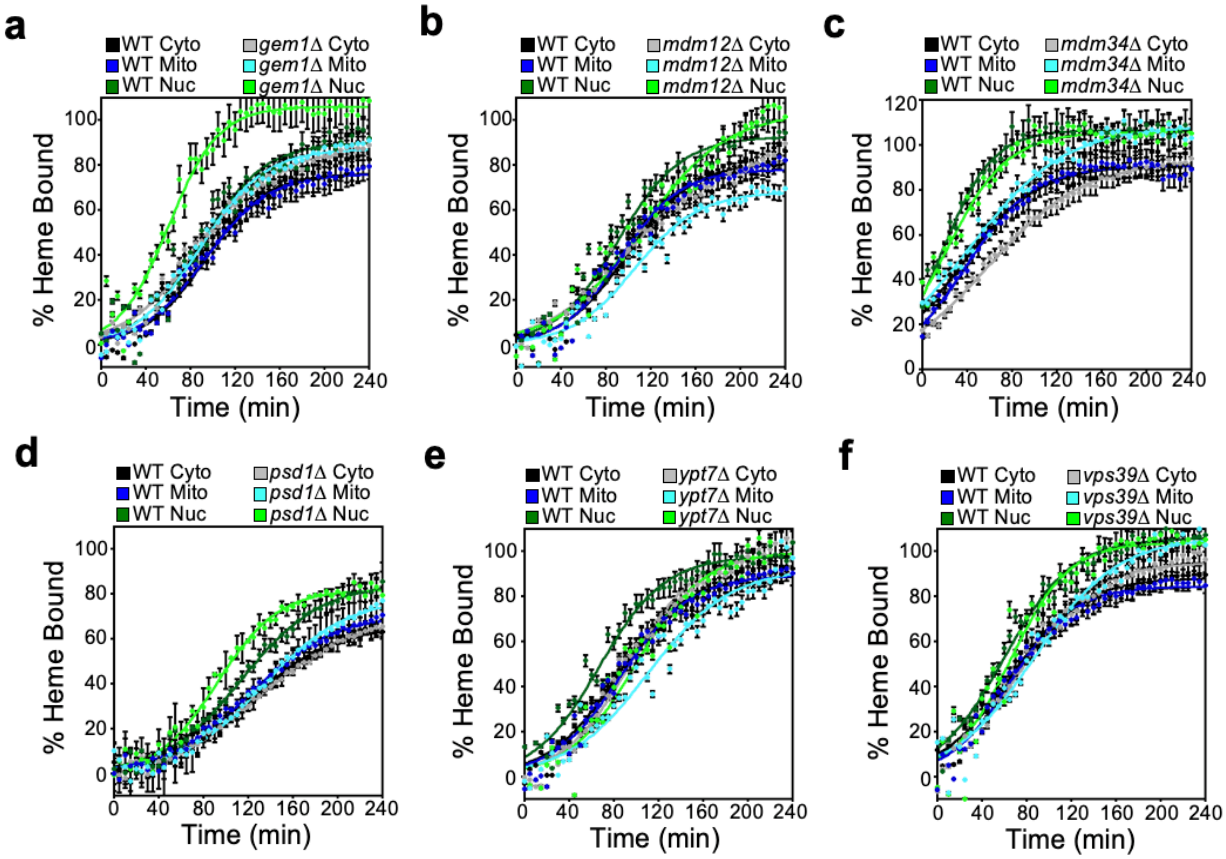

Figure 4.7 - Gem1 is a negative regulator of mitochondrial-nuclear heme trafficking. Inter-compartmental heme trafficking rates were monitored using the SA pulse- chase assay for (**a**) *gem1*Δ, (**b**) *mdm12*Δ, (**c**) *mdm34*Δ, (**d**) *psd1*Δ, (**e**) *ypt7*Δ, and (**f**) *vps39*Δ cells. The data represent the mean ± SD of independent triplicate cultures and the kinetic parameters derived from the fits to the data using equation 2 are indicated in **Appendix Table 1.**

4.2.3.1 Mgm1 and Dnm1 are positive and negative regulators of mitochondrial-nuclear heme trafficking, respectively

The mitochondrial network is highly dynamic and is constantly remodeled by fusion and fission events. The dynamic behavior of the mitochondrial network is thought to be responsible for the proper cellular distribution and trafficking of a number of mitochondrial-derived metabolites, including various lipids[140, 141]. Given that we identified Gem1, an ERMES regulating GTPase that modulates mitochondrial-nuclear heme trafficking, and that ERMES are associated

with sites of mitochondrial division and their frequency can be impacted by mitochondrial fission and fusion dynamics[119, 123], we reasoned that other GTPases that regulate mitochondrial dynamics might regulate mitochondrial-nuclear heme trafficking.

4.2.3.2 Mitochondrial Fusion

Mitochondrial fusion occurs at both the IM and OM in coordinated but physically separable steps. In yeast, a pair of dynamin-like GTPases, Fzo1 and Mgm1, drive OM and IM fusion, respectively[142]. In order to coordinate double membrane fusion, a protein spanning the mitochondrial intermembrane space, Ugo1, physically tethers Fzo1 and Mgm1. Mgm1 exists in equilibrium between long (l-Mgm1) and short (s-Mgm1) isoforms, which are generated upon proteolytic cleavage by the rhomboid protease Pcp1[143, 144]. It is thought that l-Mgm1, which has an inactive GTPase domain, acts as an anchor in the IM and interacts with and activates the GTPase activity of s-Mgm1 in the intermembrane space to promote IM fusion[143, 144].

Relative to WT cells, the *mgm1*Δ strain exhibits a marked defect in nuclear heme trafficking, with a > 50% reduction in HS1 heme loading (**Figure 4.8a**). On the other hand, heme trafficking to the mitochondrial matrix and cytosol is not significantly impacted in *mgm1*Δ cells. Interestingly, heme availability to HS1 in the nucleus is similar between WT and *mgm1*Δ cells after prolonged growth, ~16 hours, suggesting that there are compensatory mechanisms that overcome the defects in nuclear heme trafficking in *mgm1*Δ cells (**Figure 4.9a**). The rate of heme synthesis is un-perturbed by loss of Mgm1, indicating that the nuclear trafficking defect is not related to general defects in heme synthesis (**Figure 4.9b**). The effects of the *mgm1*Δ mutant on nuclear heme trafficking is not due to the loss of mitochondrial DNA, which occurs with high

frequency in *mgm1*Δ cells; *rho*^{0} cells that lack mitochondrial DNA do not exhibit an appreciable defect in nuclear heme trafficking (**Figure 4.8b**).

In order to determine if the nuclear heme trafficking defect observed in *mgm1*Δ cells is specific to Mgm1 or more generally due to ablation of mitochondrial fusion, we tested other essential components of the mitochondrial fusion machinery, including Fzo1 and Ugo1. Interestingly, the *fzo1*Δ (**Figure 4.8c**) and *ugo1*Δ (**Figure 4.8d**) mutants do not exhibit defects in mitochondrial-nuclear heme trafficking, indicating that general perturbations to mitochondrial fusion do not impact nuclear heme trafficking.

Since the regulation of nuclear heme transport is specific to Mgm1, we tested a mutant with altered Mgm1 function. *pcp1*Δ cells are defective in fusion due to an inability to proteolytically convert l-Mgm1 to its short isoform. As seen in **Figure 4.8e**, *pcp1*Δ cells do not exhibit a defect in mitochondrial-nuclear heme trafficking. These data indicate that full-length Mgm1 regulates mitochondrial-nuclear heme transport, but the short Mgm1 isoform is dispensable.

In addition to mediating mitochondrial inner-membrane fusion, Mgm1 is also responsible for maintaining the proper folding and structure of cristae in the inner- membrane[145]. In order to determine if the defect in mitochondrial- nuclear heme trafficking in *mgm1*Δ cells is related to defects in inner-membrane architecture, we determined if heme trafficking was altered in a mutant with a defect in the mitochondrial contact site and cristae organizing system (MICOS). Mic60 is a core component of MICOS and is required for proper inner-membrane folding[146]. As seen in **Figure 4.8f,** *mic60*Δ cells do not exhibit a defect in mitochondrial-nuclear heme trafficking. Altogether, our data strongly suggest that full length Mgm1, but not mitochondrial fusion or inner-

membrane architecture *per se*, positively regulates mitochondrial-nuclear heme trafficking (**Figure 4.8**).

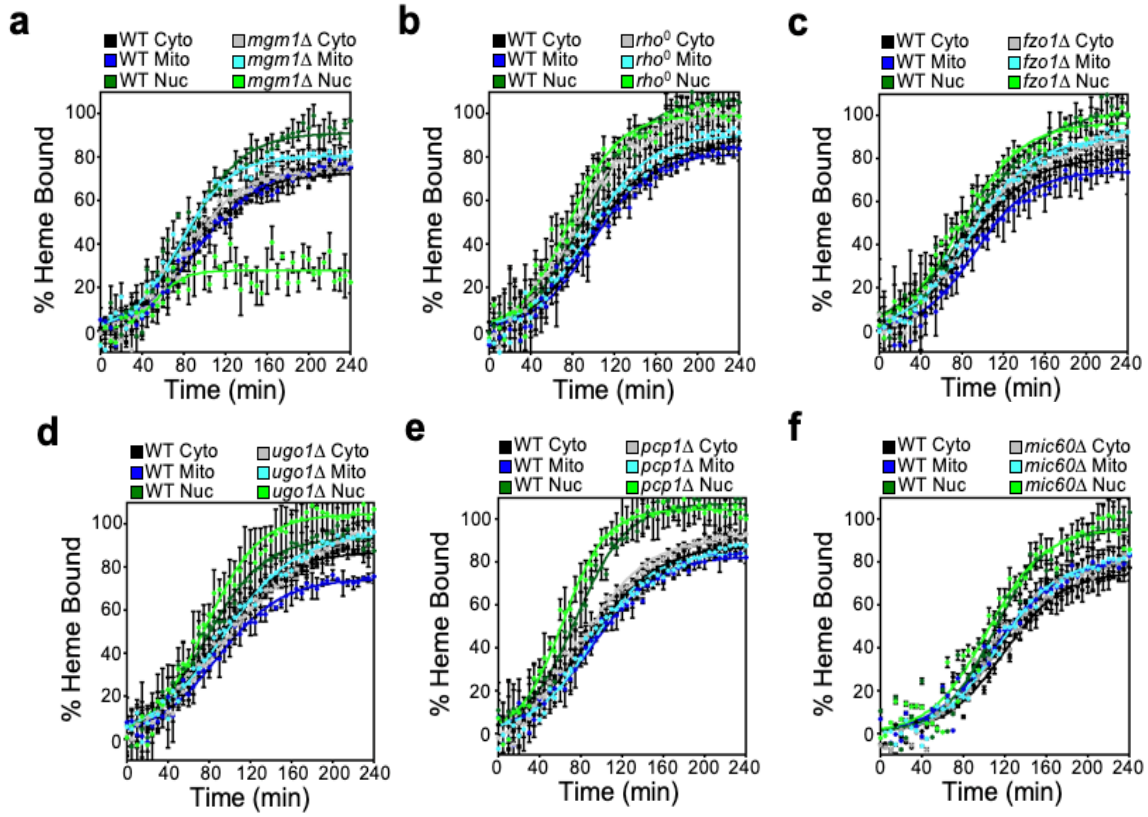

Figure 4.8 - Mgm1 is a positive regulator of mitochondrial-nuclear heme trafficking. Inter- compartmental heme trafficking rates were monitored using the SA pulse- chase assay for (**a**) *mgm1*Δ, (**b**) *rho*^{0}, (**c**) *fzo1*Δ, (**d**) *ugo1*Δ, (**e**) *pcp1*Δ cells, and (**f**) *mic60*Δ cells. The data represent the mean ± SD of independent triplicate cultures and the kinetic parameters derived from the fits to the data using equation 2 are indicated in **Appendix Table 1**.

4.2.3.3 Mitochondrial Fission

In yeast, mitochondrial fission involves recruitment of the GTPase Dnm1 to its receptor Fis1 on the mitochondrial outer-membrane (OM), which is dependent on paralogous adapter proteins Mdv1 and Caf4[142]. Once assembled and oligomerized around the OM, Dnm1 drives the GTP-dependent constriction and scission of mitochondrial tubules.

Relative to WT cells, the *dnm1*Δ strain exhibits an increase in the rate of heme trafficking to the mitochondrial matrix, cytosol, and nucleus, with the most pronounced effect on nuclear heme trafficking; $k^{NUC} / k^{CYTO} = 1.5 \pm 0.1$ in *dnm1* cells vs. $k^{NUC} / k^{CYTO} = 1.2 \pm 0.1$ in WT cells, one-way ANOVA, $p < 0.01$, $n = 3$ (**Figure 4.10a**). After prolonged growth, 16 hours, heme availability to HS1 in all three compartments is similar between WT and *dnm1*Δ cells (**Figure 4.9a**). Additionally, the rate of heme synthesis is unperturbed by loss of Dnm1, indicating that the increase in the rate of heme trafficking is not due to an increase in the rate of heme synthesis (**Figure 4.9c**).

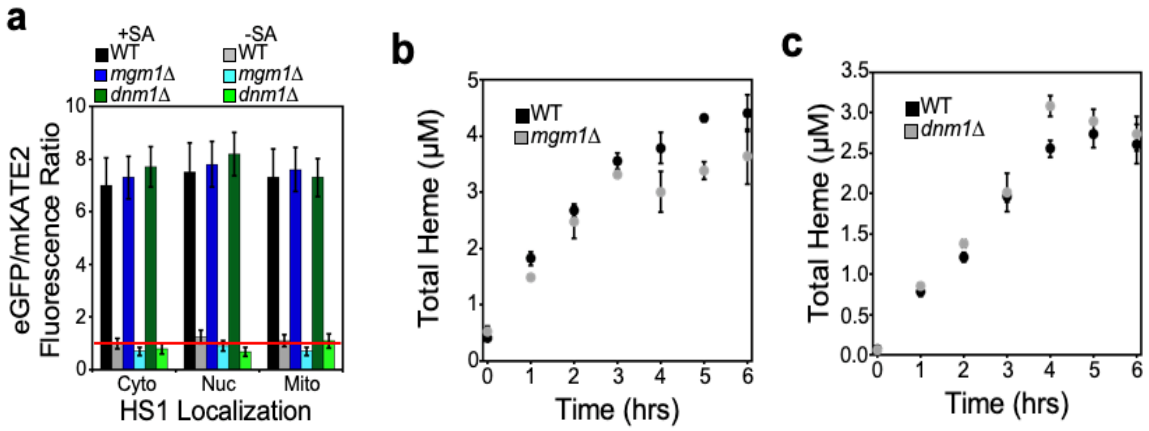

Figure 4.9 - The effects of *mgm1*Δ and *dnm1*Δ on steady-state HS1 heme loading and heme synthesis. (**a**) Cytosolic (Cyto), nuclear (Nuc), or mitochondrial (Mito) HS1 expressed in WT (black, gray*), dnm1*Δ (dark and light green), and *mgm1*Δ (dark and light blue) cells were cultured for 16 hours in SCE-LEU media with (+SA, dark colors) or without (-SA, light colors) 500 μM succinylacetone (SA). Following growth and washing cells with ultrapure water, HS1 sensor fluorescence was measured in a 100 μL suspension of 5 OD's/mL in PBS. (**b and c**) The rates of heme synthesis were measured in (**b**) *mgm1*Δ and (**c**) *dnm1*Δ cells by first heme depleting cells with 500 μM SA for 15 hours and then re-initiating heme synthesis by re-suspending cells in media lacking SA. 2 x 10^8 cells were harvested every hour and analyzed for heme content as described in the Materials and Methods. All data represent the mean ± SD of triplicate cultures.

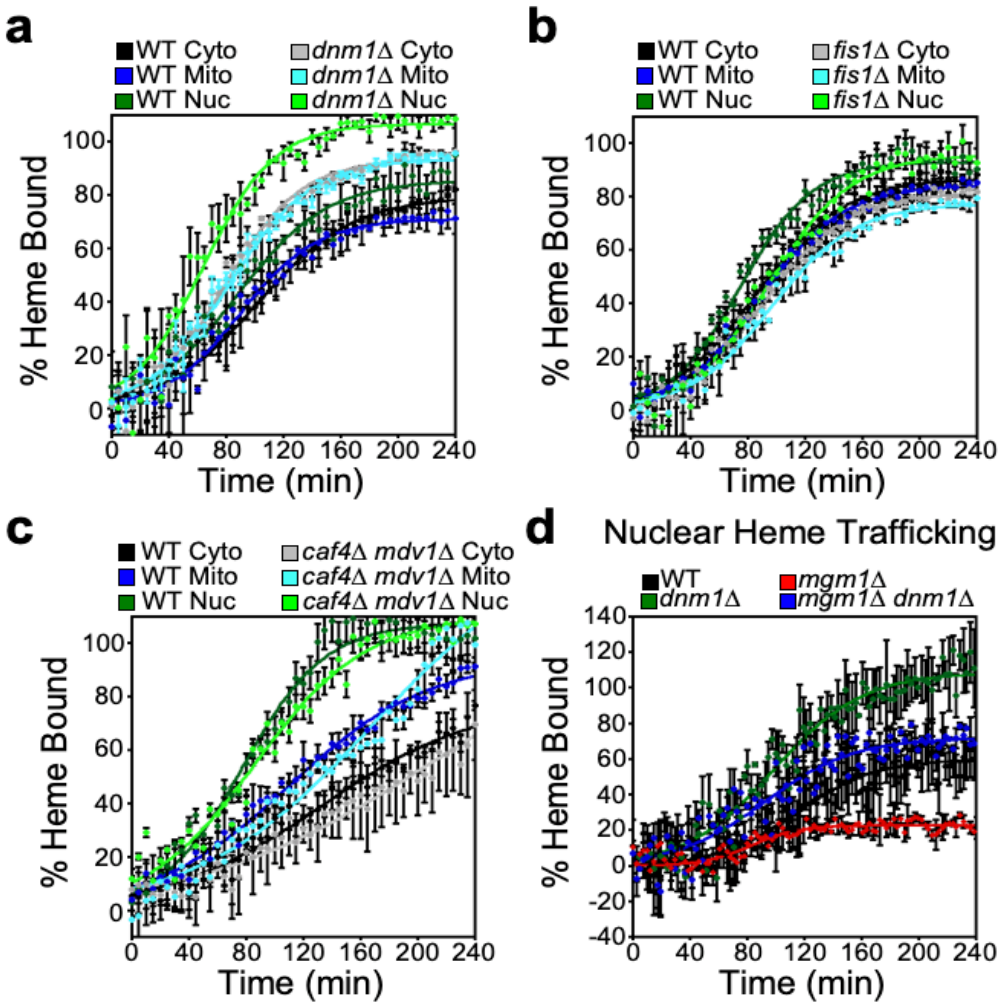

Figure 4.10 - Dnm1 is a negative regulator of mitochondrial-nuclear heme trafficking. Inter- compartmental heme trafficking rates were monitored using the SA pulse- chase assay for (**a**) *dnm1*Δ , (**b**) *fis1*Δ , and (**c**) *caf4*Δ *mdv1* cells, and (**d**) *mgm1*Δ *dnm1*Δ cells. Fluorimetry data represent the mean ± SD of three independent cultures and the kinetic parameters derived from the fits to the data using equation 2 are indicated in **Appendix Table S1**.

In order to determine if the increased rate of nuclear heme trafficking observed in *dnm1*Δ cells is specific to Dnm1 or more generally due to ablation of mitochondrial fission, we tested other essential components of the mitochondrial fission machinery, including Fis1, Caf4, and Mdv1. Interestingly, *fis1*Δ (**Figure 4.10b**) and *caf4*Δ *mdv1*Δ (**Figure 4.10c**) mutants do not exhibit perturbations to mitochondrial-nuclear heme trafficking. Altogether, our data indicate that Dnm1,

but not mitochondrial fission per se, negatively regulates mitochondrial-nuclear heme trafficking (**Figure 4.10**).

We next sought to determine the consequence of ablating both Mgm1 and Dnm1 on mitochondrial-nuclear heme trafficking. Most interestingly, *mgm1*Δ *dnm1*Δ double mutants exhibit WT-like rates of mitochondrial-nuclear heme trafficking (**Figure 4.10d**). Therefore, Mgm1 and Dnm1 regulate heme trafficking in opposing directions with similar magnitude.

4.2.4 Mgm1 and Dnm1 regulate the activation of the nuclear heme-regulated transcription factor Hap1.

Given that Mgm1 and Dnm1 are positive and negative regulators of mitochondrial-nuclear heme trafficking, we sought to determine their impact on the activation of the heme-regulated transcription factor Hap1. Heme binding to Hap1 alters its ability to promote or repress transcription of a number of target genes, including *CYC1*, which Hap1 positively regulates[3, 85, 147-149]. In order to probe Hap1 activity, we used a transcriptional reporter that employs the promoter of a Hap1 target gene, p*CYC1*, driving the expression of enhanced green fluorescent protein (eGFP)[3]. Cells were first pre-cultured with 500 μM SA for 16 hours and, following this initial growth period, the SA conditioned cells were diluted into fresh media with (+) or without (-) 500 μM SA for an additional 4 hours. A parallel set of cells continuously grown without SA (-) was cultured to provide a read out of steady-state Hap1 activity. As demonstrated in Figure 4.12a, not only is steady-state Hap1 activity greatly diminished in a heme deficient *hem1*Δ mutant and with SA conditioning (+), as expected, loss of Mgm1 results in a nearly 3-fold reduction in Hap1 activity. On the other hand, loss of Dnm1 does not affect basal Hap1 activity (**Figure 4.11a, -**). Since basal Hap1 activity in WT cells may already reflect heme saturation of Hap1, it is possible

that the effects of the loss of Dnm1 are masked. To address this, we also measured Hap1 activity under non-heme saturating conditions in which Hap1 activity was probed just 4 hours after alleviation of the SA-mediated block in heme synthesis. Under these conditions, *dnm1*Δ cells have increased Hap1 activity and *mgm1*Δ cells exhibit diminished Hap1 activity relative to WT cells (**Figure 4.11a, Δ**).

In order to determine if the effects of Hap1 activation by Mgm1 and Dnm1 are unique to these factors, and not general fusion and fission per se, we analyzed Hap1 activity in *fis1*Δ and *fzo1*Δ cells. While steady-state Hap1 activity is diminished in both *fis1*Δ and *fzo1*Δ strains (**Figure 4.11b, -**), Hap1 activity probed 4 hours after alleviation of the SA mediated block in heme synthesis results in Hap1 activity that is similar to WT cells (**Figure 4.11b, Δ**). Altogether, the positive and negative effects of Mgm1 and Dnm1 on nuclear heme trafficking, respectively, correlate with their effects on heme activation of Hap1, and appear to be distinct from their roles in fusion and fission dynamics (**Figures 4.11a and 4.11b, Δ**).

We next addressed if Mgm1- and Dnm1-regulated nuclear heme trafficking affected heme-dependent growth of cells. Towards this end, we determined the degree to which heme depleted cells pre-cultured with SA were able to recover in media lacking SA ($G_{\Delta SA}$) relative to cells continually maintained with (G_{+SA}) or without SA (G_{-SA}). As such, the "% Recovery" can be calculated using **Equation 3**:

$$[\%\ \text{Recovery}] = ([G_{\Delta SA} - G_{+SA}] / [G_{-SA} - G_{+SA}])*100 \quad \textbf{Equation 3 Equation 1}$$

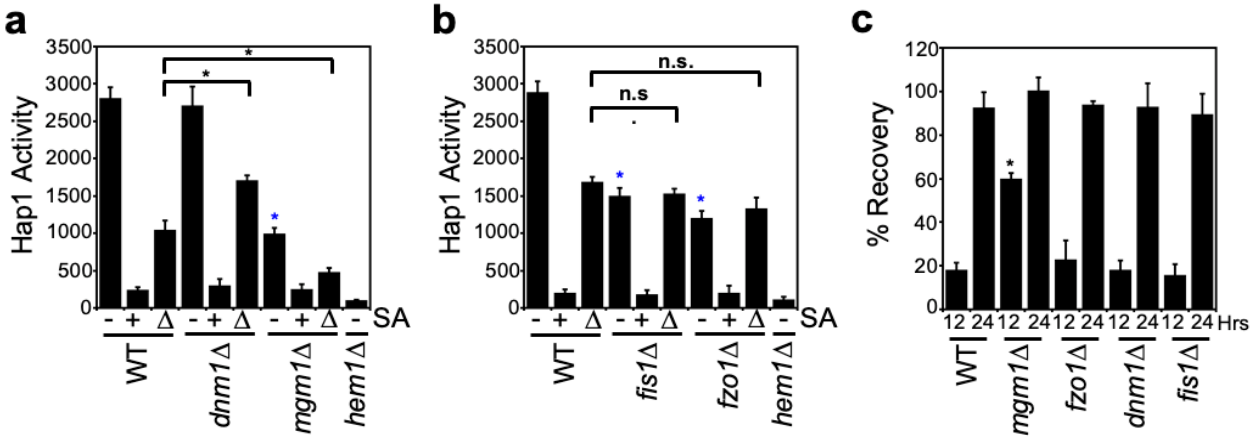

Figure 4.11 - Mitochondrial-nuclear heme trafficking regulates Hap1 activity and sensitivity to new heme synthesis. (**a** and **b**) Hap1p activity in the indicated strains as measured by a transcriptional reporter that uses eGFP driven by the *CYC1* promoter, a Hap1p target gene. We report HAP1 activity in cells that were untreated with succinylacetone (SA) (-), treated with 500 μM SA (+), or were treated with 500 μM SA followed by shifting to media lacking SA for 4 hours (Δ). Fluorimetry data represent the mean ± SD of three biological replicates; *p<0.001 using a one-way ANOVA with Bonferroni's post-hoc test. Asterisks not associated with an indicated pair-wise comparison were compared to WT untreated samples (-SA). (**c**) Cellular tolerance to new heme synthesis. Cells were pre- cultured overnight with or without 500 μM SA then allowed to recover on media without SA. Sensitivity to new heme synthesis was scored as "% Recovery", described in Equation 3, by comparing growth to cells continually maintained in media without SA and with SA. Growth data represent the mean ± SD of three biological replicates; *p<0.001 using a one-way ANOVA with Dunnett's post-hoc test relative to WT cells.

Interestingly, as seen in **Figure 4.11c**, after 12 hours of growth, *mgm1*Δ cells are better able to tolerate the re-synthesis of heme compared to WT cells. The superior ability of *mgm1*Δ cells grown with SA to recover in media lacking SA is not phenocopied by another fusion mutant, *fzo1*Δ, suggesting that Mgm1-mediated nuclear heme trafficking may be growth inhibitory. On the other hand, fission mutants, *dnm1*Δ and *fis1*Δ have WT levels of recovery from the alleviation of the SA-mediated block in heme synthesis, presumably because sufficient heme is accessing the nucleus to control growth in a WT-like manner. After 24 hours, all cells achieved maximal growth recovery after re- initiation of heme synthesis (**Figure 4.11c**). In total, our data suggests that Mgm1 is not only a positive regulator of mitochondrial-nuclear heme trafficking, but this trafficking is negatively correlated with tolerance to the re-initiation of heme synthesis.

4.3 Discussion

Herein, we developed a live-cell assay in yeast to monitor inter-compartmental heme transport dynamics between the mitochondrial IM and the mitochondrial matrix, cytosol, and nucleus in order to identify new aspects of heme trafficking and distribution. *S. cerevisiae* is an unparalleled model system to probe heme distribution dynamics because, unlike many eukaryotes, including mammalian cells, yeast lacking heme can be made viable if supplemented with ergosterol and oleic acid. Thus, heme trafficking and transport dynamics can be monitored without a background associated with pre- existing heme pools. By integrating the heme trafficking dynamics assay with yeast molecular genetics approaches, we have for the first time probed the biodistribution of heme as it is being synthesized in live cells and identified new factors that regulate heme trafficking, including the heme biosynthetic enzyme, ALAS (Hem1) (**Figure 4.6**), and GTPases that regulate ERMES, Gem1 (**Figure 4.7a**), and mitochondrial fusion, Mgm1 (**Figure 4.8a**), and fission, Dnm1 (**Figure 4.10**). As discussed below, our results provide fundamental new insights into heme trafficking and signaling.

The heme trafficking kinetics data challenge the current conceptual paradigm for the cellular distribution of mitochondrial heme. The discovery of the first putative mitochondrial heme exporter, Flvcr1b, the only mitochondrial heme transporter identified to date[30], has often been taken to imply that heme distribution is sequential, with heme first transported into the cytosol followed by its mobilization to other organelles[2, 4, 87]. However, we found that heme distribution to the mitochondrial matrix, cytosol, and nucleus occurs virtually simultaneously, suggesting the existence of parallel pathways for heme mobilization to different cellular locales (**Figures 4.3 and 4.6**). Thus, there must be additional factors and mechanisms that distribute heme, in addition to mitochondrial heme transporters that export heme into the cytosol. Our data suggest that GTPases

that regulate mitochondrial dynamics and ER contact sites constitute novel components of a new heme distribution network.

We propose that the 25% faster rate of heme trafficking to the nucleus relative to the cytosol or mitochondrial matrix (**Figure 4.3f**) is suggestive of heme acting as a mitochondrial-nuclear retrograde signal that enables cells to adapt metabolism and physiology for life with heme and properly functioning mitochondria. Indeed, the activity of the heme regulated nuclear transcription factor, Hap1, correlates with perturbations to mitochondrial-nuclear heme trafficking caused by deletion of Mgm1 or Dnm1, positive and negative regulators of heme trafficking, respectively (**Figure 4.11a**). Rather surprisingly, as part of this heme-based retrograde signal, diminished mitochondrial-nuclear heme trafficking in *mgm1*Δ cells correlate with enhanced cellular growth in response to the re-initiation of heme synthesis (**Figure 4.11c**). This may be due to the detrimental effects of potentially cytotoxic levels of heme accumulating in the nucleus. Indeed, as an iron containing, redox active, hydrophobic molecule, heme may catalyze spurious redox reactions that promote oxidative damage in the nucleus[2-4]. Alternatively, heme may act as an anti-proliferation signal through its ability to act as a transcriptional regulator by binding G-quadruplexes in DNA[150-152] or controlling transcription via Hap1 and the HAP complex[147-149, 153, 154]. Taken together, our results indicate that the relatively fast rate of nuclear heme acquisition may serve an important role in mitochondrial-nuclear retrograde signaling.

Interestingly, we find that the first enzyme in the heme biosynthetic pathway, ALAS, negatively regulates mitochondrial-nuclear heme trafficking (**Figure 4.6**). This result may explain the functional role of a proposed heme biosynthetic supercomplex, or "heme metabolon", in the IM. The heme metabolon includes the first and last enzymes in the heme synthesis pathway, ALAS and FECH, as well as mitochondrial iron importers and putative heme trafficking factors

PGRMC1/2[24, 118]. The typical biochemical rationale for protein-protein interactions in a biosynthetic pathway usually invokes the requirement for substrate channeling in order to mitigate the dissociation of potentially toxic substrates and ensuring rapid flux. In the case of eukaryotic heme biosynthesis, which is an 8-step process, the first and last two steps occur in the mitochondria with the remaining steps occurring in the cytosol. Thus, the biochemical necessity for an ALAS interaction with FECH is not immediately clear in the context of substrate channeling. Our results suggest that the interaction between ALAS and FECH may be functionally significant from a regulatory perspective because we find that ALAS negatively regulates the flow of heme from FECH in the mitochondrial IM to the nucleus. Since a number of factors are known to regulate ALAS expression and/or mitochondrial import, including glucose, iron, and heme[155, 156], we propose that the regulation of mitochondrial-nuclear heme trafficking by ALAS may be part of a complex circuit that links nutrient status to heme-based retrograde signaling. However, the precise physiological context and mechanism of ALAS-mediated regulation of mitochondrial-nuclear heme trafficking needs to be further explored.

What is the elusive mechanism of mitochondrial-nuclear heme trafficking? Herein, we identified three conserved GTPases in control of mitochondrial fusion (Mgm1) and fission (Dnm1), and ER-mitochondrial contact sites (Gem1), as regulators of mitochondrial-nuclear heme trafficking. One unifying model consistent with our data is that mitochondrial-ER contact sites facilitate the distribution of heme to the nucleus and other extra-mitochondrial locales. ER tubules facilitate mitochondrial division by constricting mitochondrial tubules so that Dnm1 can oligomerize around the compressed mitochondrial outer-membrane and catalyze the GTP hydrolysis driven scission of mitochondria[123]. Gem1 is required to disengage ER- mitochondrial contacts after mitochondrial division[124, 157]. Therefore, both *dnm1*Δ and *gem1*Δ cells are expected to - and do - have more stable mitochondrial-ER contact sites[119, 124]. Thus, if heme were trafficked

through ER-mitochondrial contact sites to reach the ER and organelles contiguous with the ER like the nucleus, one would expect that *dnm1*Δ and *gem1*Δ cells exhibit increased rates of nuclear heme trafficking as was observed (**Figure 4.7a and 4.10a**).

In accordance with the model just described, we suggest that Mgm1-mediated regulation of mitochondrial-nuclear heme trafficking occurs in a Dnm1 and ERMES- dependent manner. In such a model, Mgm1 promotes mitochondrial-nuclear heme trafficking because of its ability to drive mitochondrial fusion and provide a balancing force to oppose Dnm1-dependent mitochondrial fission. As a consequence, *mgm1*Δ cells would be expected to (and do) exhibit diminished mitochondrial-nuclear heme trafficking since there is no Mgm1 present to counteract Dnm1-mediated fission (**Figure 4.8a**). Consistent with this model, we observe a restoration of WT-levels of mitochondrial nuclear heme trafficking in *mgm1*Δ *dnm1*Δ cells (**Figure 4.10d**).

However, a number of outstanding issues must be resolved regarding the proposed ERMES-dependent model for mitochondrial-nuclear heme trafficking. First, we do not currently have a means to monitor heme in the ER to more directly assess the impact of ERMES and ER-mitochondrial contact sites on heme trafficking via the ER. Second, it is unclear at this time why other fission and fusion mutants do not exhibit defects in heme trafficking (**Figures 4.8 and 4.10**). There may be some specific unknown additional roles of Mgm1 and Dnm1 that allow them to regulate heme trafficking. Third, we do no observe that mutants with defects in essential components of the ERMES complex, including *mdm12*Δ and *mdm34*Δ, exhibit altered mitochondrial-nuclear heme trafficking rates. One explanation is that there are multiple types of ER-mitochondrial contact sites in addition to ERMES that exist. Indeed, a number of factors in a conserved ER membrane protein complex (EMC) have also been found to facilitate physical

linkage between the ER and mitochondrial networks[158]. Thus, a heme distribution phenotype may only be observed in multigenic knockout cells defective in both ERMES and ECM factors.

An alternative to the unified model that we present for heme trafficking via ER-mitochondrial contact sites is that each GTPase identified may play mechanistically distinct and unrelated roles in heme trafficking. For instance, the human homolog of Mgm1, OPA1, was previously found to physically associate with FECH in the heme metabolon[24]. As such, it is possible that Mgm1/OPA1 regulates the heme metabolon and its interactions with putative heme trafficking factors, *e.g.* PGRMC1/2, to effect mitochondrial-nuclear heme trafficking. Dnm1 and Gem1, as lipid- interacting outer-membrane associated GTPases, may play roles in heme sequestration. Binding of lipids such as cardiolipin, can stimulate GTPase activity and Dnm1/Drp1-dependent membrane fission events[159]. Given heme's lipid-like properties[4], we speculate that heme may be sequestered by Dnm1 or Gem1 in the OM to suppress heme trafficking. Gem1 also has roles in mitochondrial positioning and cytoskeleton anchoring that may contribute to heme distribution dynamics[160]. We are currently exploring the molecular mechanisms underlying Mgm1, Dnm1, and Gem1-mediated heme trafficking and if they cooperate through a common mechanism or act independently of each other.

Our data indicates that factors that impact mitochondrial fission, Dnm1, and fusion, Mgm1, have a profound effect on heme distribution kinetics. Interestingly, our collaborators suggest the reverse may be true as well; namely that heme can impact mitochondrial dynamics. It is interesting to speculate that there may be feedback mechanisms by which heme itself, possibly acting through Mgm1 or Dnm1, can regulate heme distribution dynamics between the mitochondrial network and the nucleus. We are currently probing the underlying mechanisms that govern heme- regulation of mitochondrial fragmentation.

Altogether, the *in vivo* approach to monitor real-time dynamics of inter- compartmental heme trafficking coupled with molecular genetic approaches have uncovered fundamental aspects of the mechanisms underlying heme mobilization and utilization. We expect that the tools and approaches presented herein may be used to probe a number of human diseases, including certain cancers, neurodegenerative disorders, and blood diseases, that are associated with both defects in heme homeostasis and mitochondrial dynamics and membrane contact sites[7, 114, 161]. Indeed, given that mitochondrial dynamics and contact sites with the endomembrane system are conserved between yeast and man, and the factors that regulate them have homologs or functional analogs between lower and higher eukaryotes[142, 162-165], our studies in yeast may be of broad applicability to better understand how membrane and organelle dynamics impacts heme transport and trafficking.

4.4 Materials and Methods

4.4.1 Cell Strains, Transformation, Growth Conditions and Plasmids

4.4.1.1 Yeast strains and Growth Conditions

S. cerevisiae strains used in this study were derived from BY4741 (MATa, *his3*Δ1, *leu2*Δ0, *met15*Δ0, *ura3*Δ0). *fis1*Δ::*Kan*MX4, *dnm1*Δ::*Kan*MX4, *mgm1*Δ::*Kan*MX4, *pcp1*Δ::*Kan*MX4, *ugo1*Δ::*Kan*MX4, *caf4*Δ*::KanMX4*, *mdv1*Δ*::KanMX4* strains were obtained from the yeast gene deletion collection (Thermo Fisher Scientific). We also utilized the previously reported strains, LJ109 (*rho*^{0}) [102] and DH001b-3 (*hem1*Δ::*HIS3*) [3]. AR1029-3 (*mdv1*Δ::*Kan*MX4 *caf4*Δ::*HIS3*) was generated by deleting *CAF4* with pAR1047 in *mdv1*Δ::*Kan*MX4 cells. OM232 (*mgm1*Δ::*HIS3*) and OM233 (*dnm1*Δ::*Kan*MX4 *mgm1*Δ::*HIS3*) was generated by deleting *MGM1* with pAR1051 in WT and *dnm1*Δ*::KanMX4* cells, respectively. All strains were confirmed by PCR, mitochondrial

morphology (**Figure Appendix 1**), and, if derived from the yeast deletion collection, sequencing the unique barcodes flanking the *KanMX4* deletion cassette.

4.4.1.2 Yeast Transformation

Yeast transformations were performed by the lithium acetate procedure [49]. Strains were maintained at 30° C on either enriched yeast extract (1%) - peptone (2%) based medium supplemented with 2% glucose (YPD), or synthetic complete medium (SC) supplemented with 2% glucose and the appropriate amino acids to maintain selection[3]. Cells cultured on solid media plates were done so with YPD or SC media supplemented with 2% agar [3]. Selection for yeast strains containing the KanMX4 marker was done with YPD agar plates supplemented with G418 (200 μg/mL) [3]. WT cells treated with the heme synthesis inhibitor, succinylacetone (SA), and *hem1*Δ cells were cultured in YPD or SC media supplemented with 50 μg/mL of 5-aminolevulinic acid (ALA) or 15 mg/mL of ergosterol and 0.5% Tween-80 (YPDE or SCE, respectively) [3, 166]. All liquid cultures were maintained at 30 °C and shaken at 220 RPM.

4.4.1.3 Plasmids

The *caf4*::*HIS3* disruption plasmid, pAR1047, was generated by first PCR amplifying the upstream (-650 to -129) and downstream (+2110 to +2479) sequences relative to the *CAF4* translational start site, introducing 5' BamHI / 3' XhoI and 5' XbaI / 3' BamHI restriction sites, respectively. The *CAF4* PCR products were digested with the enzymes indicated and ligated in a trimolecular reaction into the *HIS3* integrating plasmid pRS403 [167] digested with XhoI and XbaI, resulting in pAR1047. Transformation of yeast strains with pAR1047 linearized with BamHI resulted in deletion of *CAF4* sequences from -128 to +2109.

The *mgm1*::*HIS3* disruption plasmid, pAR1051, was generated by first PCR amplifying the upstream (-532 to -5) and downstream (+2736 to +3023) sequences relative to the *MGM1*

translational start site, introducing 5' BamHI / 3' XhoI and 5' XbaI / 3' BamHI restriction sites, respectively. The *MGM1* PCR products were digested with the enzymes indicated and ligated in a trimolecular reaction into the *HIS3* integrating plasmid pRS403[167] digested with XhoI and XbaI, resulting in pAR1051. Transformation of yeast strains with pAR1051 linearized with BamHI resulted in deletion of *MGM1* sequences from -4 to +2735.

Cytosolic, mitochondrial, and nuclear-targeted heme sensors, HS1, were sub-cloned into pRS415 and driven by *ADH*, *TEF*, or *GPD* promoters as previously described [3]. The Hap1 reporter plasmid in which eGFP is driven by the *CYC1* promoter was also previously described [3].

4.4.2 Experimental Methods

4.4.2.1 Heme Trafficking Dynamics Assay

Overview. Inter-compartmental heme trafficking rates were monitored by: **a.** inhibiting heme synthesis with succinylacetone (SA) in sensor expressing cells; **b.** removing the block in heme synthesis by re-suspending cells into media lacking SA; and **c.** monitoring the time-dependent change in the percentage of heme bound to heme sensor 1 (HS1) localized to the cytosol, nucleus, and mitochondrial matrix upon the re-initiation of heme synthesis. The fractional heme saturation of the sensor can be determined using previously established sensor calibration protocols[3]. The % of sensor bound to heme, % Bound, is calculated by determining the sensor eGFP/mKATE2 fluorescence ratio (R) under a given test condition relative to the eGFP/mKATE2 fluorescence ratio when the sensor is 100% (R_{max}) or 0% (R_{min}) bound to heme as described in **Equation 1** [3].

R_{min} is determined by measuring the HS1 eGFP/mKATE2 ratio in parallel cultures that are conditioned with succinylacetone (SA), which inhibits the second enzyme in the heme biosynthetic

pathway, ALA dehydratase (ALAD) [168], and R_{max} can be determined by permeabilizing cells and adding an excess of heme to saturate the sensor [3]. Given HS1 is quantitatively saturated with heme in the cytosol, nucleus, and mitochondria of WT yeast, we typically determine R_{max} by measuring the HS1 eGFP/mKATE2 ratio in parallel WT cultures grown without SA [3].

Growth for SA-pulse chase assay. HS1-expressing cells were cultured with or without 500 μM SA (Sigma-Aldrich) in SCE-LEU media. Triplicate 5 mL cultures were seeded at an initial optical density of OD_{600nm} = .01-.02 (2-4 x 10^5 cells/mL) and grown for 14-16 hours at 30 °C and shaking at 220 RPM until cells reached a final density of OD_{600nm} ~ 1.0 (2 x 10^7 cells/mL). After culturing, 1 OD or 2 x 10^7 cells were harvested, washed twice with 1 mL of ultrapure water, and resuspended in 1 mL of fresh SC-LEU media. The cells that were pre-cultured without SA provided HS1 R_{max} values. The SA-conditioned cells were split into two 500 μL fractions. One fraction was treated with 500 μM SA to give HS1 R_{min} values. The other fraction was not treated with SA so that heme synthesis could be re-initiated to give compartment-specific heme trafficking rates. HS1 fluorescence was monitored on 200 uL of a 1 OD/mL (2 x 10^7 cells/mL) cell suspension using black Greiner Bio-one flat bottom fluorescence plates and a Synergy Mx multi-modal plate reader. eGFP (ex. 488 nm, em. 510 nm) and mKATE2 (ex. 588 nm, em. 620 nm) fluorescence was recorded every 5 minutes for 4 hours, with the plate being shaken at medium-strength for 30 seconds prior to each read. Background fluorescence of cells not expressing the heme sensors were recorded and subtracted from the eGFP and mKATE2 fluorescence values.

Growth for ALA pulse-chase assay. HS1-expressing *hem1*Δ cells were cultured with or without 400 μM 5-aminolevulinic acid (ALA) (Sigma-Aldrich) in SCE-LEU media. Triplicate 5 mL cultures were seeded at an initial optical density of OD_{600nm} = .01-.02 (2-4 x 10^5 cells/mL) and grown for 14-16 hours at 30 °C and shaking at 220 RPM until cells reached a final density of OD_{600nm} ~ 1.0 (2 x 10^7 cells/mL). After culturing, 1 OD or 2 x 10^7 cells were harvested, washed

twice with 1 mL of ultrapure water, and resuspended in 1 mL of fresh SC-LEU media. The cells that were pre-cultured with ALA provided HS1 R_{max} values. The cells that were cultured without ALA were split into two 500 µL fractions. One fraction was used to give HS1 R_{min} values. The other fraction was treated with 400 µM ALA so that heme synthesis could be initiated to give compartment-specific heme trafficking rates. HS1 fluorescence was monitored on 200 uL of a 1 OD/mL (2 x 10^7 cells/mL) cell suspension using black Greiner Bio-one flat bottom fluorescence plates and a Synergy Mx multi-modal plate reader. eGFP (ex. 488 nm, em. 510 nm) and mKATE2 (ex. 588 nm, em. 620 nm) fluorescence was recorded every 5 minutes for 4 hours, with the plate being shaken at medium-strength for 30 seconds prior to each read. Background fluorescence of cells not expressing the heme sensors were recorded and subtracted from the eGFP and mKATE2 fluorescence values.

It should be noted that due to evaporation and drying of cell cultures in the plate reader, reliable measurements could not be achieved after 4 hours of continuous monitoring.

4.4.2.2 Total heme quantification

Measurements of total heme were accomplished using a fluorimetric assay designed to measure the fluorescence of protoporphyrin IX upon the release of iron from heme as previously described [58]. For all total heme measurements, ~1 x 10^8 cells were harvested, washed in sterile ultrapure water, and resuspended in 500 µL of 20 mM oxalic acid and stored in a closed box at 4 °C overnight (16-18 hours). Next, an equal volume (500 µL) of 2 M oxalic acid was added to the cell suspensions in 20 mM oxalic acid. The samples were split, with half the cell suspension transferred to a heat block set at 95 °C and heated for 30 minutes and the other half of the cell suspension kept at room temperature (~25 °C) for 30 minutes. All suspensions were centrifuged for 2 minutes on a table-top microfuge at 21000 x g and the porphyrin fluorescence (ex: 400 nm, em: 620 nm) of 200 µL of each sample was recorded on a Synergy Mx multi-modal plate reader

using black Greiner Bio-one flat bottom fluorescence plates. Heme concentrations were calculated from a standard curve prepared by diluting 500-1500 μM hemin chloride stock solutions in 0.1 M NaOH into ultrapure water, which was then added back to extra cell samples as prepared above. In order to calculate heme concentrations, the fluorescence of the unboiled sample (taken to be the background level of protoporphyrin IX) is subtracted from the fluorescence of the boiled sample (taken to be the free base porphyrin generated upon the release of heme iron). The cellular concentration of heme is determined by dividing the moles of heme determined in this fluorescence assay and dividing by the number of cells analyzed, giving moles of heme per cell, and then converting to a cellular concentration by dividing by the volume of a yeast cell, taken to be 50 fL [3].

In order to measure heme synthesis rates, exponential phase cells were pre-conditioned with 500 μM SA for 14-16 hours in SCE-LEU media as described above for the heme trafficking dynamics assay. Following this, cells were washed and resuspended in media lacking SA and aliquots of cells were harvested and washed for total heme quantification as described above.

4.4.2.3 Hap1 activity

Cells expressing p415-*CYC1-eGFP*, or *eGFP* driven by the Hap1 regulated *CYC1* promoter, were cultured in 50 mLs of SCE-LEU in 250 mL Erlenmeyer flasks, with or without 500 μM SA, for 14-16 hours to an optical density of OD_{600nm} ~ 1.0 (2 x 10^7 cells/mL). Cells were washed with sterile ultrapure water and diluted into fresh SC-LEU media at an optical density of OD_{600nm} = 0.25 and allowed to grow for an additional 4 hours. The culture that was initially not conditioned with SA remained untreated during the 4-hour growth phase and these cultures represented basal Hap1 activity. The culture that was pre-conditioned with SA was split into two fractions. One fraction was treated with 500 μM SA for the 4-hour growth phase and these cultures served as a negative control, representing minimal Hap1 mediated activation of *CYC1*. The other

fraction was not treated with SA for the 4-hour growth phase and these cultures represented Hap1 activity under conditions in which Hap1 was not saturated with heme. After growth for 4 hours, cells were washed in sterile ultrapure water and resuspended in PBS to a concentration of 1 x 10^8 cells/mL and 100 uL was used to measure eGFP fluorescence (ex. 488 nm, em. 510 nm). Background auto-fluorescence of cells not expressing eGFP was recorded and subtracted from the p415-*CYC1-eGFP* expressing strains.

4.4.2.4 Isolation of mitochondria and nuclei to confirm heme sensor localization

Mitochondria and nuclei were isolated using yeast mitochondrial (Cat # K259-50) and nuclear (Cat # K289-50) isolation kits from BioVision according to the manufacturer's instructions. All reagents were supplied by the isolation kits. For isolation of mitochondria, 50 mLs of sensor expressing cells were cultured in SC-LEU in 250 mL Erlenmeyer flasks to a final density of OD_{600nm} = 1.0 (2 x 10^7 cells/mL). 4 x 10^8 cells were harvested, washed in ultrapure water, and resuspended in "Buffer A" containing 10 mM DTT for 30 minutes at 30 °C with occasional gentle agitation. Cells were then harvested by centrifugation at 1,500 x g for 5 minutes at room temperature. Cells were then re-suspended in 1 mL of "Buffer B" containing manufacturer provided Zymolyase and incubated at 30 °C with occasional gentle inversion. Spheroplast formation was monitored by diluting 10 uL of the cell suspension into ultrapure water and monitoring the decrease in OD_{600nm} such that it was > 80% less than the initial value, which typically took 30-60 minutes. Spheroplasts were harvested by centrifugation at 1500 x g for 5 minutes, resuspended in "Homogenization Buffer" containing a protease inhibitor cocktail, and lysed with 15 strokes of a Dounce Homogenizer on ice. The lysate was centrifuged at 600 x g for 5 minutes at 4 °C to remove cell debris. The supernatant, which contained the mitochondria, was again centrifuged for 5 minutes at 600 x g to remove additional debris. Finally, mitochondria was harvested by centrifugation at 12000 x g for 10 minutes at 4 °C. The mitochondrial pellet was

resuspended in 50 µL of “Storage Buffer”. In order to validate sensor mitochondrial localization, 5% of the total spheroplast fraction, mitochondrial fraction, and the post-mitochondrial fraction (supernatant from the 12000 x g centrifugation step) were electrophoresed on a 14% tris-glycine SDS-PAGE gel and immunoblotted using α-PGK1 (Life Technologies; Cat # PA528612; 1:5000 dilution), a cytosolic marker protein, α-porin (Life Technologies; Cat # 459500; 1:5000 dilution), a mitochondrial marker protein, and α-GFP (Genetex; Cat # GTX30738; 1:5000 dilution) to probe HS1 expression. A goat α-rabbit secondary antibody conjugated to a 680 nm emitting fluorophore (VWR/Biotium; Cat # 89138-520; 1:10000 dilution) was used to probe for PGK1 and GFP. A goat α-mouse secondary antibody conjugated to a 680 nm emitting fluorophore (VWR/Biotium; Cat # 89138-516; 1:10000 dilution) was used to probe for Porin. All gels were imaged on a LiCOR Odyssey Infrared imager [3, 102].

For isolation of nuclei, 50 mLs of sensor expressing cells were cultured in SC-LEU in 250 mL Erlenmeyer flasks to a final density of OD_{600nm} = 1.0 (2 x 10^7 cells/mL). 4 x 10^8 cells were harvested, washed in ultrapure water, and resuspended in “Buffer A” containing 10 mM DTT for 30 minutes at 30 °C with occasional gentle agitation. Cells were then harvested by centrifugation at 1,500 x g for 5 minutes at room temperature. Cells were then re-suspended in 1 mL of “Buffer B” containing manufacturer provided Zymolyase and incubated at 30 °C with occasional gentle inversion. Spheroplast formation was monitored by diluting 10 uL of the cell suspension into ultrapure water and monitoring the decrease in OD_{600nm} such that it was > 80% less than the initial value, which typically took 30-60 minutes. Spheroplasts were harvested by centrifugation at 1500 x g for 5 minutes, resuspended in 1 mL of “Buffer N” containing a protease inhibitor cocktail, and lysed with 5 strokes of a Dounce Homogenizer on ice. The suspension was incubated for 30 minutes at room temperature with gentle agitation every 3-5 minutes. The lysate was centrifuged at 1500 x g for 5 minutes at 4 °C to remove cell debris. Finally, nuclei were harvested by

centrifugation at 20000 x g for 10 minutes at 4 °C. The nuclear pellet was resuspended in 100 µL of "Buffer N". In order to validate sensor nuclear localization, 5% of the total spheroplast fraction, nuclear fraction, and the post-nuclear fraction (supernatant from the 20000 x g centrifugation step) were electrophoresed on a 14% tris-glycine SDS-PAGE gel and immunoblotted using α-PGK1 (Life Technologies; Cat # PA528612; 1:5000 dilution), a cytosolic marker protein, α-NOP1 (Life Technologies; Cat # MA110025; 1:10000 dilution), a nuclear marker protein, and α-GFP (Genetex; Cat # GTX30738; 1:5000 dilution) to probe HS1 expression. A goat α-rabbit secondary antibody conjugated to a 680 nm emitting fluorophore (VWR/Biotium; Cat # 89138-520; 1:10000 dilution) was used to probe for PGK1 and GFP. A goat α-mouse secondary antibody conjugated to a 680 nm emitting fluorophore (VWR/Biotium; Cat # 89138-516; 1:10000 dilution) was used to probe for NOP1. All gels were imaged on a LiCOR Odyssey Infrared imager [3, 102].

4.4.2.5 Confirmation of heme sensor localization by microscopy

To confirm mitochondrial or nuclear localization of the sensors, prior to microscopy, 1 x 10^7 exponential phase cells were incubated with 2.0 µg/mL 4', 6-diamidino- 2-phenylindole (DAPI) (Invitrogen) in SC-LEU media for 45-60 minutes to stain nuclear or mitochondrial DNA[3]. Laser scanning confocal microscopy was accomplished on a Zeiss ELYRA LSM 780 Super-resolution Microscope equipped with a 63x, 1.4 numerical aperture oil objective. DAPI was excited at 405 nm and emission was collected using 410-483 nm band pass filters. eGFP was excited with the 488 nm line of an argon ion laser, while mKATE2 was excited using the 594 nm of a HeNe laser line. The 491-588 nm and 599-690 nm band pass filters were used to filter emission for eGFP and mKATE, respectively. Images were collected using Zeiss software and analyzed with ImageJ 1.48v (Rasband, W.S., ImageJ, U. S. National Institutes of Health, Bethesda, Maryland, USA, http://rsb.info.nih.gov/ij/, 1997-2007). Auto-fluorescence of unlabeled cells was subtracted from the DAPI, eGFP, and mKATE2 channels to produce the finalized images in **Figure 1b**.

4.4.2.6 Confirmation of mitochondrial morphology in fission and fusion

To visualize the mitochondrial network, 1 x 10^7 exponential phase cells were incubated with 500 μM Mito Tracker Red CM-H_2XRos (Thermo Fisher) in SC-LEU media for 45-60 minutes. Confocal microscopy was done on a Zeiss ELYRA LSM 780 Super-resolution Microscope equipped with a 63x, 1.4 numerical aperture oil objective. Mito Tracker Red was excited using the 594 nm of a HeNe laser line and emission was collected using a 415-735 nm band pass filter. Images were collected using Zeiss software and analyzed with ImageJ 1.48v (Rasband, W.S.,ImageJ, U. S. National Institutes of Health, Bethesda, Maryland, USA, http://rsb.info.nih.gov/ij/, 1997-2007). The various mitochondrial network morphology types observed are outlined in **Figure 1a Appendix** and ~50 cells from each strain were analyzed to confirm the expected mitochondrial morphology (**Figure 1b Appendix**). A representative image of the mitochondrial network from each strain is depicted in **Figure 1c Appendix**. Fission and fusion mutants have characteristic elongated or punctate mitochondrial networks, respectively.

CHAPTER 5. UPTAKE AND UTILIZATION OF HEME AND HEME INTERMEDIATES.

5.1 Introduction

Most heme requiring cells have the capacity to both acquire heme via *de novo* synthesis and import it from its environment. While heme synthesis is very well understood process, the mechanisms underlying heme uptake are not known. Moreover, it is important to understand if the imported heme can be used intact in metabolism. The current dogma is that every cell lives and dies with its own heme and any imported heme is degraded, with the released iron being recycled for new heme synthesis. In this context, the traditional view is that dietary heme acquisition is primarily a source for iron. However, if exogenous heme can be used intact, it is unclear how its bioavailability and subcellular distribution differs from endogenous heme.

In order to identify factors that regulate heme uptake and distribution, we employed a *hem1*Δ strain of yeast that is incapable of synthesizing heme due to a deletion in the first enzyme in the heme synthesis pathway, aminolevulinic acid synthase (ALAS; Hem1). ALAS catalyzes the formation of aminolevulinic acid (ALA) from succinyl-CoA and glycine[1]. A *hem1*Δ deletion mutant is not viable unless cultured with ergosterol and oleic acid, two essential metabolites that are biosynthesized using heme-dependent cytochrome P450 enzymes. Thus, *hem1*Δ strains offer a unique model system to probe the biodistribution and availability of biosynthesized endogenous heme, through ALA supplementation, versus nutritionally acquired exogenous heme, through heme supplementation. Herein, we utilized genetically encoded heme sensors in *hem1*Δ cells to elucidate differences in heme utilization and distribution of endogenous and exogenous heme.

Moreover, we screened the haploid yeast deletion collection to identify factors, e.g. transporters or chaperones, that regulate heme uptake and availability.

Our results demonstrated that indeed, *S. cerevisiae* could acquire and utilize exogenous heme under high concentrations but not in an efficient way. Endogenous heme is more bioavailable than exogenous heme as it can activate heme dependent processes such as catalase activity and Hap1 activity, a heme dependent transcription factor, more efficiently. We observed that conditions like iron starvation promoted heme acquisition in a heme oxygenase (HO) depended manner. From the 4,470 genes screened for heme availability under heme supplementation, we identified 33 deletion mutants that had improved heme uptake. One of these mutants is a mitochondrial magnesium transporter, Mfm1, which serves to facilitate heme uptake through a membrane potential dependent mechanism.

5.2 Results

5.2.1 A hem1Δ mutant can use intact exogenous heme.

In *Saccharomyces cerevisiae* eight enzymatic steps are responsible for heme biosynthesis. The condensation of succinyl-CoA with glycine to form aminoleuvilinic acid (ALA) is the first step. The aminolevulinic acid synthase (ALAS or Hem1) is an essential gene and is lethal upon deletion, but growth can be rescued by either supplementing with ALA or exogenous heme. Heme deficient cells such as *hem1Δ,* could also be rescued by the addition of ergosterol and oleic acid to the media. To investigate if exogenous heme could be acquired and utilized by *S. cerevisiae,* we compared the abilities of ALA and heme to rescue *hem1*Δ cells.

When heme deficient cells were titrated with ALA, we observed a dose dependent cell growth (**Figure 5.1**). We found that 50 μg/mL of ALA afforded the maximal rescue for *hem1*Δ cells, but this rescue never fully matched WT growth. This suggested that ALA uptake or integration into heme synthesis was limiting. To measure if higher doses of ALA would allow the heme deficient mutant to reach WT levels of cell growth, we decided to supplement with 400 μg/m/L and 800 μg/mL of ALA. Higher doses of ALA did not seem to improve growth, since both of the high ALA supplementation only allowed half of the WT cell growth. (**Figure 5.2**) Supplementation with heme intermediate protoporphyrin IX (PPIX) and heme displayed similar cell growth as the cells treated with ALA, indicating a similar rescue and that heme was able to be acquired and utilized intact. (**Figure 5.2**)

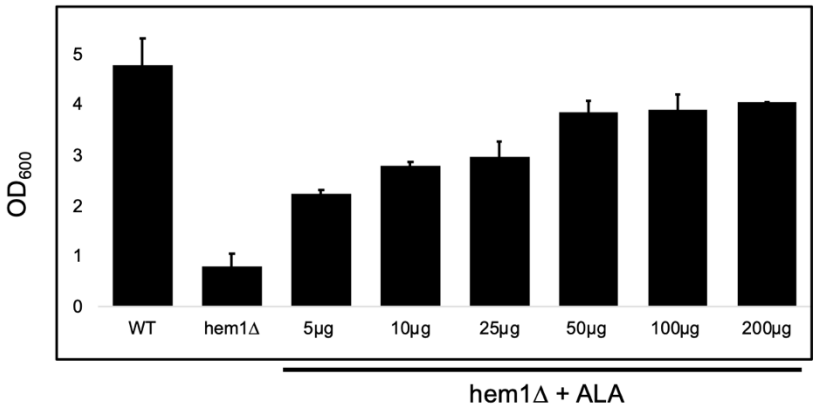

Figure 5.1- Growth rescue of *hem1*Δ with ALA treatment. Heme deficient cells were supplemented with heme intermediates to rescue growth. Growth density reported represent the mean of three biological replicates.

Overall, we observed that *hem1*Δ mutant growth could be recovered by heme and heme intermediates such as ALA and PPIX. The cell growth of a heme deficient mutant was not able to be matched to a WT through the supplementation of heme and heme intermediates judging by the lower cell growth. Because of the anionic carboxylates of ALA, heme, and PPIX, we surmise that transport across the cell membrane is limiting.

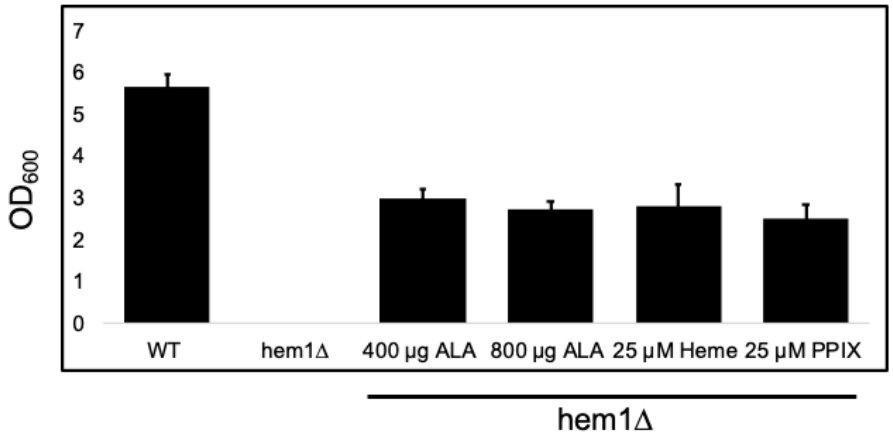

Figure 5.2- Growth rescue of *hem1*Δ with higher concentrations of ALA, PPIX and heme treatment. Heme deficient cells were supplemented with heme intermediates to rescue growth. Growth density reported represent the mean of three biological replicates.

We next quantified intracellular heme concentrations in order to determine the extent to which ALA, heme, and PPIX contributed to cellular heme stores for heme rescue. Total heme quantification was done with the high-performance liquid chromatography (HPLC) using a protocol adapted from the method of Woods and Simmonds[101]. In the initial trial, most interestingly, we observed *hem1*Δ cells supplemented with high doses of ALA contained similar levels of total heme as a WT cell. (**Figure 5.3a**) This indicated that there are other heme-independent factors that limit the growth of *hem1*Δ cells supplemented with ALA.

ALA titrations revealed that 5 µg/mL ALA was a dose that resulted in similar intracellular total heme levels to the 25 µM concentration of heme and PPIX. (**Figure 5.3b**). Despite the fact that intracellular heme levels were identical between 5 µg/mL ALA and 25 µM heme, exogenous heme rescued *hem1*Δ cells better than ALA treatment. This suggested that exogenous heme was more efficient at rescuing growth per molecule of intracellular heme than ALA.

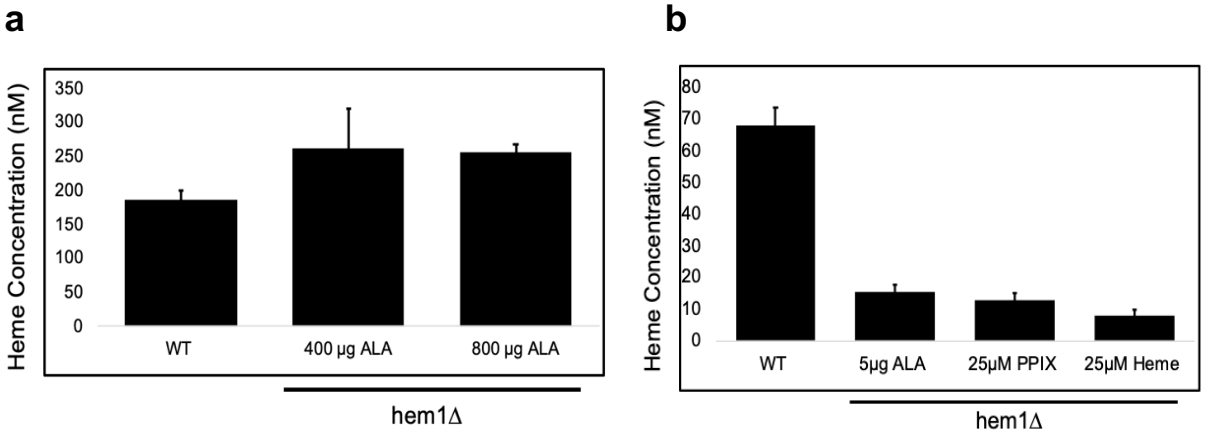

Figure 5.3- Total heme concentrations of heme deficient cells supplemented with heme and heme intermediates. **a.** Total heme measurements for the initial concentrations with best growth rescue for *hem1*Δ. **b.** Concentrations of heme and heme intermediates that present similar total heme levels. Total heme concentrations represented in the figures were taken by three biological replicates and measure using the protocol for HPLC.

5.2.2 Heme Availability for Different Compartments of a hem1Δ Mutant Provided with Exogenous Heme and Heme Intermediates.

Given the fact that concentrations of 25 µM of heme, PPIX and 5 µg/ mL of ALA resulted in similar total heme levels, we sought to understand if endogenous and exogenous heme would be mobilized, distributed and used differently. To identify labile heme distribution, we used the genetically encoded fluorescent heme sensor HS1, which is the highest heme affinity from the library of heme sensors, being 100% bound in WT cells. Since the total heme levels from the supplemented cells are 25% of a WT strain, the tight binding heme sensor is the most appropriate sensor for these measurements. To study labile heme distribution and if there are any changes by supplementation of heme and heme intermediates, the HS1 sensor can be localized to the different organelles using specific organelle targeting sequences that allow them to be targeted to different compartments, including the cytosol, nucleus, and mitochondrial matrix. These sensors will help us determine differences in heme availability and distribution between endogenous and exogenous heme sources.

Measurements of heme availability in the cytosol demonstrate none of the treatments were capable of generating enough heme to load the sensor more than 20%. (**Figure 5.4**) Additionally, we observed endogenous heme made from ALA was more efficiently distributed and more bioavailable in the cytosol than the porphyrins since the sensor had increased heme loading. PPIX and heme display similar levels of saturation in the cytosol, indicating similar uptake and distribution pathways.

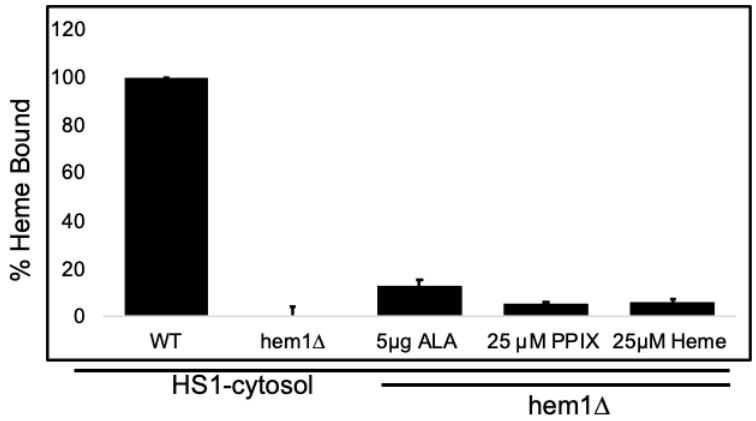

Figure 5.4 – ALA supplementation populates our sensor in the cytosol better than any other treatment. % Heme bound is calculated from the fluorimetric determination of EGFP/mKATE2 fluorescence ratios of the indicated yeast strains expressing HS1 in the cytosol. Measurements represent the mean of three biological clones.

In the case of heme availability for the nucleus, the result that stands out the most is the fact that PPIX seems to generate and make heme more bioavailable in the nucleus than ALA or heme. (**Figure 5.5**) The addition of ALA results in less bioavailable heme in the nucleus than the cytosol, while exogenous heme did not exhibit any bioavailable heme in the nucleus. Endogenous heme seems to be more efficiently mobilized and made bioavailable than exogenous heme for the nucleus and also the cytosol. It is surprising that PPIX and ALA, both heme biosynthetic intermediates, exhibit difference in heme loading in the nucleus.

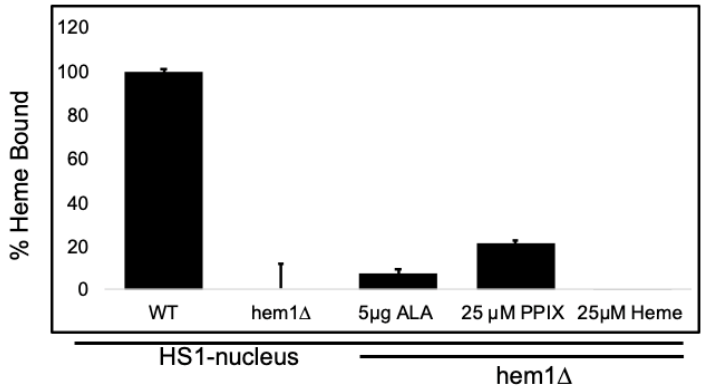

Figure 5.5 - PPIX supplementation binds to our nuclear sensor more than any other treatment or compartment. % Heme bound is calculated from the fluorimetric determination of EGFP/mKATE2 fluorescence ratios of the indicated yeast strains expressing HS1 in the nucleus. Measurements represent the mean of three biological clones.

For mitochondrial heme availability, it was very interesting to observe that supplementation with ALA, heme, or PPIX were incapable of making heme bioavailable to interact with our sensor. (**Figure 5.6**) It is possible that endogenous heme made in these supplemented cells with ALA and PPIX are being used for cytochromes in the mitochondria, preventing the formation of a labile pool. For the case of exogenous heme, it might not be regulated and delivered to the hemoproteins in the mitochondria due to the inability to transport it.

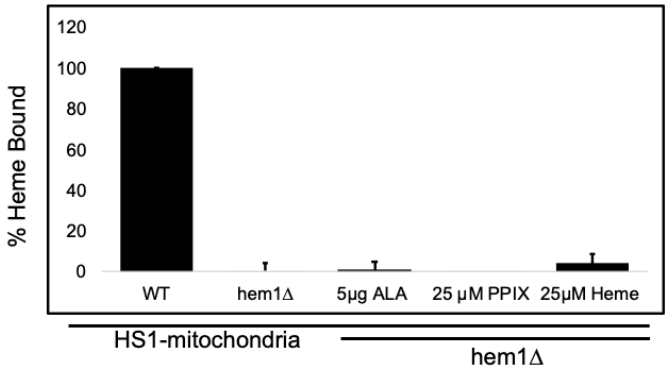

Figure 5.6 – No treatment made heme bioavailable in the mitochondria. Only heme supplementation seemed to have some heme available in the mitochondria. % Heme bound is calculated from the fluorimetric determination of EGFP/mKATE2 fluorescence ratios of the indicated yeast strains expressing HS1 in the mitochondria. Measurements represent the mean of three biological clones.

Overall, we were able to observe the changes in cellular heme distribution between exogenous and endogenous heme. Endogenous heme was more efficiently made bioavailable than exogenous

heme, especially in cells supplemented with ALA. Cells provided with ALA showed a higher mobilization of heme in the cytosol than any other compartment measured. Upon addition of PPIX in the media, it was observed that the majority of the heme made was mobilized to the nucleus.

5.2.3 Heme Dependent Processes of a hem1Δ with Supplementation of Exogenous Heme and Heme Intermediates.

We next tested the activity of certain heme dependent processes upon the addition of exogenous heme or heme intermediates to make endogenous heme. The activation of heme dependent nuclear transcription factors such as Hap1 is one process we were very interested in measuring due to the relatively high amount of nuclear heme when cells are supplemented with PPIX. The other heme dependent process we were interested in measuring was the activity of catalase, a cytosolic protein that requires heme to facilitate the decomposition of hydrogen peroxide to water and oxygen. The activity readout of this heme dependent protein will allow us to confirm the heme levels in the cytosol observed with the thigh binding heme sensor.

To further examine the activity of the heme dependent transcription factor Hap1, a transcriptional reporter was designed in which an eGFP expression is driven by Hap1 regulated CYC1. Upon heme binding, Hap1 protein will be heme loaded and activated, consequently leading to binding the CYC1 promoter and activating the expression of eGFP. The more eGFP present in the cell is translated as more heme available to activate Hap1 inducing the higher expression of this fluorescent protein. In these experiments we observed that only endogenous heme activated Hap1, especially the ALA treated sample. (**Figure 5.7**) The sample supplemented with PPIX displayed half the Hap1 activation than the ALA treated samples but double the activation than the exogenous heme treated. Even though ALA had half the heme availability than PPIX in the

nucleus according to the targeted sensor, we observed that it was more efficient at activating the transcription factor Hap1 than PPIX.

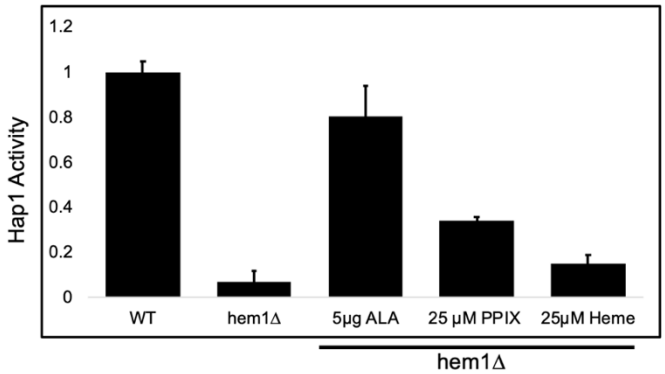

Figure 5.7 – PPIX displayed the highest Hap1 activity correlating with heme availability in the nucleus. Hap1p activity in the indicated strains as measured by a transcriptional reporter that used EGFP driven by the CYC1 promoter, a Hap1p target gene. Measurements represent the mean of three biological clones.

For the catalase activity measurements, an in-gel activity stain was utilized that contains a staining solution of H_2O_2, DMSO, dopamine and para-phenylenediaminein dissolved in a 0.2 M potassium phosphate buffer. This staining method takes advantage of the catalase reaction by generating a 2-electron oxidation to dopamine that will facilitate the attack of para-phenylenediamine to the quinone in the amine in a Michael type addition to make the benzoquinone, which is purple. The more the purple coloration corresponds with more catalase activity. This due to either increased heme availability or to increased catalase expression, which is addressed by the western blot probing for cytosolic catalase (Ctt1). When we tested the catalase activity for endogenous or exogenous heme, we observed that the only supplementation treatment capable of generating some active catalase was the heme intermediate ALA. (**Figure 5.8**) For the case of PPIX and heme, even though these supplementations generated similar total heme concentrations as the ALA treated sample, they did not make the heme bioavailable to the cytosol or catalase. According to the western blot, the lack of catalase activity is mainly due to the fact

that there was not expression of catalase with the addition of heme or PPIX. This is consistent with the fact that Ctt1 expression is driven by Hap1.

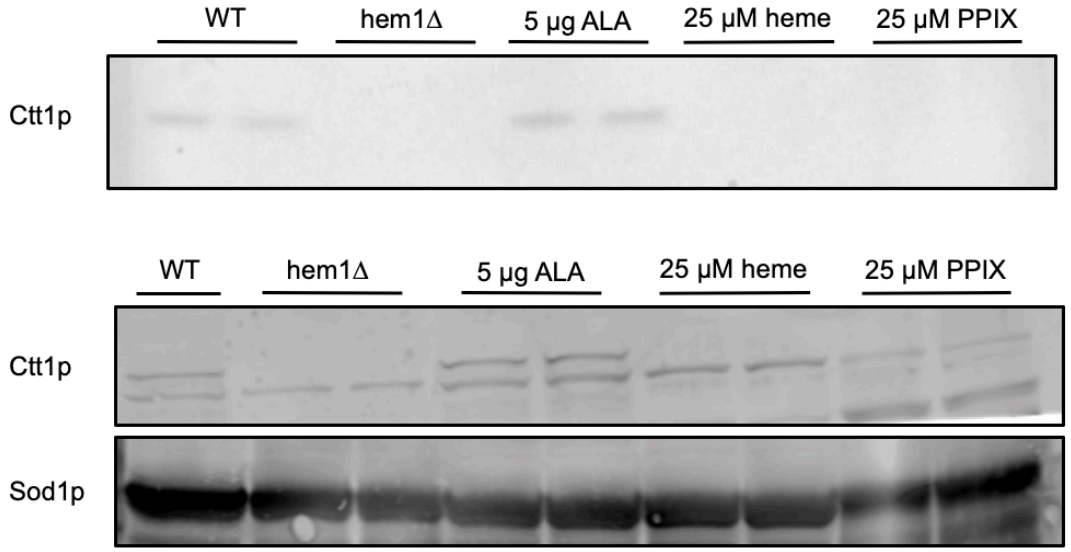

Figure 5.8 – Only endogenous heme by supplementing with ALA presented catalase activity and expression. In-gel activity assay for cytosolic catalase, Ctt1p, in the indicated strains. Cells were grown to mid-log phase in SC media. Immunoblots and catalase activity are representative of two independent trials.

5.2.4 Heme Uptake Improvement by Iron Starving S. cerevisiae.

In order to identify conditions that improve heme acquisition in *S. cerevisiae* we decided to test labile heme availability for different organelles in a WT cell that has been iron starved. In *C. albicans* iron starvation models have been a crucial method for the identification of heme transporters such as Shu1 and Str3[41, 42]. To test this model in Bakers' yeast, we utilized the iron chelator bathiphenanthrolinedisulfonic acid disodium salt hydrate (BPS) in WT cells to generate the iron starvation conditions. Iron starve cells were then supplemented with or without heme and the labile heme was measured in the cytosol with our high affinity heme sensor. A heme acquisition improvement was observed for all the BPS plus heme samples and 10μM BPS was identified as the proper concentration for generating the iron starvation. (**Figure 5.9**)

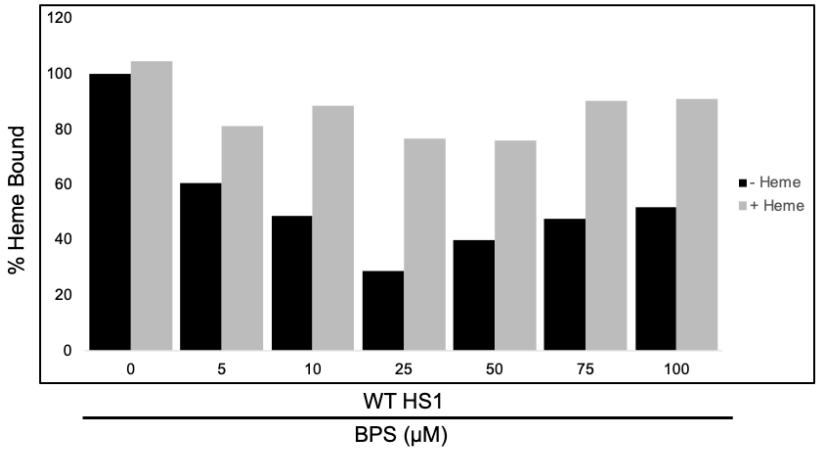

Figure 5.9 – Heme acquisition improves during iron starvation conditions. Heme uptake was measured by titrating *hem1*Δ with iron chelator BPS and then treated with and without heme. % Heme bound is calculated from the fluorimetric determination of EGFP/mKATE2 fluorescence ratios of the indicated yeast strains expressing HS1 in the mitochondria. Measurements represent the mean of three biological clones.

To characterize the heme distribution upon heme uptake under iron starvation conditions, targeted sensors to the cytosol, nucleus, and mitochondria were used. In addition, heme synthesis inhibitor succinylacetone (SA) was used to test inorganic iron deficiency and not a heme deficiency was the reason of heme uptake improvement. Labile heme measurement demonstrated that heme acquisition was improved in every organelle upon iron starvation conditions. (**Figure 5.10**) Heme starved cells in which SA was supplemented did not displayed a heme uptake in any of the organelles measured. Similar results were observed for WT iron starved cells expressing the weaker binding heme sensor.

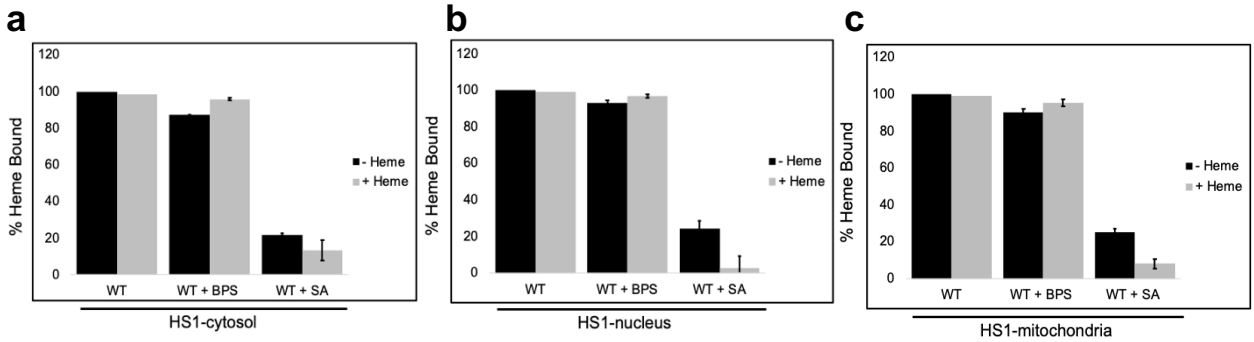

Figure 5.10 – Iron starvation facilitates heme uptake in every quantified organelle. Heme uptake was measured by titrating *hem1*Δ with iron chelator BPS or SA and then treated with and without heme. % Heme bound is calculated from the fluorimetric determination of EGFP/mKATE2 fluorescence ratios of the indicated yeast strains expressing HS1 in the **a.** cytosol, **b.** nucleus, **c.** mitochondria. Measurements represent the mean of three biological clones.

5.2.5 Heme uptake improvement under iron starvation is controlled by Heme Oxygenase

To identify if the uptake improvement under iron starvation conditions in *S. cerevisiae* was heme oxygenase dependent, similar heme availability measurements in the cytosol were performed in a heme oxygenase deficient mutant. Heme oxygenase (Hmx1) is the protein in charge of degrading heme into biliverdin, ferrous iron and carbon monoxide. The majority of organisms that are capable of heme uptake, the heme is usually degraded providing an iron source for biological functions. The *hmx1Δ* cells treated with or without the iron chelator BPS displayed similar heme availability, indicating there was no uptake under iron starvation conditions. Additionally, BPS treated *hem1*Δ did not exhibit any heme uptake for the cytosol.

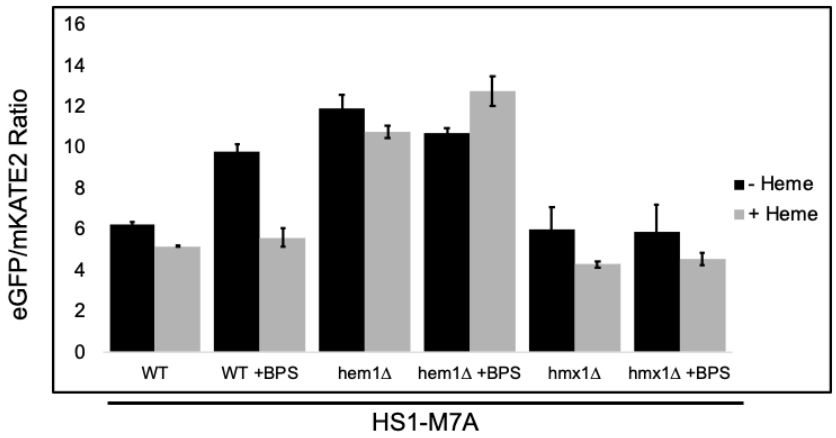

Figure 5.11 - Heme acquisition improvement by iron starvation is dependent upon heme oxygenase expression. Heme uptake was measure by titrating *hem1*Δ with iron chelator BPS and then treated with and without heme. % Heme bound is calculated from the fluorimetric determination of EGFP/mKATE2 fluorescence ratios of the indicated yeast strains expressing HS1 in the mitochondria. Measurements represent the mean of three biological clones.

5.2.6 High through-put screen for the identification of genes that regulate heme uptake.

To identify factors such as transporters or chaperones, that regulate heme uptake and availability, we screened the haploid yeast deletion collection by measuring heme acquisition using the weaker binding heme sensor, HS1-M7A. We based this method on the idea of if a certain gene that prevents uptake is deleted, we would observe an improvement in heme uptake, allowing us to

identify negative regulators for heme acquisition. From the screen we will be able to identify three possible groups: first, genes involved in a specific pathway that generates a condition that facilitates heme uptake. The second group is the transporters in which upon deletion they can no longer facilitate heme mobilization into the cell. Finally, the third group is the receptors that can sense heme outside the cell and prevent heme acquisition through signaling events.

For the heme availability measurements, cells were grown until saturation and then diluted in media supplemented with and without heme. The next day, fluorescence reads for the eGFP and mKATE2 channels were measured and the sensor fluoresce ratio for cells supplemented with and without heme were calculated. To identify increases and decreases of heme uptake, a ratio of the ratios was calculated in which the sensor fluorescence ratio of the non-heme treated sample was divided by the ratio of the heme treated sample. A ratio of ratios that is higher than one means an increase in heme acquisition. If the ratio of ratios is lower than one, this indicates a decrease in heme acquisition or heme availability. Finally, if the number is one it indicates that both samples have similar number of heme availability.

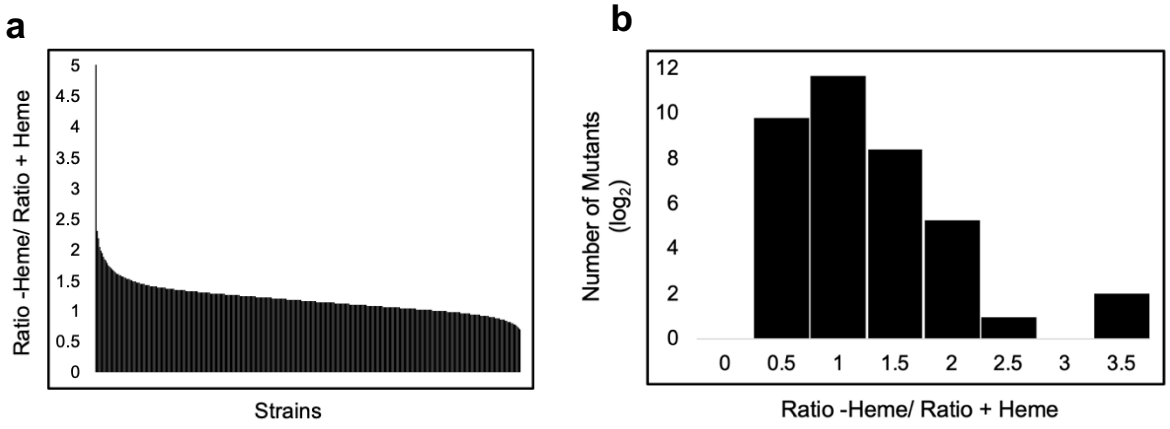

Figure 5.12 – Genome-wide high through-put screen data for heme acquisition. **a**. Ratio of ratios were calculated from the fluorescence ratios eGFP/mKATE2 expressed on the mutants with and without heme treatment. Positive numbers indicate high heme uptake and negative numbers indicate low heme uptake upon heme supplementation. **b.** Distribution of ratio of ratios in which the majority of the deletion mutants accumulate in no uptake change around a ratio of ratios of 1. Data was calculated from duplicated samples.

In Figure 5.12a we can observe an overview of the data from the heme uptake screen in which shows the distribution of the ratio of ratios. It could be observed that the majority of the gene deletion mutants did not seem to present any changes in heme uptake since they clustered in the area of ratio of ratios of one. In the screen, 4,470 genes stably expressed the sensor and were screened in which we were able to identify 33 genes with a ratio of ratios of 2.0 or higher, indicating an increase in heme availability in the heme treated sample. (**Figure 5.12a**) Around 3,438 genes, which accounts for 77% of all genes screened, displayed similar sensor fluorescence ratios for non-heme treated and heme treated samples. (**Figure 5.12b**)

5.2.6.1 Genes that regulate heme acquisition.

33 deletion mutants displayed a ratio of ratios of 2.0 or higher indicating that the heme availability for the heme treated sample in these mutants was higher than the non-treated sample. (**Table 5.1**) To identify localization enrichments for the 33 genes, we analysed the list of genes using PANTHER, which is a publicly available web-based resources that conducts gene ontology analysis. The results did not point out any specific compartment with a statistical significance and the majority of the cellular components had only one gene represented. We next assessed the biological function of these genes in order to determine if there were common pathways that might regulate heme availability. Similar to the cellular component classification data, the results did not point out any specific pathway or biological process with a statistical significance.

Due to the inability to establish any cellular component or biological process relationship, we proceeded by analysing the genes individually. We identified a couple of genes involved in regulating protein expression such as GAT1, URM1 and MIG3. They genes are interesting in the sense that they could be regulating the expression of factors that facilitate heme uptake. Ribosomal proteins were also identified including RSM23 and MRPL22, in which they could be acting as

heme delivery factors while they translate proteins. Two cell wall membranes were included in the list: BGL2, is a cell wall maintenance protein involved in newly synthesize mannoprotein incorporation. The second one was FLO1, which is a GPI-anchored cell surface glycoprotein required for the formation of fibrous interconnections between cells possibly helping in the communication between the cells about the environment. The ERV29 gene, involved in vesicle formation and incorporation of specific secretory cargo is also an interesting protein due to our conclusions in Chapter 2 of heme being mobilized through vesicles. And finally, two very compelling genes were identified for being transporters of metals into the cell, SFM3 that is an iron transporter and MFM1, a mitochondrial magnesium transporter.

Table 5.1: Genes identified to improve heme acquisition from the high through-put screen.

Systematic name	Gene name	Ratio of Ratios	Name description
YGR282C	BGL2	2.5	Beta-GLucanase
YIL088C	AVT7	2.4	Amino acid Vacuolar Transport
YGR284C	ERV29	2.4	ER-Vesicle
YER183C	FAU1	2.4	Folinic Acid Utilization
YIL059C	YIL059C	2.4	Not characterized
YGR287C	IMA1	2.3	IsoMAltase
YGR288W	MAL13	2.3	MALtose fermentation
YFL021W	GAT1	2.3	Trancriptional activator
YGL129C	RSM23	2.3	Ribosomal Small subunit of Mitochondria
YFL015C	YFL015C	2.3	Not characterized
YPR158W	CUR1	2.2	Curing of [URe3]

Table 5.1 (continued)

YIL084C	SDS3	2.2	Suppressor of Defective Silencing
YNL177C	MRPL22	2.2	Mitochondrial ribosomal protein of large subunit
YGR256W	GND2	2.2	6-phosphoGlucoNateDehydrogenase
YDR459C	PFA5	2.2	Protein Fatty Acyltransferase
YPL046C	ELC1	2.2	ELongin C
YHR033W	YHR033W	2.2	Not characterized
YPL056C	LCL1	2.1	Long Chronological Lifespan
YMR302C	YME2	2.1	Yeast Mitochondrial Escape
YIL087C	AIM19	2.1	Altered Inheritance rate of Mitochondria
YPL021W	ECM23	2.1	ExtraCellular Mutant
YIL008W	URM1	2.1	Ubiquitin Related Modifier
YIR019C	FLO11	2.1	FLOcculation
YGR122C-A	YGR122C-A	2.0	Not characterized
YFR016C	YFR016C	2.0	Not characterized
YER137C	YER137C	2.0	Not characterized
YGL151W	NUT1	2.0	Negative regulation of URS Two
YKR067W	GPT2	2.0	Glycerol-3-Phosphate acylTransferase
YER028C	MIG3	2.0	Multicopy Inhibitor of Growth
YLR034C	SMF3	2.0	Metal ion trasnporter
YPR106W	ISR1	2.0	Inhibition of Staurosporine Resistance
YOR241W	MET7	2.0	METhionine requiring

5.2.7 Role of mfm1Δ in heme uptake.

From the 33 genes identified to improve heme acquisition upon deletion, the protein Mfm1 was one that displayed an extreme phenotype for heme uptake. Mfm1 is a mitochondrial inner membrane magnesium transporter involved in the maintenance of magnesium concentration in the mitochondria and also membrane potential. We observed a higher heme availability in a *mfm1*Δ cell when it was supplemented with heme. (**Figure 5.13a**) Total heme measurement in *mfm1*Δ and a WT were done in order to validate the heme mobilization into the cell. Total heme levels demonstrated heme uptake for both WT and the *mfm1*Δ strains. (**Figure 5.13b**)

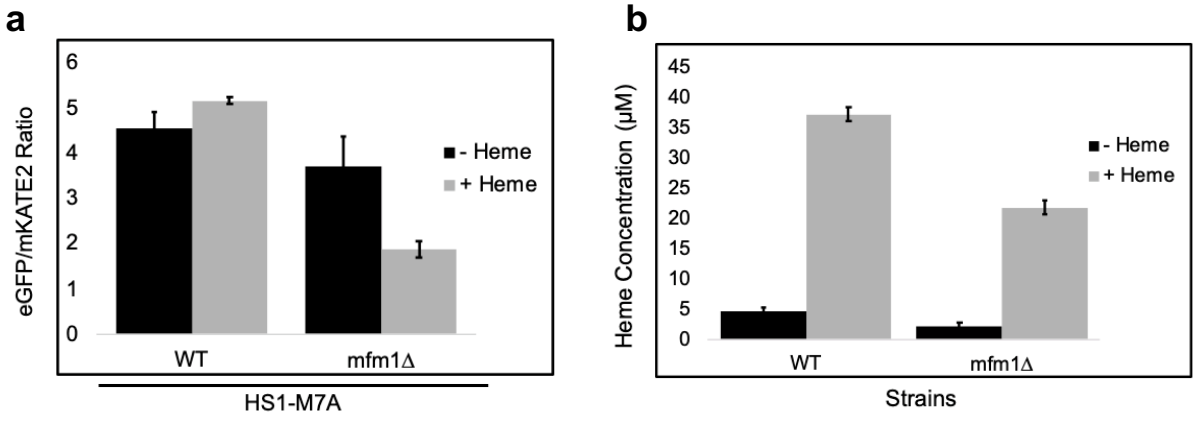

Figure 5.13- Mfm1 is a negative regulator for heme acquisition. **a.** Cytosolic fluorimetric determination of EGFP/mKATE2 fluorescence ratios of the indicated yeast strains expressing HS1-M7A. **b.** Total heme levels of the indicated strains as determined by HPLC. Measurements represent the mean of three biological clones.

Since Mfm1 is responsible to maintain the membrane potential of the mitochondria, we wanted to understand if disruption in membrane potentials is a condition that favors heme acquisition. Heme uptake in a rho0 mutant, a strain that is deficient on mitochondrial DNA, displayed no changes in heme uptake between the heme supplemented and non-heme supplemented samples. Similar results of no heme acquisition were observed in the case of WT cells, while for the *hem1*Δ we noticed small increased in heme uptake. (**Figure 5.14**)

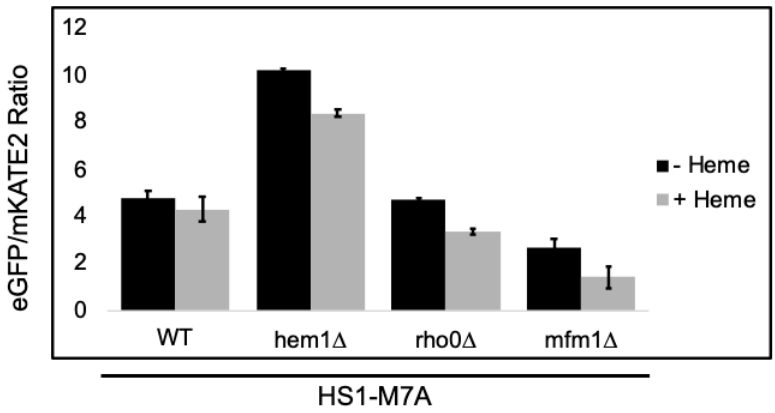

Figure 5.14- Mfm1 deletion facilitates heme uptake through changes in mitochondrial membrane potential. Heme uptake was measured by treating cells overnight with and without heme. Fluorimetric determination of EGFP/mKATE2 fluorescence ratios of the indicated yeast strains expressing HS1-M7A in the cytosol. Measurements represent the mean of three biological clones.

5.3 Discussion

In order to understand how *S. cerevisiae* is capable of importing heme into the cell and if endogenous and exogenous heme are distributed and utilized differently, we measured heme availability using genetically encoded fluorescent heme sensors under high supplementation of heme. The measurements of growth rescue displayed a rescue when supplemented with heme and heme intermediates, but not in the same degree or density as WT cells. For PPIX and heme supplementation, similar growth rescue to high ALA concentrations were achieved, but their total heme levels were half of the cells supplemented with ALA. Inefficient uptake of the protoporphyrin and accumulation of the heme intermediate could be causing PPIX to not be turnover into heme quickly enough by ferrochelatase. Cytotoxicity due to ALA accumulation in the supplemented cells might explain the similar cell rescue as the cells treated with PPIX and heme. Even though 5 μg/mL ALA only displayed half the growth rescue than 25 μM of heme and PPIX, we identified that they contain similar total heme concentrations. More readily and intact incorporation of heme in the PPIX and heme supplemented cells can explain the better rescue these samples have in comparison to the lower doses of ALA. A delay in heme biosynthesis in the ALA

supplemented cell could be responsible for slower mobilization of heme and not incorporating it into the hemoproteins as fast and supplemented with heme.

For the labile heme distribution, we observed endogenous heme was made bioavailable more efficiently than exogenous heme, localizing mainly in the cytosol and the nucleus. Supplementation with exogenous heme was observed to be made more bioavailable in the mitochondria. In erythroid cells, mitochondrial heme biosynthesis enzymes have been found to be through the formation of a metabolon or a heme biosynthetic complex in which PGRMC1, a progesterone receptor membrane component that required heme, was identified to interact with ferrochelatase and suggested to be a heme chaperone[23, 24]. If exogenous heme is not loaded into ferrochelatase in the same manner than when it is made endogenously, then it might not be able to be delivered to heme chaperones through a hem15 interaction. This would result in an accumulation of heme in the mitochondria since is not being mobilized through canonical pathways that can be detected by our heme sensors.

Cells treated with PPIX displayed a higher labile heme pool in the nucleus than any other compartment and supplementation. This high accumulation of heme in the nucleus could be explained if once PPIX is introduced into the cell facilitated by its transporter Pug1[169], it gets mobilized through intraorganellar membrane contact points in which it can get converted into heme and mobilized preferentially to the nucleus. Ferrochelatase activity has been identified in not only the mitochondria, but also the ER[170] and intraorganellar contact points such as ERMES[171, 172]. The ER was also found to be a very important localization for the mobilization of exogenous and endogenous heme in mammalians cells, suggesting a hierarchical subcellular compartment localization for heme[173]. Perhaps PPIX gets mobilized to the ER, loaded with iron through the ferrochelatase activity there or in ERMES and favored to be moved into the nucleus. More

experiments will need to be done in order to test this model. Heme trafficking kinetics experiments supplementing heme and ALA to the cell would determine if heme is mobilized to the nucleus first in PPIX supplementation, but not in ALA supplementation.

To verify the heme availability levels for endogenous and exogenous heme determined by the heme sensor, we tested the activity of heme dependent proteins localized in a certain compartment. Using the transcriptional reporter for Hap1, a heme dependent transcription factor, we observed that indeed endogenous heme, preferentially heme synthesized after ALA supplementation, seemed to have a higher activation of Hap1 than any other supplementation. PPIX treatment indeed displayed the highest labile heme concentration in the nucleus but not the highest Hap1 activation, in which ALA was the most successful one. Overall, endogenous heme was more efficient than exogenous heme in the activation of heme dependent transcription factors possibly due to pathways of heme mobilization that are more efficient in delivering heme to the low affinity hemoproteins.

In order to confirm the levels of bioavailable heme in the cytosol, catalase activity was measured using a colorimetric assay[100]. Only endogenous heme was capable of activating catalase activity, mainly because catalase expression was only active when supplemented with ALA. Why was catalase was not being expressed under PPIX and heme treatments, if all of the supplementation conditions generated similar levels of total heme? Since ALA treatment displayed the highest heme availability in the cytosol, catalase expression might be regulated by a specific cytosolic heme concentration that PPIX and heme are not necessarily reaching. Expression of catalase being regulated by ALA availability could be another possibility. Possible higher concentrations of PPIX and heme for supplementation that are buffered to prevent cytotoxicity and increase solubility could be used to test catalase expression in the future.

In *S. pombe* iron regulated heme transporters Shu1 and Str3 were identified under iron starvation conditions[41, 42]. Since *S. cerevisiae* has not been shown to be efficient at heme uptake in a high affinity manner, we decided to test if iron starvation affected heme uptake. Using the tight and weak binding sensors we observed iron starvation increased heme uptake in every single compartment measured. This increase was iron specific since heme depleted cells treated with and without heme did not seem to have any differences in heme availability. Cells seem to uptake heme mainly as an iron source since iron starve *hmx1*Δ cells supplemented with heme did not seem to uptake it. To characterize further the heme acquisition by iron starving the cells, more experiments will need to be done. For example, measuring iron levels on the samples treated with BPS and BPS plus heme to confirm iron starvation and heme degradation. Measuring transcriptional levels and increases upon iron starvation will allow us to elucidate factors facilitating heme insertion into the cell under these conditions.

From the 4,470 genes screened for heme availability supplemented with and without heme, we observed that almost 77% of the deletion mutants did not displayed any divergence under the different conditions. This result establishes the high number of genes that are not related to heme acquisition; very different from what we observed for heme homeostasis, in which the majority of the deletion mutants displayed even a minimal change. From the screen we were able to identify 33 genes acting as negative regulators, upon deletion they improve heme availability in the cell. While we were not able to identify a common function or cellular location that stood out form these genes, several were of interest. Two genes that we consider very compelling were SFM3 that is an iron transporter and MFM1, a mitochondrial magnesium transporter. We observed that iron starvation facilitates heme uptake which can explain the results of SMF3, but what is the effect of affecting magnesium uptake.

We were able to identify the negative regulator for heme uptake Mfm1 that upon deletion increased heme acquisition. Additionally, we were able to observe that mitochondrial membrane potential seems to play a role in heme uptake, since *rho0* mutants displayed increased heme uptake similar to the *mfm1*Δ cells. It is known that under limited magnesium bioavailability, fluid-phase endocytosis seems to be upregulated facilitating the transferring of solutes taken into the vacuole[174]. Mfm1 deletions could cause disruptions of Mg^{2+} availability, activating then this fluid-phase endocytosis that lead to the uptake of not only magnesium but heme as well since it is in high concentrations in the media. In the membrane potential case in *rho0*, the solutes inside the cell are disrupted and potentially signals the cell to activate diffusion in order to recover the membrane potential facilitating the entry of heme.

Overall, we were able to demonstrate that exogenous and endogenous heme seem to distribute heme differently. We show *S. cerevisiae* is capable of heme acquisition under high heme conditions and that heme uptake could be improved by iron starving the cells. Endogenous heme seems to populate and activate heme dependent processes more efficiently than exogenous heme. We were also able to identify genes that act as negative regulators for heme uptake, Mfm1 being one that the deletion facilitated heme uptake. This might be due to a decrease of magnesium in the mitochondria upon deletion of Mfm1, which would upregulate endocytosis that might favor heme entry. Deletion of Mfm1, could also alter mitochondrial membrane potential, since a *rho0* mutant similarly increased heme uptake. Experiments like overexpression screens, heme availability screen under iron starvation conditions and more characterization of the genes identify would help to elucidate more novel factors for heme acquisition. This work paves the path to further understanding of heme mobilization and utilization and identification of novels heme regulators for heme uptake.

5.4 Materials and Methods

5.4.1 Cell Strains, Transformation, Growth Conditions and Plasmids

5.4.1.1 Yeast Strains and Growth

S. cerevisiae strains used in this study were derived from BY4741 (MATa, *his3*Δ1, *leu2*Δ0, *met15*Δ0, *ura3*Δ0). All yeast haploid deletion mutant strains were obtained from the yeast gene deletion collection (Thermo Fisher Scientific). We also utilized the previously reported strain DH001b-3 (*hem1*Δ::*HIS3*) [3]. All strains derived from the yeast deletion collection were confirmed by sequencing the unique barcodes flanking the *KanMX4* deletion cassette.

5.4.1.2 Yeast Transformation

Yeast transformations were performed by the lithium acetate procedure [49]. Strains were maintained at 30° C on either enriched yeast extract (1%) - peptone (2%) based medium supplemented with 2% glucose (YPD) and G418 (200 μg/mL) or synthetic complete medium (SC) supplemented with 2% glucose and the appropriate amino acids to maintain selection[3]. Cells cultured on solid media plates were done so with YPD or SC media supplemented with 2% agar [3]. Selection for yeast strains containing the KanMX4 marker was done with YPD agar plates supplemented with G418 (200 μg/mL) [3]. Cells for the screen were resuspended in SC media supplemented with 15 mg/mL of ergosterol and 0.5% Tween-80 (SCE). All liquid cultures were maintained at 30 °C and most were done in standing cultures.

5.4.1.3 Plasmids

Cytosolic, mitochondrial, and nuclear-targeted heme sensors, HS1, were sub-cloned into pRS415 and driven by *ADH*, *TEF*, or *GPD* promoters as previously described[3]. PCR based

mutagenesis was used to generate the affinity variants of HS1 (M7A)[3]. The Hap1 reporter plasmid in which eGFP is driven by the *CYC1* promoter was also previously described [3].

5.4.2 Experimental Methods

5.4.2.1 Catalase Activity Measurements in Yeast

WT yeast cells expressing empty vector (p415-GPD), or HS1-M7A driven by the GPD, TEF1, or ADH1 promoters (p415-GPD-HS1-M7A, p415-TEF1-HS1-M7A, p415-ADH1-HS1-M7A) were cultured in SC-LEU media for ~14-16 hours to mid-exponential phase (an optical density at 600 nm of $OD_{600\ nm}$ ~ 1-2). Cells were harvested and lysed in phosphate buffer and 10 μg of protein lysate were subjected to native PAGE on a 10% tris-glycine gel (Invitrogen). After electrophoresis, an in-gel activity stain was utilized to measure catalase activity[100]. Briefly, a catalase staining solution containing 1 part Dopamine (20mg/mL) in pH 8 0.2 M KP_i buffer, 1 part para-phenylenediamine (3.5mg/mL) in pH 8 0.2M KP_i, 1 part 15 % H_2O_2, and 2 parts DMSO were mixed in the order listed. The staining solution was added directly to the gel and allowed to stain for 2 minutes, followed by rinsing in Milli-Q water and imaging.

5.4.2.2 Total Heme Quantification in Yeast

Heme was quantified using a protocol adapted from the method of Woods and Simmonds[101]. Briefly, yeast were cultured in 25 mL of YPDE media for 15 hours to a density of 1 $OD_{600\ nm}$/mL. Cells were harvested, washed in ice-cold Milli-Q water, and lysed in three pellet volumes of acid-acetone (9.75 mL acetone, 0.250 mL concentrated HCl). Lysis was achieved at 4 C using one pellet volume of zirconium oxide beads and a bead beater (Bullet Blender, Next Advance) on a setting of 8 for 3 minutes. After homogenization, lysates were clarified by centrifugation at maximum speed on a table-top centrifuge. 50 μL of an acid-acetone extract of heme was diluted into 50 μL of 0.1% trifluoroacetic acid in a 1:1 mixture of water and acetonitrile.

Heme was quantitated by HPLC using a flow rate of 1 mL/min and elution gradients going from 50% acetonitrile in water, 0.1% TFA to 100% acetonitrile, 0.1% TFA over 10 minutes on a C-18 column (Poroshell 120, SB-C18, 4.6 x 100 mm, 2.7 um). Heme was quantified relative to hemin chloride standards run in parallel and normalized for cell number. Cellular heme concentration was determined by assuming a yeast cell volume of 50 fL. Heme was unambiguously identified from its retention time and characteristic UV/visible spectrum using a photodiode array detector coupled to the HPLC.

5.4.2.3 HAP1 Transcriptional Reporter Assay

Yeast cells expressing p416-CYC1- EGFP, or EGFP driven by the Hap1p regulated CYC1 promoter, were cultured in 10 mL of SCE-URA media for 15 hours to a to a density of 1 OD_{600} nm/mL. Cells were resuspended in PBS to a concentration of 1 x 10^8 cells/mL and 100 uL was used to measure EGFP fluorescence (ex. 488 nm, em. 510 nm). As a positive and negative control, WT and *hem1*Δ cells were cultured for each experiment. Background auto- fluorescence of cells not expressing EGFP was recorded and subtracted from the EGFP expressing strains.

5.4.2.4 Immunoblotting

Yeast were cultured in 10 mL of SC media for 15 hours to a density of 1 $OD_{600\ nm}$ /mL. Cells were harvested, washed in ice-cold Milli-Q water, and lysed in two pellet volumes of phosphate buffer supplemented with protease inhibitors as described previously[102, 103]. Lysis was achieved at 4 C using one pellet volume of zirconium oxide beads and a bead beater (Bullet Blender, Next Advance) on a setting of 8 for 3 minutes[102, 103]. Lysate protein concentrations were determined by the Bradford method (Bio-rad) and 12% tris-glycine gels (Invitrogen) were employed for SDS-PAGE[102, 103]. Anti-GFP rabbit or anti-GAPDH polyclonal antibodies (Genetex) and a goat anti-rabbit secondary antibody conjugated to a 680 nm emitting fluorophore (Biotium)

were used to probe for GAPDH. All gels were imaged on a LiCOR Odyssey Infrared imager[102, 103].

5.4.2.5 High Through-put transformation

Yeast high through-put transformations were performed in the standard clear sterile 96 well plates and by: a. preculturing the cells in 200 µL YPD G418 (200 µg/mL) media until saturation (48 hours); b. diluted the cells in 200 µL of YPD G418 and grown for 14-16 hour at 30°C standing; c. transforming cells using the lithium acetate procedure adapted for 96 well plates[57]; d. incubating the cells with the transformation reagents for 6 hours at 42°C on the standing incubator on a Mary bath set up; e. resuspending cells in SCE media with the appropriate amino acids to maintain selection[3]. Plates were incubated for 96 hours and then diluted in fresh SCE media supplemented with the appropriate amino acids to confirm and maintain selection until saturation (48 hours.).

5.4.2.6 High Through-put Screen

Cytosolic HS1-M7A expressing cells were cultured in standard clear sterile 96 well plates. Duplicate cultures were seeded in 200 µLof SCE media with the appropriate amino acids to maintain selection[3] standing until saturation (48 hours.). The cells were diluted into 200 µL SCE-LEU supplemented with heme dissolved in 50% DMSO and 50% 0.1M Tris HCL and grown standing for 14-16 hours at 30°C. After culturing cells were harvested, washed twice in 200 µL of sterile ultrapure water and finally resuspended in 200 µL of 1x PBS. HS1-M7A fluorescence was monitored on 200 uL of a 4 OD/mL (2 x 10^7 cells/mL) cell suspension using black Greiner Bio-one flat bottom fluorescence plates and a Synergy Mx multi-modal plate reader. eGFP (ex. 488 nm, em. 510 nm) and mKATE2 (ex. 588 nm, em. 620 nm) fluorescence was recorded every 30 seconds for 5 min.

CHAPTER 6. CONCLUSION AND FUTURE WORK

During the last ten years the understanding of heme homeostasis mechanism has been transformed and advanced significantly. The view for this essential cofactor has evolved from being a static cofactor to be a signaling molecule involved in many biological functions. Even though the knowledge about heme has increased thanks to the development of imaging tool, more questions have risen about the factors that regulate its homeostasis. Despite the tremendous importance of heme in physiology, the cellular and molecular mechanisms that govern the safe assimilation of heme into metabolism remain poorly understood. All the work done in this thesis is to contribute in the understanding of heme homeostasis by identifying factors that regulate steady-state heme availability, the dynamics of heme mobilization to different subcellular compartments as it is being synthesized, and heme uptake.

6.1 Genome-Wide Determinants of Heme Homeostasis

Through the use of the yeast haploid deletion collection in combination with genetically encoded fluorescent heme sensors we were able to identify genes involved in heme homeostasis. From the 4,470 genes screened, we were able to identify 114 strains that upon deletion displayed a higher cytosolic heme availability and 323 deletion mutants with low cytosolic heme availability. The screen was validated through the successful identification of heme biosynthetic factors including pyruvate transporters, pyruvate dehydrogenase, FAD transporters, glycine transporters, iron homeostasis, ALAS maturation and heme maturation as genes with low cytosolic heme availability. Proteins like GAPDH were identified from this screen as heme buffering factors, which was previously suggested as a heme binding protein. Functional groups like ESCRT proteins and vesicular trafficking proteins were identified to have an important role in heme

homeostasis and distribution. Even though this work will help in the understanding of heme trafficking, the regulation of heme homeostasis and as a tool for discovering heme buffering elements and new factors for heme biosynthesis and degradation, further characterization experiments are required.

This screen has provided us with abundant information on heme homeostasis, but further characterization is needed to validate that the factors identified are indeed playing a role in heme homeostasis. The identified genes have been arranged by localization and function, but further characteristic analysis by size, abundance, or solubility could assist in predicting protein functions as either buffering factors or transporters. For the case of the vesicular proteins and the ESCRT complex, further experiments such as deletion of genes in the ESCRT pathway and measuring heme distribution in different organelles are required in order to identify the crucial point for heme mobilization and to validate our model.

6.2 GAPDH

From the genome-wide screen for heme availability we were able to identify GAPDH as a possible heme buffering factor. This glycolytic enzyme was demonstrated to be a heme buffering factor that regulates heme mobilization and delivery to heme dependent transcription factors such as Hap1p. Additionally, the His53 in hGAPDH and His51 in yeast were characterized as crucial heme binding residue that not only regulated the heme buffering capacity but also the delivery to Hap1p. These results give us a new insight into how heme gets distributed and regulated within the cell. Our data suggest that the GAPDH heme pool is in equilibrium with the overall labile heme pool in the cell that is detected by the heme sensor, and that GAPDH is responsible for managing a significant portion of it. Once GAPDH binds heme, it makes it bioavailable to be inserted into cytosolic proteins like iNOS and for delivery to heme dependent transcription factors like Hap1p.

How exactly GAPDH is delivering heme to the Hap1p is still unknow, but we can suggest two possible pathways. One possibility is that GAPDH delivers heme through the direct contact with Hap1p, which could be supported by the idea of being able to shuttle or mobilized from the cytosol to the nucleus in specific conditions[92]. The alternative would be that heme delivery is mediated via an intermediary. Experiments to determine if the mechanism is through direct contact or an intermediary could be performed by targeting GAPDH to the mitochondria. This would maintain glycolytic functions, while probing heme distribution to the nucleus or testing activity of the transcription factor Hap1. Hap1 could also be truncated or targeted in the nucleus and do similar experiments. Overall, the identification of GAPDH as a heme buffering factor helps to expand the knowledge on how intracellular heme is trafficked and how heme homeostasis is maintained.

6.3 The Heme Biosynthesis Enzyme, 5-aminolevulinic Acid Synthase (ALAS), and GTPases in Control of Mitochondrial Dynamics and ER Contact Sites, Regulate Heme Mobilization to the Nucleus.

To understand the dynamics of heme mobilization out of the mitochondria, we developed a live-cell assay in yeast that uses the genetically encoded ratiometric fluorescent heme sensors (HS1) targeted to the mitochondrial matrix, cytosol, or nucleus[3, 87, 125], to monitor heme distribution kinetics and identify processes important for subcellular heme trafficking. Surprisingly, we found that heme trafficking rates from the matrix side of the IM to the mitochondrial matrix and cytosol are similar, while trafficking to the nucleus is ~25% faster. This indicates that heme is distributed from the mitochondrial IM to other locales simultaneously via multiple parallel pathways rather than sequentially. We were able to discover that the heme biosynthetic enzyme, ALAS, negatively regulates mitochondrial-nuclear heme trafficking, highlighting the close coordination of heme

synthesis and trafficking. In addition, we identified GTPases that directly (Gem1) and indirectly (Dnm1 and Mgm1) regulate ERMES as being modulators of nuclear heme transport. Based on our results, we propose a model in which heme is trafficked via ER- mitochondrial membrane contact sites to other organelles such as the nucleus.

One interesting observation from all of the deletion mutants analyzed for this project was how most of them presented their heme homeostasis disruptions mainly in the nucleus. Why mainly in the nucleus? There is the possibility that the disruption might be happening through the ER, but currently we do not possess an ER targeted sensor restricting our ability to observe it. The development of an ER targeted sensor would allow us to perform similar trafficking kinetics studies in the ER. Could it be due by nucleus volume and size? Titrations with the heme synthesis inhibitor SA, would allow us to measure if changes in total heme levels affect heme distribution only in the nucleus or if it gets disrupted in a similar manner as to the other compartments.

Altogether, the *in vivo* approach to monitor real-time dynamics of inter- compartmental heme trafficking coupled with molecular genetic approaches have uncovered fundamental aspects of the mechanisms underlying heme mobilization and utilization. We expect that the tools and approaches presented here may be used to probe a number of human diseases, including certain cancers, neurodegenerative disorders, and blood diseases, that are associated with both defects in heme homeostasis and mitochondrial dynamics and membrane contact sites[7, 114, 161]. Indeed, given that mitochondrial dynamics and contact sites with the endomembrane system are conserved between yeast and man, and the factors that regulate them have homologs or functional analogs between lower and higher eukaryotes[142, 162-165], our studies in yeast may be of broad applicability to better understand how membrane and organelle dynamics impacts heme transport and trafficking.

6.4 Uptake and Utilization of Heme and Heme Intermediates

In this chapter we demonstrated that exogenous and endogenous heme seem to distribute heme differently, showing *S. cerevisiae* is capable of heme acquisition under high heme conditions and iron starvation. We also identified genes that act as positive and negative regulators for heme uptake, Mfm1 being one that the deletion facilitated heme uptake. Membrane potential was observed to play a role since a *rho0* mutant seem to improve heme uptake too. From the 4,470 genes screened for heme availability supplemented with and without heme, we observed that almost 75% of the deletion mutants did not displayed any divergence under the different conditions. This result establishes the high number of genes that are not related to heme acquisition; very different from what we observed for heme homeostasis, in which the majority of the deletion mutants displayed even a minimal change. From the screen we were able to identify 374 genes acting as negative regulators, upon deletion they improve heme insertion into the cell. We also identified 113 genes as possible positive regulators, since the deletion of the genes seemed to decrease the amount of heme inserted into the cell.

Since in the screen we were mainly able to identify genes that acted as negative regulators for heme acquisition, we believed that an overexpression screen would be a good complementary data set to help us identify novel factors that regulate heme uptake. A heme availability screen under iron starvation conditions coupled with transcript expression levels will allow us to expand our knowledge of heme uptake factors and identify positive regulators for heme uptake. Further characterization of the genes identified in this screen would also help for elucidate the functional role these genes have in exogenous heme uptake and heme utilization. This body of work cements the foundation for further exploration of heme mobilization, utilization, and the identification of novel heme regulators for heme uptake.

6.5 Conclusions

- Genome-wide screen for bioavailable heme reveals that heme may be trafficked via intracellular vesicles.
- We identified transporters, metabolic enzymes, and uncharacterized Open Reading Frames that impact heme bioavailability; they remain to be characterized.
- GAPDH was identified as a heme chaperone responsible for the heme delivery to heme dependent transcription factors such as Hap1.
- We identified His51 in yeast GAPDH and His53 in human GAPDH to be important for heme binding in GAPDH and for the delivery of heme to the heme dependent transcription factors such as Hap1.
- Heme goes to the nucleus first, presumably to signal the presence of heme.
- Heme synthesis and trafficking are closely coupled, suggesting ALAS to not only be involved in heme biosynthesis but also regulating heme mobilization throughout the cell.
- Factors that regulate mitochondrial dynamics and ER-contact sites gate the flow of heme to the nucleus.
- Endogenous heme is more efficient in distributing heme throughout the cell and activating heme dependent processes than exogenous heme.
- Iron starvation is a condition that promotes heme uptake from the environment in *Saccharomyces cerevisiae* in a heme oxygenase dependent manner.
- The mitochondrial magnesium transporter, Mfm1 was identified as a negative regulator for heme uptake.

APPENDIX A. SUPPLEMENTAL TABLES AND FIGURES

A.1 Introduction

This appendix is meant to be used as supplementary information that was crucial for the research, but with much more detail. Kinetic information from the Pulse chase assay for measuring heme dynamics in Chapter 4 are also included. Microscopy data to confirm the mitochondrial phenotypes of the strains used in Chapter 4 are also included in this appendix.

A.2 Supplemented Tables

Table A.1 - Kinetic parameters derived from fits to the heme trafficking data using Equation 2. The values indicated represent the mean ± SD of independent triplicate cultures. *p<0.05, **p<0.01, ***p<0.001 by one-way ANOVA with Dunnett's post-hoc test. Red asterisks indicate statistical significance relative to the cytosol within a given strain. Black asterisks indicate statistical significance relative to the WT strain of a given compartment.

Strain	Location	$t_{1/2}$ (min)	k (min^{-1})	Amplitude (% Bound)	Lag Time (min)	Figure	Goodness of Fit (R^2)
WT	Cyt	86(4)	.032(.003)	93(5)	24(4)	Fig. 2e	.9908
	Nuc	75(3)*	.041(.002)*	87(4)	26(3)		.9851
	Mito	89(4)	.034(.003)	88(5)	29(4)		.9942
*hem1*Δ + ALA	Cyt	171(7)	.030(.003)	86(7)	104(7)	Fig. 3a	.9596
	Nuc	150(2)***	.055(.005)***	108(5)*	113(2)		.9739
	Mito	173(9)	.028(.004)	75(8)	102(9)		.9445

Table A.1
(continued)

WT	Cyt Nuc Mito	92(2) 84(3)* 93(2)	.033(.001) .039(.002)* .033(.002)	75(5) 91(6)* 75(4)	31(2) 33(3) 32(2)	Fig. 5a	.9926 .9724 .9914
*mgm1*Δ	Cyt Nuc Mito	90(4) 53(5)***/*** 85(5)	.034(.002) .06(.03) .037(.003)	74(6) 27(5)***/*** 77(6)	31(4) 20(5)*/* 31(5)	Fig. 5a	.9901 .8742 .9908
WT	Cyt Nuc Mito	97(3) 82(4)* 99(3)	.033(.002) .041(.001)* .034(.003)	85(6) 105(5)* 82(4)	36(3) 33(4) 40(3)	Fig. 5b	.9805 .9779 .9668
rho^{0}	Cyt Nuc Mito	85(2) 77(2)* 96(3)	.035(.002) .044(.003)* .034(.002)	98(5) 99(4) 93(5)	27(2) 31(2) 37(3)	Fig. 2b	.9797 .9768 .9795
WT	Cyt Nuc Mito	87(2) 78(3)* 93(3)	.033(.002) .042(.002)* .030(.002)	80(4) 100(6)* 78(4)	26(2) 30(3) 26(3)	Fig. 5c	.9854 .9692 .9783
*fzo1*Δ	Cyt Nuc Mito	89(2) 79(2)* 89(2)	.033(.002) .039(.002)* .032(.002)	87(5) 95(4) 90(4)	28(2) 28(2) 27(2)	Fig. 5c	.9888 .9805 .9897
WT	Cyt Nuc Mito	85(3) 75(2)* 87(2)	.031(.001) .041(.002)* .031(.002)	87(4) 94(5) 75(3)	20(3) 26(2) 22(2)	Fig. 2d	.9908 .9840 .9867
*ugo1*Δ	Cyt Nuc Mito	100(4) 77(3)* 96(3)	.028(.003) .039(.002)* .028(.001)	95(4) 102(6) 96(4)	28(4) 25(3) 25(3)	Fig. 5d	.9924 .9854 .9906

Table A.1
(continued)

WT	Cyt	89(2)	.030(.002)	88(4)	22(2)		.9889
	Nuc	75(2)*	.041(.002)*	105(5)*	26(3)	Fig. 5e	.9873
	Mito	92(2)	.032(.002)	83(4)	28(2)		.9824
*pcp1*Δ	Cyt	85(2)	.033(.002)	90(4)	24(2)		.9872
	Nuc	69(3)*	.045(.003)*	105(6)	24(3)	Fig. 5e	.9898
	Mito	90(3)	.034(.001)	86(5)	31(3)		.9859
WT	Cyt	119(3)	.033(.003)	78(5)	58(3)		.9886
	Nuc	110(4)	.041(.003)*	96(5)*	61(4)	Fig. 5f	.9488
	Mito	111(3)	.033(.002)	80(4)	50(3)		.9767
*mic60*Δ	Cyt	114(3)	.033(.003)	78(6)	54(3)		.9874
	Nuc	104(3)	.039(.003)*	96(5)*	53(3)	Fig. 5f	.9686
	Mito	114(2)	.031(.002)	81(4)	50(2)		.9876
WT	Cyt	102(3)	.030(.002)	80(4)	35(3)		.9833
	Nuc	88(4)*	.038(.002)*	85(6)	35(4)	Fig. 6a	.9449
	Mito	99(4)	.031(.001)	75(5)	34(4)		.9778
*dnm1*Δ	Cyt	80(2)	.038(.002)	93(4)	27(2)		.9874
	Nuc	64(2)*/*	.055(.003)*/**	105(5)*	27(2)	Fig. 6a	.9669
	Mito	82(2)	.036(.002)	93(3)	26(2)		.9885
WT	Cyt	86(2)	.032(.002)	87(3)	24(2)		.9876
	Nuc	75(3)*	.042(.003)*	93(4)	27(3)	Fig. 6b	.9827
	Mito	89(2)	.033(.002)	84(3)	28(2)		.9931
*fis1*Δ	Cyt	92(2)	.032(.002)	84(3)	30(2)		.9898
	Nuc	83(3)*	.040(.001)*	95(5)	33(3)	Fig. 6b	.9714
	Mito	95(3)	.032(.002)	80(4)	32(3)		.9820

A.3 Supplemental Figure

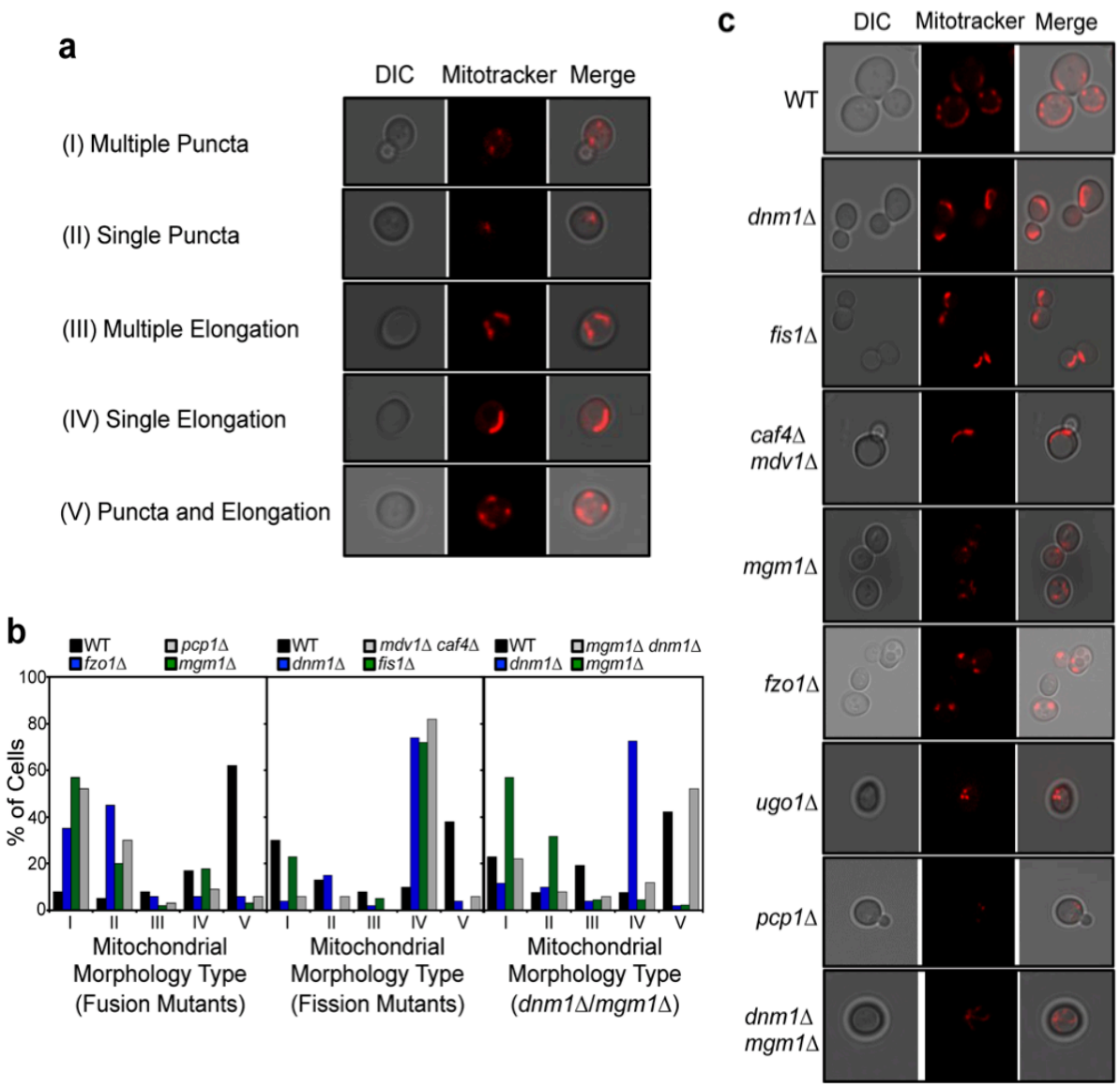

Figure A.1 - Validation of the mitochondrial network morphology defects in yeast fission and fusion mutants. (**a**) Sampling and classification of mitochondrial network morphologies observed using Mitotracker staining of cells. (**b**) Histograms of mitochondrial network morphology in the fission and fusion mutants used throughout this study. Mutants defective in mitochondrial fission exhibit an elongated mitochondrial network. Mutants defective in mitochondrial fusion exhibit a punctate mitochondrial network. WT and *mgm1*Δ *dnm1*Δ cells tend to have a more equal distribution of elongated and punctate mitochondrial networks. The histograms were generated by analyzing ~50 cells per mutant. (**c**) Representative images of the mitochondrial network in the fission and fusion mutants utilized in this study.

References:

[1] Donegan, R. K., Moore, C. M., Hanna, D. A., and Reddi, A. R. (2019) Handling heme: The mechanisms underlying the movement of heme within and between cells, *Free radical biology & medicine 133*, 88-100.

[2] Hanna, D. A., Martinez-Guzman, O., and Reddi, A. R. (2017) Heme Gazing: Illuminating Eukaryotic Heme Trafficking, Dynamics, and Signaling with Fluorescent Heme Sensors, *Biochemistry 56*, 1815-1823.

[3] Hanna, D. A., Harvey, R. M., Martinez-Guzman, O., Yuan, X., Chandrasekharan, B., Raju, G., Outten, F. W., Hamza, I., and Reddi, A. R. (2016) Heme dynamics and trafficking factors revealed by genetically encoded fluorescent heme sensors, *Proceedings of the National Academy of Sciences of the United States of America 113*, 7539-7544.

[4] Reddi, A. R., and Hamza, I. (2016) Heme Mobilization in Animals: A Metallolipid's Journey, *Accounts of chemical research 49*, 1104-1110.

[5] Severance, S., and Hamza, I. (2009) Trafficking of heme and porphyrins in metazoa, *Chemical reviews 109*, 4596-4616.

[6] Atamna, H., and Boyle, K. (2006) Amyloid-beta peptide binds with heme to form a peroxidase: relationship to the cytopathologies of Alzheimer's disease, *Proceedings of the National Academy of Sciences of the United States of America 103*, 3381-3386.

[7] Atamna, H., and Frey, W. H., 2nd. (2004) A role for heme in Alzheimer's disease: heme binds amyloid beta and has altered metabolism, *Proceedings of the National Academy of Sciences of the United States of America 101*, 11153-11158.

[8] Sassa, S. (2004) Why heme needs to be degraded to iron, biliverdin IXα, and carbon monoxide?, *Antioxidants & redox signaling 6*, 819-824.

[9] Kumar, S., and Bandyopadhyay, U. (2005) Free heme toxicity and its detoxification systems in human, *Toxicol Lett 157*, 175-188.

[10] Dawson, J. H. (1988) Probing structure-function relations in heme-containing oxygenases and peroxidases, *Science (New York, N.Y.) 240*, 433-439.

[11] Atamna, H., Brahmbhatt, M., Atamna, W., Shanower, G. A., and Dhahbi, J. M. (2015) ApoHRP-based assay to measure intracellular regulatory heme, *Metallomics 7*, 309-321.

[12] Song, Y., Yang, M., Wegner, S. V., Zhao, J., Zhu, R., Wu, Y., He, C., and Chen, P. R. (2015) A genetically encoded FRET sensor for intracellular heme, *ACS chemical biology 10*, 1610-1615.

[13] Heinemann, I. U., Jahn, M., and Jahn, D. (2008) The biochemistry of heme biosynthesis, *Archives of biochemistry and biophysics 474*, 238-251.

[14] Kikuchi, G., Yoshida, T., and Noguchi, M. (2005) Heme oxygenase and heme degradation, *Biochemical and biophysical research communications 338*, 558-567.

[15] Chuang, J.-Y., Lee, C.-W., Shih, Y.-H., Yang, T., Yu, L., and Kuo, Y.-M. (2012) Interactions between amyloid-β and hemoglobin: implications for amyloid plaque formation in Alzheimer's disease, *Plos One 7*, e33120.

[16] Seyfried, N. T., Dammer, E. B., Swarup, V., Nandakumar, D., Duong, D. M., Yin, L., Deng, Q., Nguyen, T., Hales, C. M., and Wingo, T. (2017) A multi-network approach identifies protein-specific co-expression in asymptomatic and symptomatic Alzheimer's disease, *Cell systems 4*, 60-72. e64.

[17] Wu, C.-W., Liao, P.-C., Yu, L., Wang, S.-T., Chen, S.-T., Wu, C.-M., and Kuo, Y.-M. (2004) Hemoglobin promotes Aβ oligomer formation and localizes in neurons and amyloid deposits, *Neurobiology of disease 17*, 367-377.

[18] Cullen, K. M., Kócsi, Z., and Stone, J. (2006) Microvascular pathology in the aging human brain: evidence that senile plaques are sites of microhaemorrhages, *Neurobiology of aging 27*, 1786-1796.

[19] Sankar, S. B., Donegan, R. K., Shah, K. J., Reddi, A. R., and Wood, L. B. (2018) Heme and hemoglobin suppress amyloid β–mediated inflammatory activation of mouse astrocytes, *Journal of Biological Chemistry 293*, 11358-11373.

[20] Muller-Eberhard, U., and Fraig, M. (1993) Bioactivity of heme and its containment, *American journal of hematology 42*, 59-62.

[21] Atamna, H., and Ginsburg, H. (1995) Heme degradation in the presence of glutathione A proposed mechanism to account for the high levels of non-heme iron found in the membranes of hemoglobinopathic red blood cells, *Journal of Biological Chemistry 270*, 24876-24883.

[22] Contreras, H., Chim, N., Credali, A., and Goulding, C. W. (2014) Heme uptake in bacterial pathogens, *Current opinion in chemical biology 19*, 34-41.

[23] Piel III, R. B., Dailey Jr, H. A., and Medlock, A. E. (2019) The mitochondrial heme metabolon: Insights into the complex (ity) of heme synthesis and distribution, *Molecular genetics and metabolism*.

[24] Piel III, R. B., Shiferaw, M. T., Vashisht, A. A., Marcero, J. R., Praissman, J. L., Phillips, J. D., Wohlschlegel, J. A., and Medlock, A. E. (2016) A novel role for progesterone receptor membrane component 1 (PGRMC1): a partner and regulator of ferrochelatase, *Biochemistry 55*, 5204-5217.

[25] Khan, A. A., and Quigley, J. G. (2013) Heme and FLVCR-related transporter families SLC48 and SLC49, *Molecular aspects of medicine 34*, 669-682.

[26] Rajagopal, A., Rao, A. U., Amigo, J., Tian, M., Upadhyay, S. K., Hall, C., Uhm, S., Mathew, M., Fleming, M. D., and Paw, B. H. (2008) Haem homeostasis is regulated by the conserved and concerted functions of HRG-1 proteins, *Nature 453*, 1127.

[27] Korolnek, T., Zhang, J., Beardsley, S., Scheffer, G. L., and Hamza, I. (2014) Control of metazoan heme homeostasis by a conserved multidrug resistance protein, *Cell metabolism 19*, 1008-1019.

[28] Yang, Z., Philips, J. D., Doty, R. T., Giraudi, P., Ostrow, J. D., Tiribelli, C., Smith, A., and Abkowitz, J. L. (2010) Kinetics and specificity of feline leukemia virus subgroup C receptor (FLVCR) export function and its dependence on hemopexin, *Journal of Biological Chemistry 285*, 28874-28882.

[29] Quigley, J. G., Burns, C. C., Anderson, M. M., Lynch, E. D., Sabo, K. M., Overbaugh, J., and Abkowitz, J. L. (2000) Cloning of the cellular receptor for feline leukemia virus subgroup C (FeLV-C), a retrovirus that induces red cell aplasia, *Blood 95*, 1093-1099.

[30] Chiabrando, D., Marro, S., Mercurio, S., Giorgi, C., Petrillo, S., Vinchi, F., Fiorito, V., Fagoonee, S., Camporeale, A., and Turco, E. (2012) The mitochondrial heme exporter FLVCR1b mediates erythroid differentiation, *The Journal of clinical investigation 122*, 4569-4579.

[31] White, C., Yuan, X., Schmidt, P. J., Bresciani, E., Samuel, T. K., Campagna, D., Hall, C., Bishop, K., Calicchio, M. L., and Lapierre, A. (2013) HRG1 is essential for heme transport from the phagolysosome of macrophages during erythrophagocytosis, *Cell metabolism 17*, 261-270.

[32] Taketani, S., Adachi, Y., Kohno, H., Ikehara, S., Tokunaga, R., and Ishii, T. (1998) Molecular characterization of a newly identified heme-binding protein induced during differentiation of urine erythroleukemia cells, *Journal of Biological Chemistry 273*, 31388-31394.

[33] Iwahara, S., Satoh, H., Song, D. X., Webb, J., Burlingame, A. L., Nagae, Y., and Mullereberhard, U. (1995) Purification, Characterization, and Cloning of a Heme-Binding Protein (23 Kda) in Rat-Liver Cytosol, *Biochemistry 34*, 13398-13406.

[34] Ketley, J. N., Habig, W., and Jakoby, W. (1975) Binding of nonsubstrate ligands to the glutathione S-transferases, *Journal of Biological Chemistry 250*, 8670-8673.

[35] Zylka, M. J., and Reppert, S. M. (1999) Discovery of a putative heme-binding protein family (SOUL/HBP) by two-tissue suppression subtractive hybridization and database searches, *Molecular brain research 74*, 175-181.

[36] Vincent, S. H., and Muller-Eberhard, U. (1985) A protein of the Z class of liver cytosolic proteins in the rat that preferentially binds heme, *Journal of Biological Chemistry 260*, 14521-14528.

[37] Watanabe, Y., Ishimori, K., and Uchida, T. (2017) Dual role of the active-center cysteine in human peroxiredoxin 1: Peroxidase activity and heme binding, *Biochemical and biophysical research communications 483*, 930-935.

[38] Labbe, S., Khan, M. G. M., and Jacques, J.-F. (2013) Iron uptake and regulation in Schizosaccharomyces pombe, *Current opinion in microbiology 16*, 669-676.

[39] Askwith, C., and Kaplan, J. (1997) An oxidase-permease-based iron transport system in Schizosaccharomyces pombe and its expression in Saccharomyces cerevisiae, *Journal of Biological Chemistry 272*, 401-405.

[40] Pelletier, B., Beaudoin, J., Philpott, C. C., and Labbé, S. (2003) Fep1 represses expression of the fission yeast Schizosaccharomyces pombe siderophore-iron transport system, *Nucleic acids research 31*, 4332-4344.

[41] Mourer, T., Jacques, J.-F., Brault, A., Bisaillon, M., and Labbé, S. (2015) Shu1 is a cell-surface protein involved in iron acquisition from heme in Schizosaccharomyces pombe, *Journal of Biological Chemistry 290*, 10176-10190.

[42] Normant, V., Mourer, T., and Labbé, S. (2018) The major facilitator transporter Str3 is required for low-affinity heme acquisition in Schizosaccharomyces pombe, *Journal of Biological Chemistry 293*, 6349-6362.

[43] Mourer, T., Normant, V., and Labbé, S. (2017) Heme assimilation in Schizosaccharomyces pombe requires cell-surface-anchored protein Shu1 and vacuolar transporter Abc3, *Journal of Biological Chemistry 292*, 4898-4912.

[44] Kuznets, G., Vigonsky, E., Weissman, Z., Lalli, D., Gildor, T., Kauffman, S. J., Turano, P., Becker, J., Lewinson, O., and Kornitzer, D. (2014) A relay network of extracellular heme-binding proteins drives C. albicans iron acquisition from hemoglobin, *PLoS pathogens 10*, e1004407.

[45] Weissman, Z., and Kornitzer, D. (2004) A family of Candida cell surface haem-binding proteins involved in haemin and haemoglobin-iron utilization, *Molecular microbiology 53*, 1209-1220.

[46] Weissman, Z., Shemer, R., Conibear, E., and Kornitzer, D. (2008) An endocytic mechanism for haemoglobin-iron acquisition in Candida albicans, *Molecular microbiology 69*, 201-217.

[47] Hooda, J., Shah, A., and Zhang, L. (2014) Heme, an essential nutrient from dietary proteins, critically impacts diverse physiological and pathological processes, *Nutrients 6*, 1080-1102.

[48] Ponka, P., Sheftel, A. D., English, A. M., Bohle, D. S., and Garcia-Santos, D. (2017) Do mammalian cells really need to export and import heme?, *Trends in biochemical sciences 42*, 395-406.

[49] Gietz, R. D., and Schiestl, R. H. (1991) Applications of high efficiency lithium acetate trasformation of intact yeast cells using single-stranded nucleic acids as carrier, *Yeast 7*, 253-263.

[50] Gietz, R. D., and Schiestl, R. H. (1991) Applications of high efficiency lithium acetate transformation of intact yeast cells using single-stranded nucleic acids as carrier, *Yeast 7*, 253-263.

[51] Waxman, H. S., and Rabinovitz, M. (1966) Control of reticulocyte polyribosome content and hemoglobin synthesis by heme, *Biochimica et Biophysica Acta (BBA)-Nucleic Acids and Protein Synthesis 129*, 369-379.

[52] Lennon, R., Singh, A., Welsh, G. I., Coward, R. J., Satchell, S., Ni, L., Mathieson, P. W., Bakker, W. W., and Saleem, M. A. (2008) Hemopexin induces nephrin-dependent reorganization of the actin cytoskeleton in podocytes, *Journal of the American Society of Nephrology 19*, 2140-2149.

[53] Ye, W., and Zhang, L. (2004) Heme controls the expression of cell cycle regulators and cell growth in HeLa cells, *Biochemical and biophysical research communications 315*, 546-554.

[54] Di Fiore, P. P., and De Camilli, P. (2001) Endocytosis and signaling: an inseparable partnership, *Cell 106*, 1-4.

[55] Chen, A. J., Yuan, X., Li, J., Dong, P., Hamza, I., and Cheng, J.-X. (2018) Label-free imaging of heme dynamics in living organisms by transient absorption microscopy, *Analytical chemistry 90*, 3395-3401.

[56] Roh, H. C., Collier, S., Guthrie, J., Robertson, J. D., and Kornfeld, K. (2012) Lysosome-related organelles in intestinal cells are a zinc storage site in C. elegans, *Cell metabolism 15*, 88-99.

[57] Liu, G., Lanham, C., Buchan, J. R., and Kaplan, M. E. (2017) High-throughput transformation of Saccharomyces cerevisiae using liquid handling robots, *Plos One 12*, e0174128.

[58] Michener, J. K., Nielsen, J., and Smolke, C. D. (2012) Identification and treatment of heme depletion attributed to overexpression of a lineage of evolved P450 monooxygenases, *Proc Natl Acad Sci U S A 109*, 19504-19509.

[59] Sirover, M. A. (1999) New insights into an old protein: the functional diversity of mammalian glyceraldehyde-3-phosphate dehydrogenase, *Biochimica et Biophysica Acta (BBA)-Protein Structure and Molecular Enzymology 1432*, 159-184.

[60] Carlile, G. W., Chalmers-Redman, R. M., Tatton, N. A., Pong, A., Borden, K. L., and Tatton, W. G. (2000) Reduced apoptosis after nerve growth factor and serum withdrawal: conversion of tetrameric glyceraldehyde-3-phosphate dehydrogenase to a dimer, *Molecular pharmacology 57*, 2-12.

[61] Engel, M., Seifert, M., Theisinger, B., Seyfert, U., and Welter, C. (1998) Glyceraldehyde-3-phosphate dehydrogenase and Nm23-H1/nucleoside diphosphate kinase A two old enzymes combine for the novel Nm23 protein phosphotransferase function, *Journal of Biological Chemistry 273*, 20058-20065.

[62] GY, M. (2002) Proliferative and nutritional dependent regulation of glyceraldehyde-3-phosphate dehydrogenase expression in the rat liver, *Cell proliferation 35*, 173-182.

[63] Cool, B. L., and Sirover, M. A. (1989) Immunocytochemical localization of the base excision repair enzyme uracil DNA glycosylase in quiescent and proliferating normal human cells, *Cancer research 49*, 3029-3036.

[64] McAlister, L., and Holland, M. J. (1985) Isolation and characterization of yeast strains carrying mutations in the glyceraldehyde-3-phosphate dehydrogenase genes, *The Journal of biological chemistry 260*, 15013-15018.

[65] McAlister, L., and Holland, M. J. (1985) Differential expression of the three yeast glyceraldehyde-3-phosphate dehydrogenase genes, *The Journal of biological chemistry 260*, 15019-15027.

[66] Delgado, M. L., O'Connor, J. E., Azorin, I., Renau-Piqueras, J., Gil, M. L., and Gozalbo, D. (2001) The glyceraldehyde-3-phosphate dehydrogenase polypeptides encoded by the Saccharomyces cerevisiae TDH1, TDH2 and TDH3 genes are also cell wall proteins, *Microbiology 147*, 411-417.

[67] Sirover, M. A. (1997) Role of the glycolytic protein, glyceraldehyde-3-phosphate dehydrogenase, in normal cell function and in cell pathology, *Journal of cellular biochemistry 66*, 133-140.

[68] Baxi, M. D., and Vishwanatha, J. K. (1995) Uracil DNA-glycosylase/glyceraldehyde-3-phosphate dehydrogenase is an Ap4A binding protein, *Biochemistry 34*, 9700-9707.

[69] Meyer-Siegler, K., Mauro, D. J., Seal, G., Wurzer, J., Deriel, J. K., and Sirover, M. A. (1991) A human nuclear uracil DNA glycosylase is the 37-kDa subunit of glyceraldehyde-3-phosphate dehydrogenase, *Proceedings of the National Academy of Sciences 88*, 8460-8464.

[70] Tarze, A., Deniaud, A., Le Bras, M., Maillier, E., Molle, D., Larochette, N., Zamzami, N., Jan, G., Kroemer, G., and Brenner, C. (2007) GAPDH, a novel regulator of the pro-apoptotic mitochondrial membrane permeabilization, *Oncogene 26*, 2606-2620.

[71] Kumagai, H., and Sakai, H. (1983) A porcine brain protein (35 K protein) which bundles microtubules and its identification as glyceraldehyde 3-phosphate dehydrogenase, *The Journal of Biochemistry 93*, 1259-1269.

[72] Huitorel, P., and Pantaloni, D. (1985) Bundling of microtubules by glyceraldehyde-3-phosphate dehydrogenase and its modulation by ATP, *European journal of biochemistry 150*, 265-269.

[73] Walsh, J. L., Keith, T. J., and Knull, H. R. (1989) Glycolytic enzyme interactions with tubulin and microtubules, *Biochimica et Biophysica Acta (BBA)-Protein Structure and Molecular Enzymology 999*, 64-70.

[74] Hara, M. R., Cascio, M. B., and Sawa, A. (2006) GAPDH as a sensor of NO stress, *Biochimica et Biophysica Acta (BBA)-Molecular Basis of Disease 1762*, 502-509.

[75] Hara, M. R., and Snyder, S. H. (2006) Nitric oxide–GAPDH–Siah: a novel cell death cascade, *Cellular and molecular neurobiology 26*, 525-536.

[76] Tisdale, E. J., and Artalejo, C. R. (2007) A GAPDH mutant defective in Src-dependent tyrosine phosphorylation impedes Rab2-mediated events, *Traffic 8*, 733-741.

[77] Ashmarina, L. I., Louzenko, S. E., Severin, S. E., Muronetz, V. I., and Nagradova, N. K. (1988) Phosphorylation of D-glyceraldehyde-3-phosphate dehydrogenase by Ca2+/calmodulin-dependent protein kinase II, *FEBS letters 231*, 413-416.

[78] Volker, K. W., and Knull, H. R. (1997) A glycolytic enzyme binding domain on tubulin, *Archives of biochemistry and biophysics 338*, 237-243.

[79] Durrieu, C., Bernier-Valentin, F., and Rousset, B. (1987) Binding of glyceraldehyde 3-phosphate dehydrogenase to microtubules, *Molecular and cellular biochemistry 74*, 55-65.

[80] Tristan, C., Shahani, N., Sedlak, T. W., and Sawa, A. (2011) The diverse functions of GAPDH: views from different subcellular compartments, *Cellular signalling 23*, 317-323.

[81] Chakravarti, R., Aulak, K. S., Fox, P. L., and Stuehr, D. J. (2010) GAPDH regulates cellular heme insertion into inducible nitric oxide synthase, *Proceedings of the National Academy of Sciences of the United States of America 107*, 18004-18009.

[82] Hamza, I., and Dailey, H. A. (2012) One ring to rule them all: trafficking of heme and heme synthesis intermediates in the metazoans, *Biochim Biophys Acta 1823*, 1617-1632.

[83] Hanker, J. S., and Rabin, A. N. (1975) Color reaction streak test for catalase-positive microorganisms, *Journal of clinical microbiology 2*, 463-464.

[84] Guarente, L., Lalonde, B., Gifford, P., and Alani, E. (1984) Distinctly regulated tandem upstream activation sites mediate catabolite repression of the CYC1 gene of S. cerevisiae, *Cell 36*, 503-511.

[85] Pfeifer, K., Kim, K. S., Kogan, S., and Guarente, L. (1989) Functional dissection and sequence of yeast HAP1 activator, *Cell 56*, 291-301.

[86] Andreini, C., Putignano, V., Rosato, A., and Banci, L. (2018) The human iron-proteome, *Metallomics 10*, 1223-1231.

[87] Sweeny, E. A., Singh, A. B., Chakravarti, R., Martinez-Guzman, O., Saini, A., Haque, M. M., Garee, G., Dans, P. D., Hannibal, L., Reddi, A. R., and Stuehr, D. J. (2018) Glyceraldehyde-3-phosphate dehydrogenase is a chaperone that allocates labile heme in cells, *Journal of Biological Chemistry 293*, 14557-14568.

[88] Harvey, J. W., and Beutler, E. (1982) Binding of heme by glutathione S-transferase: a possible role of the erythrocyte enzyme, *Blood 60*, 1227-1230.

[89] Iwahara, S., Satoh, H., Song, D. X., Webb, J., Burlingame, A. L., Nagae, Y., and Muller-Eberhard, U. (1995) Purification, characterization, and cloning of a heme-binding protein (23 kDa) in rat liver cytosol, *Biochemistry 34*, 13398-13406.

[90] Taketani, S., Adachi, Y., Kohno, H., Ikehara, S., Tokunaga, R., and Ishii, T. (1998) Molecular characterization of a newly identified heme-binding protein induced during differentiation of urine erythroleukemia cells, *The Journal of biological chemistry 273*, 31388-31394.

[91] Vincent, S. H., and Muller-Eberhard, U. (1985) A protein of the Z class of liver cytosolic proteins in the rat that preferentially binds heme, *J Biol Chem 260*, 14521-14528.

[92] Zheng, L., Roeder, R. G., and Luo, Y. (2003) S phase activation of the histone H2B promoter by OCA-S, a coactivator complex that contains GAPDH as a key component, *Cell 114*, 255-266.

[93] Hara, M. R., Agrawal, N., Kim, S. F., Cascio, M. B., Fujimuro, M., Ozeki, Y., Takahashi, M., Cheah, J. H., Tankou, S. K., and Hester, L. D. (2005) S-nitrosylated GAPDH initiates apoptotic cell death by nuclear translocation following Siah1 binding, *Nature cell biology 7*, 665.

[94] Fiucci, G., Beaucourt, S., Duflaut, D., Lespagnol, A., Stumptner-Cuvelette, P., Géant, A., Buchwalter, G., Tuynder, M., Susini, L., and Lassalle, J.-M. (2004) Siah-1b is a direct transcriptional target of p53: identification of the functional p53 responsive element in the siah-1b promoter, *Proceedings of the National Academy of Sciences 101*, 3510-3515.

[95] Sen, N., Hara, M. R., Ahmad, A. S., Cascio, M. B., Kamiya, A., Ehmsen, J. T., Aggrawal, N., Hester, L., Dore, S., and Snyder, S. H. (2009) GOSPEL: a neuroprotective protein that binds to GAPDH upon S-nitrosylation, *Neuron 63*, 81-91.

[96] Gietz, R. D., and Schiestl, R. H. (2007) Microtiter plate transformation using the LiAc/SS carrier DNA/PEG method, *Nature protocols 2*, 5-8.

[97] Ness, F., Achstetter, T., Duport, C., Karst, F., Spagnoli, R., and Degryse, E. (1998) Sterol uptake in Saccharomyces cerevisiae heme auxotrophic mutants is affected by ergosterol and oleate but not by palmitoleate or by sterol esterification, *J Bacteriol 180*, 1913-1919.

[98] Bertani, G. (2004) Lysogeny at mid-twentieth century: P1, P2, and other experimental, systems, *J Bacteriol 186*, 595-600.

[99] Mumberg, D., Muller, R., and Funk, M. (1995) Yeast Vectors for the Controlled Expression of Heterologous Proteins in Different Genetic Backgrounds, *Gene 156*, 119-122.

[100] Baureder, M., and Hederstedt, L. (2012) Genes Important for Catalase Activity in Enterococcus faecalis, *Plos One 7*.

[101] Woods, J. S., and Simmonds, P. L. (2001) HPLC methods for analysis of porphyrins in biological media, *Current protocols in toxicology 7*, 8.9. 1-8.9. 17.

[102] Reddi, A. R., and Culotta, V. C. (2013) SOD1 integrates signals from oxygen and glucose to repress respiration, *Cell 152*, 224-235.

[103] Reddi, A. R., and Culotta, V. C. (2011) Regulation of manganese antioxidants by nutrient sensing pathways in Saccharomyces cerevisiae, *Genetics 189*, 1261-1270.

[104] Raghuram, S., Stayrook, K. R., Huang, P., Rogers, P. M., Nosie, A. K., McClure, D. B., Burris, L. L., Khorasanizadeh, S., Burris, T. P., and Rastinejad, F. (2007) Identification of heme as the ligand for the orphan nuclear receptors REV-ERBα and REV-ERBβ, *Nature structural & molecular biology 14*, 1207.

[105] Shen, J., Sheng, X., Chang, Z., Wu, Q., Wang, S., Xuan, Z., Li, D., Wu, Y., Shang, Y., Kong, X., Yu, L., Li, L., Ruan, K., Hu, H., Huang, Y., Hui, L., Xie, D., Wang, F., and Hu, R. (2014) Iron metabolism regulates p53 signaling through direct heme-p53 interaction and modulation of p53 localization, stability, and function, *Cell Rep 7*, 180-193.

[106] Ogawa, K., Sun, J., Taketani, S., Nakajima, O., Nishitani, C., Sassa, S., Hayashi, N., Yamamoto, M., Shibahara, S., Fujita, H., and Igarashi, K. (2001) Heme mediates derepression of Maf recognition element through direct binding to transcription repressor Bach1, *The EMBO journal 20*, 2835-2843.

[107] Chen, J. J., and London, I. M. (1995) Regulation of protein synthesis by heme-regulated eIF-2 alpha kinase, *Trends Biochem Sci 20*, 105-108.

[108] Mense, S. M., and Zhang, L. (2006) Heme: a versatile signaling molecule controlling the activities of diverse regulators ranging from transcription factors to MAP kinases, *Cell research 16*, 681-692.

[109] Burton, M. J., Kapetanaki, S. M., Chernova, T., Jamieson, A. G., Dorlet, P., Santolini, J., Moody, P. C., Mitcheson, J. S., Davies, N. W., Schmid, R., Raven, E. L., and Storey, N. M. (2016) A heme-binding domain controls regulation of ATP-dependent potassium channels, *Proceedings of the National Academy of Sciences of the United States of America 113*, 3785-3790.

[110] Barr, I., Smith, A. T., Chen, Y., Senturia, R., Burstyn, J. N., and Guo, F. (2012) Ferric, not ferrous, heme activates RNA-binding protein DGCR8 for primary microRNA processing, *Proc Natl Acad Sci U S A 109*, 1919-1924.

[111] Sachar, M., Anderson, K. E., and Ma, X. (2016) Protoporphyrin IX: the good, the bad, and the ugly, *Journal of Pharmacology and Experimental Therapeutics 356*, 267-275.

[112] Shen, J., Sheng, X., Chang, Z., Wu, Q., Wang, S., Xuan, Z., Li, D., Wu, Y., Shang, Y., and Kong, X. (2014) Iron metabolism regulates p53 signaling through direct heme-p53 interaction and modulation of p53 localization, stability, and function, *Cell Rep 7*, 180-193.

[113] Wu, M.-L., Ho, Y.-C., Lin, C.-Y., and Yet, S.-F. (2011) Heme oxygenase-1 in inflammation and cardiovascular disease, *American Journal of Cardiovascular Disease 1*, 150.

[114] Atamna, H., Killilea, D. W., Killilea, A. N., and Ames, B. N. (2002) Heme deficiency may be a factor in the mitochondrial and neuronal decay of aging, *Proceedings of the National Academy of Sciences 99*, 14807-14812.

[115] Schipper, H. M., Song, W., Zukor, H., Hascalovici, J. R., and Zeligman, D. (2009) Heme oxygenase-1 and neurodegeneration: expanding frontiers of engagement, *Journal of neurochemistry 110*, 469-485.

[116] Puy, H., Gouya, L., and Deybach, J.-C. (2010) Porphyrias, *The Lancet 375*, 924-937.

[117] Yang, Z., Keel, S. B., Shimamura, A., Liu, L., Gerds, A. T., Li, H. Y., Wood, B. L., Scott, B. L., and Abkowitz, J. L. (2016) Delayed globin synthesis leads to excess heme and the macrocytic anemia of Diamond Blackfan anemia and del (5q) myelodysplastic syndrome, *Science translational medicine 8*, 338ra367-338ra367.

[118] Medlock, A. E., Shiferaw, M. T., Marcero, J. R., Vashisht, A. A., Wohlschlegel, J. A., Phillips, J. D., and Dailey, H. A. (2015) Identification of the mitochondrial heme metabolism complex, *Plos One 10*, e0135896.

[119] Elbaz-Alon, Y., Rosenfeld-Gur, E., Shinder, V., Futerman, A. H., Geiger, T., and Schuldiner, M. (2014) A dynamic interface between vacuoles and mitochondria in yeast, *Developmental cell 30*, 95-102.

[120] Lackner, L. L. (2019) The expanding and unexpected functions of mitochondria contact sites, *Trends in cell biology*.

[121] Murley, A., and Nunnari, J. (2016) The Emerging Network of Mitochondria-Organelle Contacts, *Mol Cell 61*, 648-653.

[122] Xue, Y., Schmollinger, S., Attar, N., Campos, O. A., Vogelauer, M., Carey, M. F., Merchant, S. S., and Kurdistani, S. K. (2017) Endoplasmic reticulum–mitochondria junction is required for iron homeostasis, *Journal of Biological Chemistry 292*, 13197-13204.

[123] Friedman, J. R., Lackner, L. L., West, M., DiBenedetto, J. R., Nunnari, J., and Voeltz, G. K. (2011) ER tubules mark sites of mitochondrial division, *Science (New York, N.Y.) 334*, 358-362.

[124] Murley, A., Lackner, L. L., Osman, C., West, M., Voeltz, G. K., Walter, P., and Nunnari, J. (2013) ER-associated mitochondrial division links the distribution of mitochondria and mitochondrial DNA in yeast, *Elife 2*, e00422.

[125] Hanna, D. A., Hu, R., Kim, H., Martinez-Guzman, O., Torres, M. P., and Reddi, A. R. (2018) Heme bioavailability and signaling in response to stress in yeast cells, *The Journal of biological chemistry 293*, 12378-12393.

[126] Shadel, G. S., and Seidel-Rogol, B. L. (2007) Diagnostic assays for defects in mtDNA replication and transcription in yeast and humans, *Methods in cell biology 80*, 465-479.

[127] Williamson, D. H., and Fennell, D. J. (1979) [62] Visualization of yeast mitochondrial dna with the fluorescent stain "DAPI", In *Methods in enzymology*, pp 728-733, Elsevier.

[128] Michener, J. K., Nielsen, J., and Smolke, C. D. (2012) Identification and treatment of heme depletion attributed to overexpression of a lineage of evolved P450 monooxygenases, *Proceedings of the National Academy of Sciences 109*, 19504-19509.

[129] Arosio, P., Knowles, T. P., and Linse, S. (2015) On the lag phase in amyloid fibril formation, *Physical Chemistry Chemical Physics 17*, 7606-7618.

[130] Boldogh, I. R., Nowakowski, D. W., Yang, H.-C., Chung, H., Karmon, S., Royes, P., and Pon, L. A. (2003) A protein complex containing Mdm10p, Mdm12p, and Mmm1p links mitochondrial membranes and DNA to the cytoskeleton-based segregation machinery, *Mol Biol Cell 14*, 4618-4627.

[131] Kornmann, B., Currie, E., Collins, S. R., Schuldiner, M., Nunnari, J., Weissman, J. S., and Walter, P. (2009) An ER-mitochondria tethering complex revealed by a synthetic biology screen, *Science (New York, N.Y.) 325*, 477-481.

[132] Sogo, L. F., and Yaffe, M. P. (1994) Regulation of mitochondrial morphology and inheritance by Mdm10p, a protein of the mitochondrial outer membrane, *The Journal of cell biology 126*, 1361-1373.

[133] Youngman, M. J., Hobbs, A. E. A., Burgess, S. M., Srinivasan, M., and Jensen, R. E. (2004) Mmm2p, a mitochondrial outer membrane protein required for yeast mitochondrial shape and maintenance of mtDNA nucleoids, *The Journal of cell biology 164*, 677-688.

[134] Burgess, S. M., Delannoy, M., and Jensen, R. E. (1994) MMM1 encodes a mitochondrial outer membrane protein essential for establishing and maintaining the structure of yeast mitochondria, *The Journal of cell biology 126*, 1375-1391.

[135] Kornmann, B., Osman, C., and Walter, P. (2011) The conserved GTPase Gem1 regulates endoplasmic reticulum–mitochondria connections, *Proceedings of the National Academy of Sciences 108*, 14151-14156.

[136] Kawano, S., Tamura, Y., Kojima, R., Bala, S., Asai, E., Michel, A. H., Kornmann, B., Riezman, I., Riezman, H., and Sakae, Y. (2018) Structure–function insights into direct lipid transfer between membranes by Mmm1–Mdm12 of ERMES, *The Journal of cell biology 217*, 959-974.

[137] Nguyen, T. T., Lewandowska, A., Choi, J. Y., Markgraf, D. F., Junker, M., Bilgin, M., Ejsing, C. S., Voelker, D. R., Rapoport, T. A., and Shaw, J. M. (2012) Gem1 and ERMES do not directly affect phosphatidylserine transport from ER to mitochondria or mitochondrial inheritance, *Traffic 13*, 880-890.

[138] Schuler, M.-H., Di Bartolomeo, F., Mårtensson, C. U., Daum, G., and Becker, T. (2016) Phosphatidylcholine affects inner membrane protein translocases of mitochondria, *Journal of Biological Chemistry 291*, 18718-18729.

[139] Hönscher, C., Mari, M., Auffarth, K., Bohnert, M., Griffith, J., Geerts, W., van der Laan, M., Cabrera, M., Reggiori, F., and Ungermann, C. (2014) Cellular metabolism regulates contact sites between vacuoles and mitochondria, *Developmental cell 30*, 86-94.

[140] Chan, D. C. (2012) Fusion and fission: interlinked processes critical for mitochondrial health, *Annual review of genetics 46*, 265-287.

[141] Tatsuta, T., Scharwey, M., and Langer, T. (2014) Mitochondrial lipid trafficking, *Trends in cell biology 24*, 44-52.

[142] Westermann, B. (2008) Molecular machinery of mitochondrial fusion and fission, *Journal of Biological Chemistry 283*, 13501-13505.

[143] DeVay, R. M., Dominguez-Ramirez, L., Lackner, L. L., Hoppins, S., Stahlberg, H., and Nunnari, J. (2009) Coassembly of Mgm1 isoforms requires cardiolipin and mediates mitochondrial inner membrane fusion, *The Journal of cell biology 186*, 793-803.

[144] Zick, M., Duvezin-Caubet, S., Schäfer, A., Vogel, F., Neupert, W., and Reichert, A. S. (2009) Distinct roles of the two isoforms of the dynamin-like GTPase Mgm1 in mitochondrial fusion, *FEBS letters 583*, 2237-2243.

[145] Meeusen, S., DeVay, R., Block, J., Cassidy-Stone, A., Wayson, S., McCaffery, J. M., and Nunnari, J. (2006) Mitochondrial inner-membrane fusion and crista maintenance requires the dynamin-related GTPase Mgm1, *Cell 127*, 383-395.

[146] Hessenberger, M., Zerbes, R. M., Rampelt, H., Kunz, S., Xavier, A. H., Purfürst, B., Lilie, H., Pfanner, N., van der Laan, M., and Daumke, O. (2017) Regulated membrane remodeling by Mic60 controls formation of mitochondrial crista junctions, *Nature communications 8*, 15258.

[147] Zhang, L., Bermingham-McDonogh, O., Turcotte, B., and Guarente, L. (1993) Antibody-promoted dimerization bypasses the regulation of DNA binding by the heme domain of the yeast transcriptional activator HAP1, *Proceedings of the National Academy of Sciences 90*, 2851-2855.

[148] Zhang, L., and Hach, A. (1999) Molecular mechanism of heme signaling in yeast: the transcriptional activator Hap1 serves as the key mediator, *Cellular and Molecular Life Sciences CMLS 56*, 415-426.

[149] Zhang, L., Hach, A., and Wang, C. (1998) Molecular mechanism governing heme signaling in yeast: a higher-order complex mediates heme regulation of the transcriptional activator HAP1, *Molecular and cellular biology 18*, 3819-3828.

[150] Shinomiya, R., Katahira, Y., Araki, H., Shibata, T., Momotake, A., Yanagisawa, S., Ogura, T., Suzuki, A., Neya, S., and Yamamoto, Y. (2018) Characterization of Catalytic Activities and Heme Coordination Structures of Heme–DNA Complexes Composed of Some Chemically Modified Hemes and an All Parallel-Stranded Tetrameric G-Quadruplex DNA Formed from d (TTAGGG), *Biochemistry 57*, 5930-5937.

[151] Shumayrikh, N., Huang, Y. C., and Sen, D. (2015) Heme activation by DNA: isoguanine pentaplexes, but not quadruplexes, bind heme and enhance its oxidative activity, *Nucleic acids research 43*, 4191-4201.

[152] Yamamoto, Y., Kinoshita, M., Katahira, Y., Shimizu, H., Di, Y., Shibata, T., Tai, H., Suzuki, A., and Neya, S. (2015) Characterization of Heme–DNA Complexes Composed of Some

Chemically Modified Hemes and Parallel G-Quadruplex DNAs, *Biochemistry 54*, 7168-7177.

[153] Buschlen, S., Amillet, J., Guiard, B., Fournier, A., Marcireau, C., and Bolotin-Fukuhara, M. (2003) The S. cerevisiae HAP complex, a key regulator of mitochondrial function, coordinates nuclear and mitochondrial gene expression, *International Journal of Genomics 4*, 37-46.

[154] Hon, T., Lee, H. C., Hu, Z., Iyer, V. R., and Zhang, L. (2005) The heme activator protein Hap1 represses transcription by a heme-independent mechanism in Saccharomyces cerevisiae, *Genetics 169*, 1343-1352.

[155] Kubota, Y., Nomura, K., Katoh, Y., Yamashita, R., Kaneko, K., and Furuyama, K. (2016) Novel mechanisms for heme-dependent degradation of ALAS1 protein as a component of negative feedback regulation of heme biosynthesis, *Journal of Biological Chemistry 291*, 20516-20529.

[156] Keng, T., and Guarente, L. (1987) Constitutive expression of the yeast HEM1 gene is actually a composite of activation and repression, *Proceedings of the National Academy of Sciences 84*, 9113-9117.

[157] Nezich, C. L., and Youle, R. J. (2013) Cell Biology: Make or break for mitochondria, *Elife 2*, e00804.

[158] Lahiri, S., Chao, J. T., Tavassoli, S., Wong, A. K., Choudhary, V., Young, B. P., Loewen, C. J., and Prinz, W. A. (2014) A conserved endoplasmic reticulum membrane protein complex (EMC) facilitates phospholipid transfer from the ER to mitochondria, *PLoS biology 12*, e1001969.

[159] Macdonald, P. J., Stepanyants, N., Mehrotra, N., Mears, J. A., Qi, X., Sesaki, H., and Ramachandran, R. (2014) A dimeric equilibrium intermediate nucleates Drp1 reassembly on mitochondrial membranes for fission, *Mol Biol Cell 25*, 1905-1915.

[160] Koshiba, T., Holman, H. A., Kubara, K., Yasukawa, K., Kawabata, S.-i., Okamoto, K., Macfarlane, J., and Shaw, J. M. (2011) Structure-Function Analysis of the Yeast Mitochondrial Rho GTPase, Gem1p IMPLICATIONS FOR MITOCHONDRIAL INHERITANCE, *Journal of Biological Chemistry 286*, 354-362.

[161] Wang, X., Su, B., Siedlak, S. L., Moreira, P. I., Fujioka, H., Wang, Y., Casadesus, G., and Zhu, X. (2008) Amyloid-beta overproduction causes abnormal mitochondrial dynamics via differential modulation of mitochondrial fission/fusion proteins, *Proceedings of the National Academy of Sciences of the United States of America 105*, 19318-19323.

[162] Abrams, A. J., Hufnagel, R. B., Rebelo, A., Zanna, C., Patel, N., Gonzalez, M. A., Campeanu, I. J., Griffin, L. B., Groenewald, S., and Strickland, A. V. (2015) Mutations in SLC25A46, encoding a UGO1-like protein, cause an optic atrophy spectrum disorder, *Nature genetics 47*, 926.

[163] Cipolat, S., de Brito, O. M., Dal Zilio, B., and Scorrano, L. (2004) OPA1 requires mitofusin 1 to promote mitochondrial fusion, *Proceedings of the National Academy of Sciences 101*, 15927-15932.

[164] MacVicar, T., and Langer, T. (2016) OPA1 processing in cell death and disease–the long and short of it, *J Cell Sci 129*, 2297-2306.

[165] Schrepfer, E., and Scorrano, L. (2016) Mitofusins, from mitochondria to metabolism, *Mol Cell 61*, 683-694.

[166] Ness, F., Achstetter, T., Duport, C., Karst, F., Spagnoli, R., and Degryse, E. (1998) Sterol uptake in Saccharomyces cerevisiae heme auxotrophic mutants is affected by ergosterol and oleate but not by palmitoleate or by sterol esterification, *J Bacteriol 180*, 1913-1919.

[167] Sikorski, R. S., and Hieter, P. (1989) A system of shuttle vectors and yeast host strains designed for efficient manipulation of DNA in *Saccharomyces ceresiviae*, *Genetics 122*, 19-27.

[168] Ebert, P. S., Hess, R. A., Frykholm, B. C., and Tschudy, D. P. (1979) Succinylacetone, a potent inhibitor of heme biosynthesis: effect on cell growth, heme content and delta-aminolevulinic acid dehydratase activity of malignant murine erythroleukemia cells, *Biochem Biophys Res Commun 88*, 1382-1390.

[169] Protchenko, O., Shakoury-Elizeh, M., Keane, P., Storey, J., Androphy, R., and Philpott, C. C. (2008) Role of PUG1 in inducible porphyrin and heme transport in Saccharomyces cerevisiae, *Eukaryotic cell 7*, 859-871.

[170] Prasad, A. R., and Dailey, H. A. (1995) Effect of cellular location on the function of ferrochelatase, *Journal of Biological Chemistry 270*, 18198-18200.

[171] Poston, C. N., Duong, E., Cao, Y., and Bazemore-Walker, C. R. (2011) Proteomic analysis of lipid raft-enriched membranes isolated from internal organelles, *Biochemical and biophysical research communications 415*, 355-360.

[172] Zhang, A., Williamson, C. D., Wong, D. S., Bullough, M. D., Brown, K. J., Hathout, Y., and Colberg-Poley, A. M. (2011) Quantitative proteomic analyses of human cytomegalovirus-induced restructuring of endoplasmic reticulum-mitochondrial contacts at late times of infection, *Molecular & Cellular Proteomics 10*, M111. 009936.

[173] Yuan, X., Rietzschel, N., Kwon, H., Nuno, A. B. W., Hanna, D. A., Phillips, J. D., Raven, E. L., Reddi, A. R., and Hamza, I. (2016) Regulation of intracellular heme trafficking revealed by subcellular reporters, *Proceedings of the National Academy of Sciences 113*, E5144-E5152.

[174] Klompmaker, S. H., Kohl, K., Fasel, N., and Mayer, A. (2017) Magnesium uptake by connecting fluid-phase endocytosis to an intracellular inorganic cation filter, *Nature communications 8*, 1879.